Lawrence Berkeley National Laboratory
Recent Work

Title

MODEL CATALYTIC SYSTEMS: REACTIONS OF SMALL MOLECULES (C4H9OH, NH3, CO,H2 ON TRANSITION METAL SURFACES

Permalink

Author

Naasz, B.

Publication Date

1986-11-01

Lawrence Berkeley Laboratory
UNIVERSITY OF CALIFORNIA

Materials & Molecular Research Division

MODEL CATALYTIC SYSTEMS: REACTIONS OF SMALL MOLECULES (C_4H_9OH, NH_3, CO, H_2) ON TRANSITION METAL SURFACES

B. Naasz
(Ph.D. Thesis)

November 1986

DISCLAIMER

MODEL CATALYTIC SYSTEMS: REACTIONS OF SMALL MOLECULES
(C_4H_9OH, NH_3, CO AND H_2) ON TRANSITION METAL SURFACES

Brian Naasz

(Ph. D. Thesis)

Materials and Molecular Research Division
Lawrence Berkeley Laboratory
University of California
Berkeley, California 94720

TABLE OF CONTENTS   Page

MODEL CATALYTIC SYSTEMS: REACTIONS OF SMALL MOLECULES

(C_4H_9OH, NH_3 CO, H_2) ON TRANSITION METAL SURFACES.

BRIAN MICHAEL NAASZ

LAWRENCE BERKELEY LABORATORY
BERKELEY, CA.

and

DEPT. OF CHEMISTRY
UNIVERSITY OF CALIFORNIA
BERKELEY, CA.

ABSTRACT

This thesis is comprised of the study of two different catalytic reactions. The first being the ammonolysis of n-butanol over model Rh(111), Rh(331), and Cu(111) single crystal surfaces. The second is the hydrogenation of CO over well defined Fe and Re polycrystalline foils and unsupported MoS_2 catalysts. These studies combine kinetic characterization of these catalytic systems and surface analysis of the catalysts used.

It is shown that both the Rh(111) and Rh(331) surfaces have the ability to selectively catalyze the formation of butyronitrile from n-butanol and ammonia. Kinetic, structural and surface science data combine in this case to suggest a mechanism in which the alcohol is dehydrogenated to the corresponding aldehyde, and then the aldehyde reacts with ammonia to form either the nitrile or the amine via an imine intermediate.

The reaction occurs on a catalyst which is almost completely covered by an overlayer containing carbon, nitrogen, and oxygen.

Only approximately 5 percent of the bare metal sites are available during the reaction. Therefore the overlayer is a very integral part of the catalyst in this case.

It was found that Cu(111) single crystals can also catalyze this reaction. Again in this case, the overlayer on the Cu surface plays a role in the catalytic process and the resulting kinetics are similar to those observed on Rh. The differences on reactivity between the Cu(111) and Rh(111) catalysts were primarily a much shorter lifetime for the Cu and an inability of Cu to catalyze the formation of amines upon addition of hydrogen.

In the studies of the CO hydrogenation reactions over rhenium and iron catalysts it was shown that rhenium produced primarily methane and exhibited a lower activity than iron. The addition of sub-monolayer amounts of alkali decreased the overall rate of reaction and caused a selectivity change towards longer chain hydrocarbons on both metal surfaces. The hydrogenation of carbon or CH_x fragments appeared to be the rate determining step in this reaction.

Finally, it was found that addition of potassium carbonate as a promoter greatly increased the selectivity to alcohol of a MoS_2 catalyst for the CO hydrogenation reaction.

ACKNOWLEDGEMENTS

In another arena, I am deeply thankful for the support of both my sets of parents who were always absolute in their encouragement. The person who deserves the most praise of all is my wife, Corrie. She has made our stay in Berkeley and the associated hard work and long hours much more bearable with her loving support. My special thanks also to Michael McKale and John Raeside, both of whom provided encouragement above and beyond the call of housemateship. Finally I acknowledge my hound, Calico Ridge Kentucky Sour Mash for many helpful conversations.

DEDICATION

TO MY FAMILY

I. INTRODUCTION

1.1 Introduction

"It has then been proved that several simple and composite, soluble and insoluble substances possess the property of exercising upon other substances an effect quite different from chemical affinity. By means of this effect they produce decomposition of the elements of these substances and different recombinations of the same elements, from which they remain separate.

This new force, which was unknown until now, is common to both organic and inorganic nature. I do not believe that it is a force completely independent of electrochemical affinities; on the contrary, I believe that this is nothing other than a new manifestation of electrochemical affinity; but inasmuch as we cannot see their connection and mutual dependence, it is more convenient to give this force a separate name. I would therefore call this the catalytic force. I would furthermore call the decomposition of substances resulting from this force catalysis, just as the decomposition of substances resulting from chemical affinity is called analysis."[1]

One hundred and fifty years ago Berzelius, in the above passage, introduced the word catalysis. In effect, he hit the nail right on the head; we know today that this "new manifestation of electrochemical affinity" to which he refers is the process of making and breaking bonds with the catalyst.

For most of the past 150 years the entire field of catalysis has been more of an art than a science. Studies were necessarily limited, for the most part by an inability to adequately characterize the actual catalyst surface. The result of this was volumes of kinetic information that were generated by recording the rates of reaction over "black box" catalysts. This situation is rapidly changing, due primarily to the information that has become accessible through modern surface analysis techniques.

Thus, this important field, one that demanded $955 million of process catalysts last year,[2] is rapidly becoming a science. It plays a major role in the modern chemical processes of oxidation, hydrogenation, ammoxidation, ammonolysis, polymerization, alkylation, dehydration and all of the reactions in the petroleum refining process.

Catalysis is, in general, an incredibly complex phenomenon. Catalysis is a kinetic phenomenon; molecules adsorb, react, and desorb continuously. Catalysis is also a thermodynamic phenomenon; if bonds between reactant, intermediate, or product molecules and the surface are too strong the catalyst can be hindered or poisoned. On the other hand, a catalyst which does not form any bonds to the molecules in question, or one that forms very weak bonds, is not effective, since catalysis generally involves the breaking of bonds and the remaking of other bonds.

The studies that comprise this thesis combine kinetic characterization of the specific catalytic systems chosen and analysis of the catalyst surface. In the kinetic characterizations the pressure dependencies, selectivities, initial rates and activation energies were studied. The surface analysis included: studies of the catalyst surface before and after reaction with Auger Electron Spectroscopy, adsorption of reactant and product molecules on the clean and post reaction catalyst surface in ultra high vacuum monitored by both Auger and Thermal Programmed Desorption Spectroscopy, and in some cases X-ray Photoelectron Spectroscopy was used to aid in the characterization of the catalyst surface.

The combination of kinetic studies with surface analysis is very complimentary. By using a catalyst that has been characterized in UHV before a reaction it is possible to determine how the kinetic variables measured during a reaction are changed by such parameters as altering the type of clean metal catalyst used, modifying the surface with an additive, or changing the surface structure of a particular catalyst.

The overlayer that is formed during a catalytic reaction (or the absence of an overlayer), can sometimes provides additional insight into the catalytic reaction. The information gained includes the relative atomic coverages obtained from Auger measurements as well as data indicating what molecules or fragments have desorbed during a Thermal Programmed Desorption experiment. This information, while often not of direct kinetic importance, can often suggest the role adsorbates play in altering the selectivity or activity of a catalyst.

The purpose of this thesis is to study two different reactions. The first being the ammonolysis of n-butanol over model Rh(111), Rh(331), and Cu(111) single crystal surfaces. The second is the hydrogenation of CO over well defined Fe and Re polycrystalline foils and unsupported MoS_2 catalysts. Obviously, the ultimate goal in all cases would be to understand at an atomic level how changes in a catalyst's surface affect the observed kinetics. This is however beyond the current level of technology. Short of this goal, the object remains to learn as much as possible about how these catalysts function. The specific questions asked and the motivation for using these systems are the focus of the next two sections.

1.2 The Ammonolysis of n-Butanol to Butyronitrile

The ammonolysis reaction is an important technology, with virtually every major chemical manufacturer producing the product amines and nitriles through this process (see Chapter 3 for references). While the indicated references in Chapter 3 show the large amount of work that has been done on various supported ammonolysis catalysts, there have been no reported surface science studies of these catalysts. Another type of C-N bond forming reaction, ammoxidation, has been studied extensively by Grasselli.[3-7] This complex reaction, which includes alkenes, oxygen, and ammonia as reactant molecules was not studied here and any comparison to it is difficult due to the complexity of the oxide catalyst used.

In this section of the thesis metal single crystals were chosen as catalysts in an attempt to simplify as much as possible the catalyst used. Two papers were influential in determining Rh as a potential catalyst for the ammonolysis reaction. In both of these papers Rh metal was shown to be an active catalyst for C-N bond formation. In the first paper Schmidt and Hasenberg[8] showed that Rh foil could form HCN from CH_4 and NH_3 at temperatures ranging from 500 to 1600K. In the second, DeLouise and Winograd[9] showed that adsorption of NO on a carbon pretreated Rh(331) crystal resulted in the evolution of RH_2CN^+ and CN- SIMS ions, indicating CN bond formation under these circumstances. While neither of these reactions are directly related to the ammonolysis reactions, they both indicate that Rh metal is a potential C-N bond forming catalyst.

The goal of this research was to begin building a knowledge base for studies of the ammonolysis reaction. The questions that prompted the specific experiments were very simple since there has been no prior work in this area. They were: Can a metal single crystal catalyze an ammonolysis reaction? What effect does variation in the metal's surface structure have? Is the actual metal important to this reaction or does an overlayer play a major role in the catalytic process? Can the selectivity between nitrile and amine, the two primary reaction products as industrially observed, be controlled by the addition of hydrogen to the reaction? Would this observation be dependent on the metal used?

Chapter 3 is the first of two chapters in this thesis that address these questions. It will be shown in this chapter that both the Rh(111) and the Rh(331) surfaces have the ability to selectively catalyze the formation of butyronitrile from n-butanol and ammonia. Kinetic, structural and surface science data combine in this case to suggest a mechanism in which the alcohol is dehydrogenated to the corresponding aldehyde, and then the aldehyde reacts with ammonia to form either the nitrile or the amine via an imine intermediate.

The reaction occurs on a catalyst which is almost completely covered by an overlayer containing carbon, nitrogen and oxygen. Only approximately 5 percent of the bare metal sites are available during the reaction. Therefore the overlayer is a very integral part of the catalyst in this case.

This fact encouraged the work described in Chapter 4. Here the same reaction, between n-butanol and ammonia, was studied over a Cu(111) single crystal catalyst. Cu was chosen as a catalyst due to its inclusion in many of the supported catalysts that have been reported in the patent literature for the ammonolysis reaction (see Chapter 3 for references). (On Cu, as with Rh, there have been no surface science studies reported on this reaction.) The results of the reaction between n-butanol and ammonia on Cu(111) are then compared with those on Rh(111). This work shows that Cu(111) can also catalyze the selective formation of butyronitrile from n-butanol and ammonia. Again in this case, the overlayer on the copper surface plays a role in the catalytic process and the resulting kinetics are similar to those observed on Rh.

The differences in reactivity between the Cu(111) and Rh(111) catalysts were primarily a much shorter lifetime for the Cu and an inability of Cu to catalyze the formation of amines upon addition of hydrogen. Both of these results are quite possibly a result of the Cu catalysts inability to dissociate H_2 easily.

1.3 The Hydrogenation of Carbon Monoxide

For the purposes of this work the hydrogenation of carbon monoxide will be viewed as either the complete hydrogenation to hydrocarbons, as in the Fischer Tropsch synthesis, or the partial hydrogenation to alcohol.

The Fischer Tropsch synthesis has been a subject of much interest as a possible synthesis of fuels from syngas.[10,11] The only place this technology is currently in use is in South Africa, where waxes and diesel fuels are produced via this synthesis.[12,13] The catalysts used are typically alkali-promoted iron.

In Chapter 5 of this work model iron and rhenium catalysts for use in the Fischer Tropsch synthesis are compared. In an effort to more clearly understand the promoter effect alkali promoters were introduced to a clean metal catalyst. The results showed that rhenium produced primarily methane and exhibited a lower activity than iron. The addition of submonolayer amounts of alkali decreased the overall rate of reaction and caused a selectivity change towards longer chain hydrocarbons on both metal surfaces. Oxidation of the surface usually caused a higher selectivity towards methane, and a decreased rate of carbon build-up, but the overall rate of methanation remained relatively constant. The hydrogenation of carbon or CH_x fragments appears to be the rate determining step in the reaction.

In Chapter 6 an unsupported MoS_2 catalyst for the production of alcohols from carbon monoxide and hydrogen is discussed. Methanol is a very important basic industrial chemical, with production in the

United States of over one billion gallons per year.[14] It is also a potentially valuable source of fuel, with the potential of becoming a gasoline additive or basic raw fuel itself. Unfortunately, methanol is one of the least thermodynamically favored products of a reaction between carbon monoxide and hydrogen. This is shown graphically in Fig. 1.1.[15] As a result, it is of utmost importance then to develop catalysts that produce alcohols with high selectivity from carbon monoxide and hydrogen.

In recent years Quarderer and Cochran[16] reported a MoS_2/K_2CO_3 catalyst with about 10% K_2CO_3 loading by weight as a catalyst for alcohol production. Similar catalysts by Murchison and Murdick[17] with a lighter loading of K_2CO_3 gave no alcohol. The work reported here was undertaken to study what effect K_2CO_3 addition has upon the selectivity of the MoS_2 catalyst to alcohol. It is shown that molybdenum disulfide is an active catalyst for the formation of alkanes from carbon monoxide and hydrogen. The addition of potassium carbonate as a promoter greatly increased the selectivity of the catalyst to alcohols. The alcohol production was also found to be dependent on the pressure; higher pressures of either carbon monoxide or hydrogen led to significant increases in the alcohol yield. In particular, at 2000 psig and 250°C, a catalyst with 30 percent by weight potassium carbonate produced a total alcohol yield of 90 percent, mostly methanol.

I. REFERENCES

1.1 Berzelius, J., Jahres-Bericht Uber Die Forschritte Der Physischen Wissenschaften, Tubingen, 243 (1836).

1.2 Stinson, S.C., Chem. Eng. News, 27 (February 17, 1986).

1.3 Grasselli, R.K., and Suresh, D.D., J. Catalysis 25, 273(1972).

1.4 Burrington, J.D., Kartisek, C.T., and Grasselli, R.K., J. Catalysis 81, 489(1983).

1.5 Burrington, J.D., Kartisek, C.T., and Grasselli, R.K., J. Catalysis 87, 363(1984).

1.6 USP 3,893,951 and USP 3,929,899 to Standard Oil (Ohio), Grasselli, R.K. et al., 22 Feb. 1972 and 20 Dec, 1967.

1.7 USP 3,978,003 and USP 4,192,776 to Standard Oil (Ohio), Grasselli, R.K. et al., 31 Aug. 1976 and 11 Mar. 1980.

1.8 Hasenberg, D., and Schmidt, L.D., J. Catalysis 91, 116(1985).

1.9 DeLouise, L.A., and Winograd, N., Surf. Sci. 154(1), 79 (1985).

1.10 Poels, E.K., and Ponec, V., "Catalysis," Vol. 6, eds. Bond, G.C., and Webb, G., The Royal Soc. of Chem., London (1983).

1.11 Bartish, C.M., and Drissel, G.M., "Kirk-Othmer Encyclopedia of Chemical Technology," Vol. 4, p. 772, eds. Mark, H.F., et al., John Wiley and Sons, New York (1978).

1.12 Dry, M.E., "Catalysis," Vol. 1, eds. Anderson, J.R., and Boudart, M., Springer-Verlag, Berlin (1981).

1.13 Dry, M.E., Ind. Eng. Chem. Prod. Res. Dev. 15, 282 (1976).

1.14 Kung, H.H., Catal. Rev. Sci. Eng. 22(2), 235 (1980).

1.15 Klier, K., Advances in Catalysis, Vol. 31, 243 (1982).

1.16 Quarderer, G.J., and Cochran, G.A., European Patent Application:
    0119609 (September 1984), and references cited therein.

1.17 Murchison, C.B. and Murdick, D.A., Hydro. Proc. $\underline{1}$, 159(1981).

11
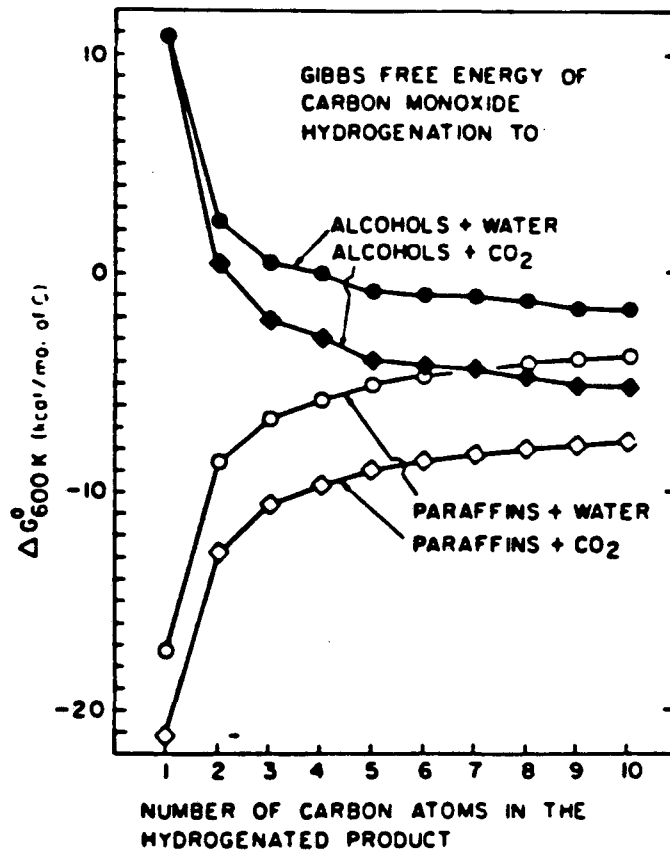
FIG. 11 Gibbs free energies ΔG at 600 K (kcal/mol of carbon) in the product alcohol or hydrocarbon of the reactions:

$$nCO + 2nH_2 \rightarrow CH_3(CH_2)_{n-1}OH + (n-1)H_2O \quad (\bullet)$$
$$(2n-1)CO + (n+1)H_2 \rightarrow CH_3(CH_2)_{n-1}OH + (n-1)CO_2 \quad (\blacklozenge)$$
$$nCO + (2n+1)H_2 \rightarrow CH_3(CH_2)_{n-2}CH_3 + nH_2O \quad (O)$$
$$2nCO + (n+1)H_2 \rightarrow CH_3(CH_2)_{n-2}CH_3 + nCO_2 \quad (\ )$$
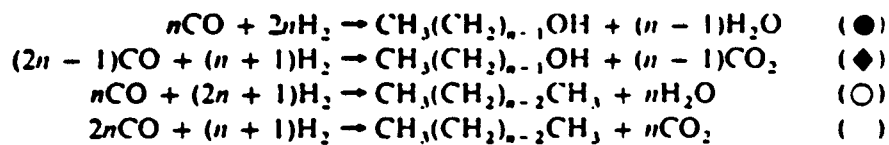
From D. R. Stull, E. F. Westrum, and G. C. Sinke, "The Chemical Thermodynamics of Organic Compounds," Wiley, New York, 1969. 1 cal = 4.184 J.

XBL 8610-4147

II. EXPERIMENTAL METHODS

A. OVERVIEW OF APPARATUS

1) Vacuum Chamber

The bulk of the experiments that comprise this work were performed in the ultrahigh vacuum (UHV) high pressure reactor system depicted schematically in Fig. 2.1.[1] The system and associated equipment are shown photographically in Figs. 2.2 and 2.3.

The system was pumped with a 6 inch Varian diffusion pump topped with an optically dense liquid nitrogen cooled cold trap. Optimal base pressure after baking was 1×10^{-10} Torr. The system was equipped with an LBL-built high pressure compatible sample holder-manipulator, a Physical Electronics (PHI) 15-2556 double pass cylindrical mirror (CMA) electron energy analyzer for use in both Auger Electron Spectroscopy (AES) and X-ray Photoemission Spectroscopy (XPS), a PHI 04-151 magnesium anode X-ray generator, a Varian 081-2043 argon ion sputter gun, and a UTI 100C mass spectrometer in its UHV application. The CMA and mass spectrometer were interfaced to a Commodore PET 256 K personal computer for use in data acquisition and analysis.

2) Sample Mounting

Single crystal or foil samples used in these experiments were mounted to the sample holder by spot welding as shown in Fig. 2.4. The sample holder consisted of 2 copper rods attached to the manipulator. The ends of the rods were drilled to allow the insertion of 1/8" tantalum rods attached by set screws. The sample was attached to these rods by spot welding two 20 mil wires, often tantalum, to the

tantalum rods and then spotwelding the other ends of the "support wires" to the sample. Thus resistive heating was possible by passing a current through the loop created by sample and holder. The geometry of the mounting system allowed 360° sample rotation. No z-motion was possible. No cooling of the sample was possible.

An appropriate thermocouple was spot welded to the top edge of the sample to allow temperature monitoring. The thermocouples used were chromel/alumel for Rh and Cu, Pt/Pt-Rh for Fe and Re, and W/W-Re for some of the Re experiments. The thermocouple was attached to a Eurotherm temperature controller via a feedback loop. This allowed the temperature to be raised at a reproducible rate of about 10°C/second to within ±0.5°C of the desired reaction temperature. This also served as the source of the heating ramp for TPD experiments.

3) High Pressure Reaction Cell

Figure 2.5 shows a picture of the high pressure reaction cell in the open position. The entire reaction loop consists of the pictured main cell inside the UHV chamber plus a network of 1/8" stainless steel tubing connecting the essential parts and forming a batch reactor. A schematic of this reactor is shown in Fig. 2.6.

Using this high pressure cell, the surface of the catalyst could be prepared in UHV and enclosed in the reaction cell without exposure to the atmosphere. In order to isolate the sample, the lower part of the cell was mechanically raised to position it against the top part of the cell which contained the sample holder. The UHV to high pressure isolation was accomplished via a knife edge that was ground

into the edges of the cell. These knife edges were pressed into a copper gasket with a backing pressure of about 2500 psig. The pressure inside the cell could be raised to 1 atm without the pressure in the chamber exceeding 1×10^{-8} Torr.

To initiate a reaction the sample was prepared and the cell closed. Immediately, gases were introduced into the cell and the micro-bellows circulation pump started. Liquid reactants were introduced via a septum that was changed weekly and which seemed to elicit no leaks. (Note – for an excellent tabulation of the equilibrium vapor pressures of many common chemicals, see Jordan[2].)

The reaction gases were monitored by a HP 5890 gas chromatograph. The gas sampling valve was equipped with a 0.10 ml sample loop. The carrier gases used were Ar or N_2, with no differences between the two noted in any of the experiments listed. In all cases, a flame ionization detector was used to analyze the gaseous mixtures. Individual product identification was made with GC/MS when necessary.

For the ammonolysis experiments a 6 foot long, 1/4 inch diameter glass column packed with 4 percent Carbowax 20M/0.8 percent KOH on 60/80 Carbopack B was used to separate gases. For the CO hydrogenation a 4 foot long 1/8 inch Chromosorb 102 stainless steel column was used.

A HP 3392A integrator interfaced to the HP 5890 gas chromatograph via a HP 19405 event control module allowed sampling to be done automatically at reproducible time intervals.

After a reaction the sample was cooled. After cooling, the reaction loop was evacuated by a mechanical pump and pumped down to about 20 microns. When the cell was reopened to UHV the pressure rose to about 5×10^{-7} Torr. The pressure in the main chamber returned to the 10^{-9} range in about 15 minutes following this pressure burst. For reactions using NH_3 this period was longer; about 1 hour in most instances. After returning to this low pressure, post reaction surface analysis was possible.

4) Gas Manifold

Gasses were introduced into the reaction loop for catalysis experiments or into the main chamber for UHV experiments via the gas manifold. A schematic of the manifold is included in Fig. 2.6.

The necessary cylinders of gases were connected to the manifold. These gases were connected via the appropriate traps to the entrance of the manifold. Liquid samples could also be connected via Cajon fittings to glass ampules. Pumping of the manifold was achieved by a mechanical pump and two molecule sieve sorption pumps. Pressures were monitored by several thermal conductivity gauges or by the appropriate Wallace and Tiernan gauges.

5) Associated Equipment

The system was also equipped with the following:

a. A G.E. light bulb, operated at 70 volts via a Variac transformer to bake out the system overnight.

b. A nude ion gauge for determining the pressure in the chamber.

c. Two leak valves for dosing into UHV from the gas manifold.

6) Materials

The materials used in all experiments are listed in Table 2.1 along with common impurities found in them.

7) High Pressure Autoclave for MoS$_2$ Studies

The experiments studying the MoS$_2$ catalyst were conducted in a different apparatus. This high pressure reactor is shown schematically in Fig. 2.7. This reactor allowed pressures of 2000 psi to be utilized.

The reactor consisted of a stainless steel autoclave with a total volume of about 300 ml. The inlet to this reactor was connected to a gas manifold to which CO, H$_2$, and Ar gas bottles were connected. A small 0.5 ml sample volume was used to take a sample from the high pressure region. This sample was then expanded to a larger region in order to lower the pressure. Following this a gas sample was extracted by a gas tight syringe via a septum. The gases were analyzed on a HP 5720A gas chromatograph with a flame ionization detector. The column was 6 ft long, 1/4 inch diameter stainless steel and was packed with Chromosorb 102. A HP 3391 integrator was used to determine peak area.

Each experiment was performed using about 0.1 gram of catalyst. After placing the catalyst in the autoclave it was flushed with Ar. A typical reaction consisted of heating the reactor to the desired temperature in about 10 atmospheres of Ar. The Ar was then evacuated and the H$_2$ and CO were introduced sequentially in the above order to initiate the reaction. The MoS$_2$ catalyst samples were exposed to air before post reaction analysis was possible.

B. SAMPLE PREPARATIONS

The first step in the preparation of the single crystal catalysts was cutting the appropriate single crystal rod along the desired crystallographic orientation to within ±0.5°. The conventional methods for this process are described in Yeates.[3]

Typical impurities in the Rh sample were C, B, and S. If B was present the surface was heated at 700°C for 15 minutes in 5×10^{-7} Torr O_2. This converted the B to an oxide which was then removed by ion sputtering. The O_2 treatment also removed any C present, without the need of sputtering. S was removed by sputtering at 700°C. The surfaces were then annealled at 900 - 1000°C. Typically a Rh crystal needed several cycles of sputtering to remove bulk B and S when initially put in vacuum. Some of the crystals used were pretreated by baking in 1 atm of H_2 for several days at 700°C before use. This substantially lowered the amount of B present in the sample.

The Cu single crystals used contained Cl, S, and C as their principle impurities. Again O_2 treatment, this time at 5×10^{-7} Torr and 500°C, was used to remove C. Cl and S were removed by argon ion sputtering. These crystals were annealed at 650°C.

Both Rh and Cu are face centered cubic metals. The crystal faces used were the hexagonally close-packed (111) for both metals, and in addition, the (331) stepped surface for Rh. These two surfaces are shown in Fig. 2.8. The (331) surface has close packed terraces 3 atoms wide with 1 atom high (111) steps. The orientation of these

surfaces was verified by back reflection Lauie X-ray diffraction and LEED prior to introduction into the UHV chamber.

The iron foil was initially cleaned by baking it in 1 atmosphere of hydrogen (to help remove bulk S and C), then by repeated sputtering in 10^{-5} Torr Argon while heat cycling between 400 and 800°C. The rhenium foil sample was cleaned by heating the sample to 1000°C in 5 x 10^{-7} Torr oxygen for several minutes, followed by argon ion sputtering at 900°C with intermittent annealing to 1300°C. To finish the cleaning both the Re and the Fe samples were argon ion sputtered at room temperature for 5 minutes then flashed to 1300°C and 650°C respectively.

For samples that were dosed with alkali an appropriate alkali SAES getter source was used to dose the surface. Water was introduced at 5 x 10^{-7} Torr to oxidize both the samples and the alkali adlayers as necessary. The alkali was readily oxidized at ambient temperature. It was necessary to heat the clean rhenium and iron samples at 800-900°C and 400-500°C respectively to enhance the rate of low pressure oxidation. Oxidation could also be achieved by introducing water into the reaction cell before or during the reaction.

The MoS_2 used in MeOH synthesis experiments, was prepared by thermally decomposing $(NH_4)_2MoS_4$ obtained from Alfa Chemical Co. in a tube furnace with flowing nitrogen at 350°C for three hours. The following reaction occurs under these conditions:

$$(NH_4)_2MoS_4 \xrightarrow{350°C, N_2} MoS_2 + (NH_4)_2S + 1/2\ S_2$$
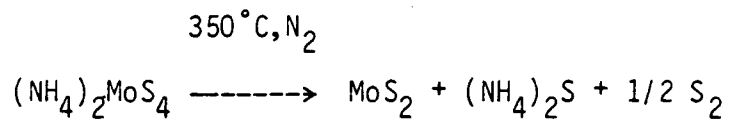
Promoted MoS_2 catalysts were prepared by impregnating MoS_2 with a 0.2% K_2CO_3 solution and drying at 110°-120°C for several hours. The catalysts were then ground before using. More information about the characterization of these catalysts is shown in Chapter 6.

Note – For an excellent review of the procedures used to clean metals in UHV see reference 4.

C. SURFACE ANALYSIS TECHNIQUES

1) Surface Analysis Technique

The most commonly used surface analysis technique in these studies was Auger Electron Spectroscopy (AES). AES was used to monitor the composition of the overlayer resulting from a catalytic reaction or a UHV dose of a gas. In addition it served as a useful tool to monitor the surface cleanliness. (For several reviews see references 5-9. Note also various electron spectroscopy reviews referenced in XPS section.) AES is an electron in electron out spectroscopy. A 2000 eV electron beam from an electron gun is focused on the sample. This electron beam provides the initial step in the Auger experiment where an inner shell electron is ejected from an atom near the surface. This excitation can also be accomplished by allowing X-rays to impinge on the surface. Once this atom has been ionized, there are two modes possible for the subsequent relaxation process. These processes are Auger electron emission and X-ray fluorescence. In the X-ray process an electron from a higher energy level fills the core hole with the accompanying emission of a photon. In the Auger process, depicted schematically in Fig. 2.9, an electron from a higher level relaxes to fill the core vacancy also; but in a radiationless process the energy is transferred to another outer shell electron which is ejected from the sample with an amount of kinetic energy characteristic of the atom involved. This emitted electron is the Auger electron.

The relative amounts of these two competing relaxation processes varies with atomic number. This trend is illustrated in Fig. 2.10.

The energy of the emitted Auger electron is given by the equation

$$E(x,y,z) = E(x) - E(y) - E(z) - \phi_a$$

where $E(x)$ is the binding energy of the primary core electron, $E(y)$ is the binding energy of the electron which fills the core hole, $E(z)$ is the binding energy of the emitted Auger electron moving in a field of increased charge, and ϕ_a is the work function of the analyzer relative to the metal.

The system of nomenclature describing this Auger process is noted in Fig. 2.9. The convention is that electrons originating in the 1s shell are labeled K, the 2s are L_I, the 2p are L_{II} and L_{III}, and so on. Valence shell electrons are labelled as V. To describe an Auger transition a series of 3 letters are strung together as xyz to describe: x, the core hole electron; y, the hole generated by the core hole being filled; and z the hole generated by the emitted electron. Thus the Auger transition described in Fig. 2.9 is a K L_I L_{III} transition where $x = K$, $y = L_I$ and $z = L_{III}$.

The Auger electron energies were analyzed by using the CMA in its Auger mode. A schematic of this analyzer operating in AES mode is shown in Fig. 2.11. For complete discussion of the details of the electron energy analysis by a CMA see Ref. 2.10. In brief, in the AES mode, the analyzer is used with the inner cylinder at ground and the outer cylinder ramped from the initial voltage to the desired final one. The energy difference between the inner and outer cylinders determines the pass energy of the electron (the amount of energy an electron must have to move through the analyzer and pass out the exit

slit to be multiplied by the channeltron and thereby registered on the spectrum). Thus, in Auger mode the pass energy is constantly varying as the voltage difference between the two cylinders is varied. As the resolution is a function of the pass energy, this results in a constantly changing resolution. This is not generally a problem for the purposes of AES due to the relatively low resolution necessary for a typical study.

The surface sensitivity of AES arises from the limit of the mean free path for the emitted Auger electron. Figure 2.12 shows the "universal curve" for the mean free path of an electron in a solid as a function of kinetic energy. This mean free path, the distance at which the electron is inelastically scattered, is a minimum in the 40 to 100 eV range. Note that typical Auger energies are in the 50-1000 eV range. This corresponds to a sampling depth of a minimum of 6 Å or about 2 atomic layers at 50 eV varying to a maximum of about 18 to 20 Å or 6 atomic layers at 1000 eV.

Figure 2.13 shows the relative cross sections for the various possible Auger transitions, plotted vs. atomic number. This gives a rough estimate of the actual atomic ratio indicated by comparing two AES peaks from different elements. Note for example that S is one of the elements with the highest sensitivity. In contrast Na is only about 30 percent as sensitive. Thus a S peak 3 times larger than a comparable Na peak translates to roughly the same number of atoms of each sampled.

A sample AES spectrum is shown in Fig. 2.14. In it we see peaks due to a Rh substrate covered with carbon, nitrogen and oxygen. Note that if one uses an intense metal peak as a reference, relative coverages of other adsorbates can be obtained by taking peak height ratios if relative Auger intensity calibrations are known. A good source for these values is found in reference 2.11 which is the source of Fig. 2.13. In addition, Ref. 2.12 provides a tabulation of calculated Auger transition energies and intensities for most elements.

2) <u>Temperature Programmed Desorption (TPD)</u>

Thermal Programmed Desorption was one of the most used techniques in this work. The experiment is simple in concept: a surface which has an adsorbate layer bound to it is heated at a constant rate; as the surface heats up the adsorbates desorb; this desorption is monitored in a mass spectrometer. This process generates a plot, for each (m/e) unit monitored, of intensity vs. temperature. From a study of the desorption products observed the nature of the adsorption state can be inferred. In addition it is possible to learn about the energetics of the bonding in the system, the chemical reactions of the bonding in the system, the chemical reactions happening on the surface and the interactions between adsorbates. Specifically, it is possible to determine the kinetic desorption order, the activation energy, the pre-exponential factor of the desorption rate, the number and relative concentrations of different binding sites, the products and mechanism for decomposition reactions and the strength of lateral interactions.

To briefly outline the idea behind these calculations note that kinetic information is obtained from an Arrhenius form of the desorption rate (Rd).

$$Rd = \frac{d\sigma}{dt} = \nu_n \sigma^n \exp(-\frac{E_d}{RT})$$

where σ is the surface coverage, n is the desorption order, ν_n is the pre-exponential factor, E_d is the activation energy of desorption, and T is the desorption temperature. If the assumption is made that ν_n and E_d are independent of σ and time t, then E_d and ν_n can be determined as shown by Redhead[15] for first and second order desorption using

$$E_d/RT_p^2 = (\nu_1/\beta) \exp [-E_d/RT_p]$$

where T_p is the temperature of the desorption maximum, β is the heating rate, and ν_1 is the first order pre-exponential factor. Thus we can see that for a first order desorption, this model predicts no coverage dependence for T_p. For a second order process this changes to

$$E_d/RT_p^2 = (\nu_2 \theta_0/\beta) \exp (-E_d/RT_p)$$

where ν_2 is now the second order pre-exponential factor and θ_0 is the initial coverage. Thus in a second order desorption T_p is dependent on the initial coverage. That is, T_p should decrease with increasing θ_0. Traditionally the pre-exponential factors ν_1 and ν_2 are taken as 10^{13} sec^{-1} and 10^{-2} cm^{2}sec^{-1} respectively. These approximations allow the estimation of E_d. For a detailed analysis of the extraction of

quantitative information from TPD spectra, information that was not used in this work, there are several excellent reviews listed in refs. 13-20.

The principle use of TPD in this work was to identify the desorbing species and their concentrations. A typical example of this technique as applied to this work is the case of H_2 desorbing from a catalyst after a reaction. Identification of the (m/e)= 2 fragment is obvious, and it is straightforward to integrate the amount desorbing for comparison with other cases. In addition it is learned that as the H_2 desorbs between 450-650K it is not desorbing from the metal surface. This can be stated due to the fact that previous experiments have shown that H_2 desorbs from Rh at about 300K. In this case the H_2 comes from decomposition of fragments on the surface.

3) X-ray Photoelectron Spectroscopy (XPS or ESCA)

X-ray photoelectron spectroscopy was used in this work for the Rh, Re, and the MoS_2 experiments. It's primary use in these experiments was to verify the oxidation state of the catalyst surfaces. XPS is a useful tool that has been the subject of many reviews. Several are listed in references 21-27.

In photoelectron spectroscopy a photon beam (ultra violet for UPS, X-ray for XPS) is directed at a sample. These beams causes the photoejection of electrons from the sample. These photoelectrons are ejected directly from filled core electronic states. To quantify this relationship we can write this process as a simple conservation of

total energy or

$$E_B = h\nu - E_k - \phi_s$$

where E_B is the binding energy of the ejected electron, $h\nu$ is the energy of the incident X-ray photon, E_k is the kinetic energy, and ϕ_s is the work function of the spectrometer relative to the sample. Note that $h\nu$ is known, ϕ_s is measurable, E_k is measured, thus E_B can be determined in a straightforward fashion to a first order approximation. However this is only true in a very uniform sample. Any mixture of signals from levels of slightly altered binding energy complicates matters considerably.

The X-ray sources used are generally the MgKα (1253.6 eV) or AlKα (1486.6 eV) lines. In this work MgKα was used. In general these X-ray sources are not monochromatic and as such have a linewidth of sufficient width to hamper the entire resolution of the technique (0.7 eV for Mg, 0.85 eV (FWHM) for Al). Monochromatic x-ray sources are becoming more common, and with the increasing availability of synchrotron radiation many high resolution photoemission techniques are being rapidly developed. However, the unmonochromatized sources are sufficient for the purpose of low resolution study.

Figure 2.15 shows a schematic diagram of the CMA while in XPS mode. In this mode the instrument resolution stays constant. The resolution of the spectrometer is governed by the relationship

$$\Delta E/E_p = C$$

where ΔE is the resolution, E_p is the pass energy of the spectrometer and C is an instrumental constant. Thus E_p becomes the parameter used to adjust the resolution. E_p is determined by the potential difference between the inner and outer cylinders in the CMA. As mentioned previously, this is constantly changing for AES resulting in the varying resolution. In XPS mode this pass energy term is kept constant by setting the potential difference between the cylinders to a given constant value and ramping a potential grid in the front of the spectrometer to determine at what energy electrons will enter the spectrometer. Note that the high resolution requires low pass energy. This results in a significant reduction in signal. Thus, a highly resolved spectrum may require 3 to 4 hours of scanning time.

The principle use of XPS in these experiments was to determine the chemical or oxidation state of the catalysts' used. This is done by looking for a chemical shift in the binding energy of a core electron. The chemical shift arises from a shift in binding energy caused by changes in the screening of core electrons by valence electrons. Thus in a higher oxidation state valence electrons are withdrawn from an atom and core electrons are held more tightly. For a detailed description of the physical basis of chemical shifts see the mentioned reviews.

XPS was used relatively little in this work, due primarily to unsolvable instrumental difficulties. Due to the limits of the reliability of my spectrometer, obtaining spectra of overlayers was diffi-

cult. As a result the spectra shown are all of the catalyst rather than the adsorbate layer on top of it.

The spectra of Rh and Re displayed as examples in this section are the only Re and Rh spectra included in this work. This is due to the fact that any XPS spectra taken of these metals after a reaction did not show any change in the catalysts oxidation state. This information is in itself important and as such is listed here. No XPS studies were done on the Cu or Fe catalysts, again due to instrumental failure. The spectra shown of MoS_2 in Chapter 6 were taken to insure that the MoS_2 we prepared exhibited the same chemical shifts as the commercially prepared MoS_2. In all cases the metal peaks and/or a convenient C 1s peak were used for spectrometer calibration. Gold foil was occasionally used to double check this standard.

Figures 2.16 and 2.17 show the type of spectra obtained. Figure 2.16 is a full width scan of Re. This spectra shows all the transitions resulting from a variety of core level emissions. This type of scan can also be used in addition to AES to monitor surface cleanliness. This spectrum was taken at pass energy of 200 eV. Figure 2.17 shows a close-up scan of the Rh 3d peaks. This spectrum, taken at a pass energy of 25 eV, is of sufficient resolution to detect any "chemical shifts" that might occur on or near the Rh surface. Reference 28 provides an excellent compilation of reference spectra for comparison.

D. METHODS FOR DETERMINING INITIAL RATES OF REACTION

The determination of the rate of reaction for reactions occurring on single crystal or polycrystalline foil catalysts is an inexact art. The problem lies in the definition of rate. The most commonly used rate expression in these works, and others similar to it, is that of turnover frequency. This is defined as product molecules produced per surface site per second. The problem occurs in determining the number of surface sites.

In virtually no instance has any sort of actual catalytic system been described so completely as to identify the actual number of catalytically active sites present on a working catalyst. This would require the knowledge of both the site geometry required for each step in the catalytic pathway and the number of these sites actually available to reactant molecules at any given time.

Given that exact determination of these parameters is not possible at present, any attempt at this time to report a turnover frequency using an "actual" number of sites has some inherent error. Thus, as we need numbers to compare rates with, we assign each surface atom present on the ideal catalyst surface as a catalytic "site." This becomes our basis for "site" calculations.

Thus, initial rates were determined by determining the volume of the reactor loop, the volume of the sampling volume, the G.C. calibration factor in molecules/count and the number of surface atoms.

Initial rates were

$$r = \frac{molecules}{site \cdot sec} = \frac{G.C.\ counts}{sampling\ volume} \times \frac{Molecules}{G.C.\ count}$$

$$\times\ Total\ Volume\ Reactor \times \frac{1}{seconds} \times \frac{1}{sites} \qquad .$$

Typical values for the gas chromatographic flame ionization detector sensitivity were in the 5 x 10^8 molecules/count range. Initial rates were typically measured at less than 3% conversion, and in no cases did conversion exceed 10%.

II. REFERENCES

2.1   Cabrera, A.L., Spencer, N.D., Kozak, E., Davies, D.W., and Somorjai, G.A., Rev. Sci. Instrum. 53(12), 1893 (1982).

2.2   Jordan, Ph. D. Thesis, Vapor Pressure of Org. Compounds, Film 16727 QC chem.

2.3   Yeates, R.C., Ph.D. thesis, Univ. of California, Berkeley, 1985.

2.4   Musket, R.G., McLean, W., Colmenares, C.A., Makowiecki, D.M., and Siekhaus, W.J., Appl. Surf. Science 10, 143 (1982).

2.5   Ertl, G., and Kuppers, J., "Low-Energy Electrons and Surface Chemistry," Verlag Chemie, Weinheim (1979).

2.6   Kane, P.F. and Larrabee, G.B., "Characterization of Solid Surfaces," Plenum Press, New York, Chapt. 20 (1974).

2.7   Alford, N.A., Barrie, A., Drummond, I.W., and Herd, Q.C., Surface and Interface Analysis, Vol. 1, No. 1, 36 (1979).

2.8   Seah, M.P., Surface and Interface Analysis Vol. 1, No. 3, 91 (1979).

2.9   Rye, R.R., Houston, J.E., Jennison, D.R., Madey, T.E., and Holloway, P.H., Ind. Eng. Chem. Prod. Res. Dev., Vol. 18(1) (1979).

2.10 Phi Manual for 15-255G Double Pass Cyclindrical Mirror Analyzer.

2.11 Palmberg, P.N., Riach, G.E., Weber, R.E., and MacDonald, N.C., "Handbook of Auger Electron Spectroscopy," Physical Electronics Ind., Minnesota (1972).

2.12 Coghlan, W.A., and Clausing, R.E., "A Catalog of Calculated Auger Transitions for the Elements," Oak Ridge National Laboratory, ORNL-TM-3576, November 1971.

2.13 Gasser, R.P.H., "An Introduction to Chemisorption and Catalysis by Metals," Clarendon Press, Oxford, Chapt. 3 (1985).

2.14 Somorjai, G.A., "Chemistry in Two Dimensions: Surfaces," Cornell Univ. Press (1981).

2.15 Redhead, P.A., Vacuum 12, 203 (1962).

2.16 King, D.A., "Chem. and Phys. of Solid Surf. II," CRC Press (1979).

2.17 Ertl, G., and Rhodin, T.N., eds., "The Nature of the Surface Chemical Bond," North-Holland, Oxford, Chapter 5 (1979).

2.18 Peterman, L.A., Prog. Surf. Science 3, 1 (1972).

2.19 Tompkins, F.C., "Chemisorption of Gases on Metals," Academic Press, London (1978).

2.20 Roberts, M.W., and McKee, C.S., "Chemistry of the Gas-Metal Interface," Oxford Univ. Press (1978).

2.21 Rhodin, T.N. Ertl, G., eds., "The Nature of the Surface Chemical Bond," Chapter 3, North-Holland Publishing Co., New York (1979).

2.22 Hercules, S.H., and Hercules, D.M., Record of Chemical Progress 32 No. 4, 183 (1971).

2.23 Delgass, A.N., Hughes, T.R., and Fadlsy, C.S., Catalysis Reviews 4(2), 179 (1970).

2.24 Carley, A.F. and Joyner, R.W., Journal of Electron Spectroscopy and Related Phenomena 16, 1 (1979).

2.25 Briggs, D. and Seah, M.P., eds., "Practical Surface Analysis," John Wiley and Sons, 1983, Chapter 3 and Appendices.

2.26 Ertl, G. and Kuppers, J., "Low Energy Electrons and Surface Chemistry," Verlag Chemie, Chapter 4 (1979).

2.27 Ibach, H. ed., "Electron Spectroscopy for Surface Analysis," Springer-Verlag, Chapter 5 (1977).

2.28 Wagner, C.D., Riggs, W.M., Davis, L.E., Moulder, J.F., and Muilenberg, G.E., "Handbook of X-ray Photoelectron Spectroscopy," Perkin-Elmer Corp., Minnesota (1978).

Table 2.1

Materials used in this work

Reagent	Supplier	Impurities
H_2	Matheson	ND
CO	Matheson	Iron carbonyls
N_2	Liquid Carbonic	ND
O_2	Matheson	CO
Ar	Liquid Carbonic	CH_4, CO_2
Na	SAES getter	ND
NH_3	Matheson	H_2O
n-butanol	MCB	ND
n-butanal	MCB	ND
butylamine	Aldrich	ND
butyronitrile	MCB	ND

Note – Impurities were identified by a variety of methods including GC, GC/MS, MS, and AES resulting from adsorption of impurities on the samples used. ND – no impurities detected.

FIGURE CAPTIONS

Fig. 2.1 Schematic diagram of combined ultra high vacuum – high pressure catalysis chamber used for study of model catalysts.

Fig. 2.2 Picture of UHV chamber used in this work.

Fig. 2.3 Picture of chamber with associated instruments and electronics.

Fig. 2.4 Schematic diagram of sample and holder-manipulator.

Fig. 2.5 Picture of high pressure cell in open position.

Fig. 2.6 Schematic diagram of high pressure reactor. Included are the circulation path for this batch reactor and the gas manifold. The abbreviations represent: CP – circulation pump, SV – sampling valve, MC – main chamber, GC – gas chromotograph, PG – pressure gas, RP – rotary vacuum pump, ECM – event control module, INT – integration, S – septum.

Fig. 2.7 Schematic diagram of high pressure autoclave. The abbreviations represent: ST – belt driven stirrer, SV – sampling volume, ER – expansion reservior, S – septum, RP – rotary mechanical pump, CH – catalyst holder.

Fig. 2.8 Drawings of the two single crystal surfaces used in this work. These are the face centered cubic (111) and (331) surfaces.

Fig. 2.9 An energy level scheme for the Auger electron emission process.

HIGH PRESSURE / LOW PRESSURE CHAMBER
FOR CATALYST SURFACE STUDIES
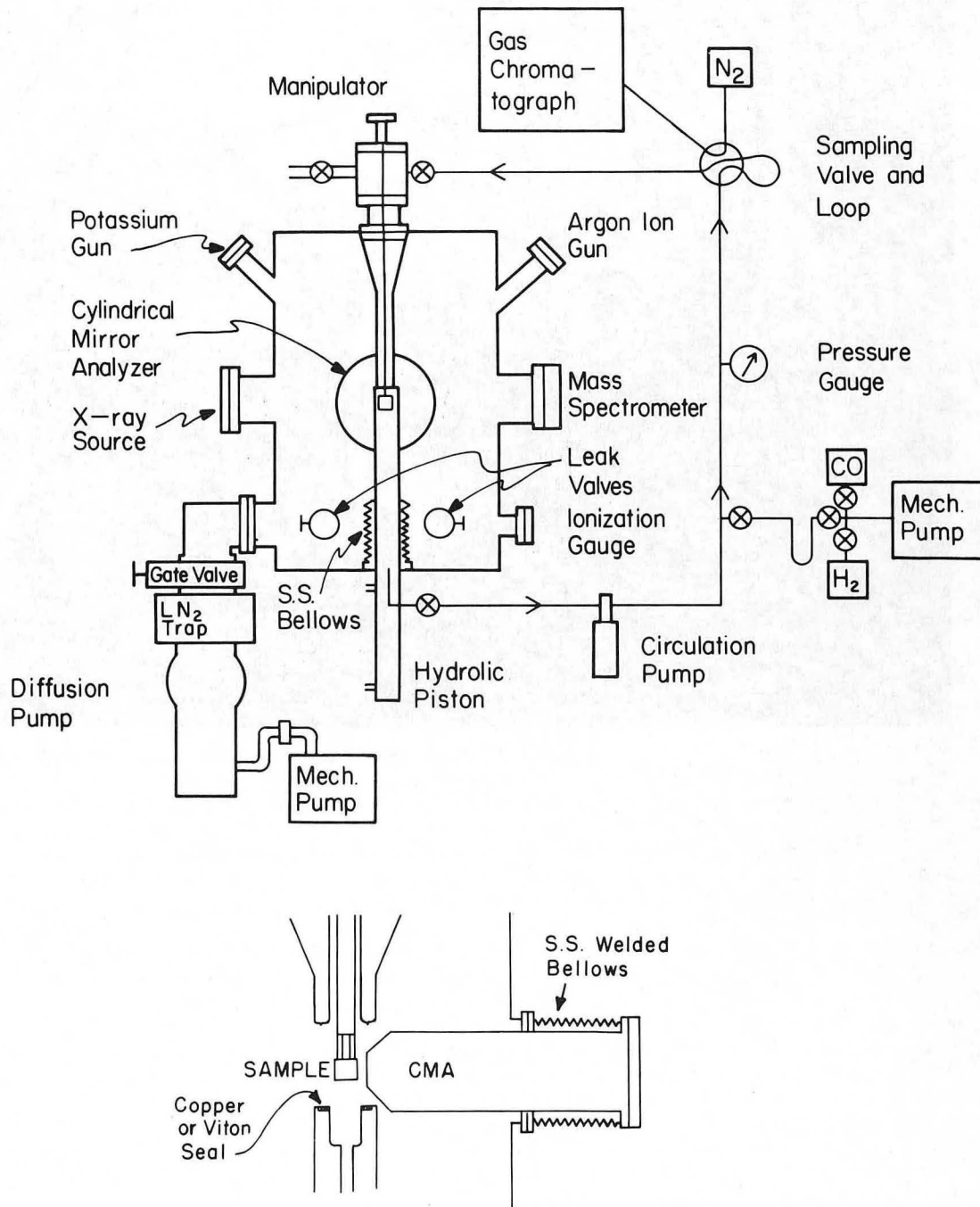
SIDE VIEW WITH HIGH PRESSURE CELL OPEN

XBL 832-8401

Fig. 2.1
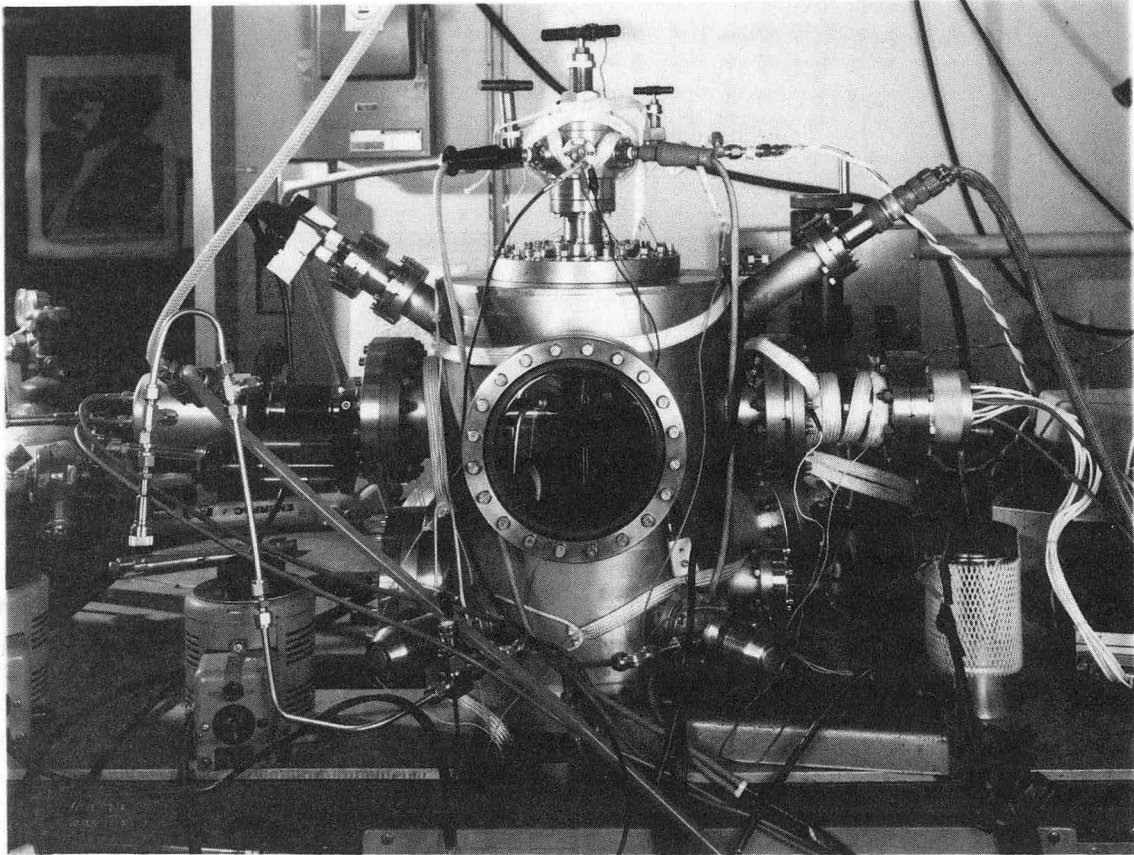
CBB 869-7285

Fig. 2.2
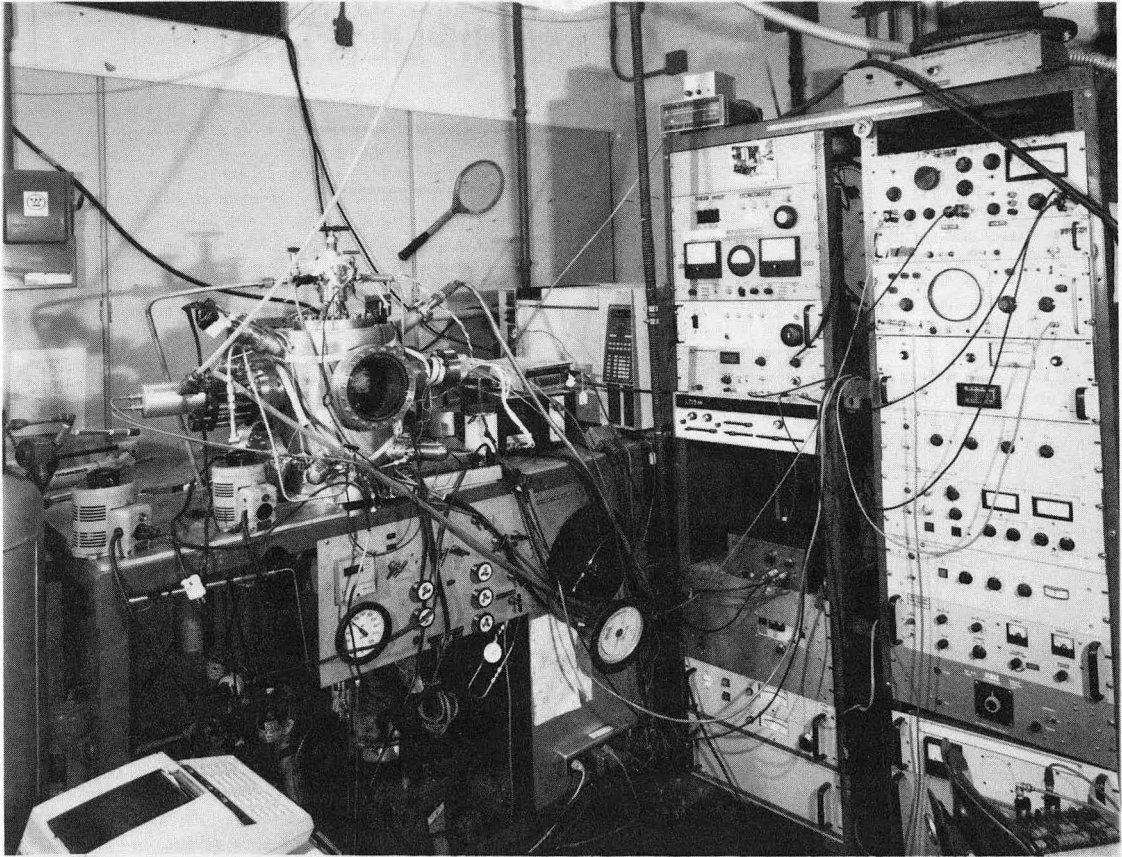
CBB 869-7283

Fig. 2.3

SCHEMATIC DIAGRAM OF SAMPLE
AND MANIPULATOR
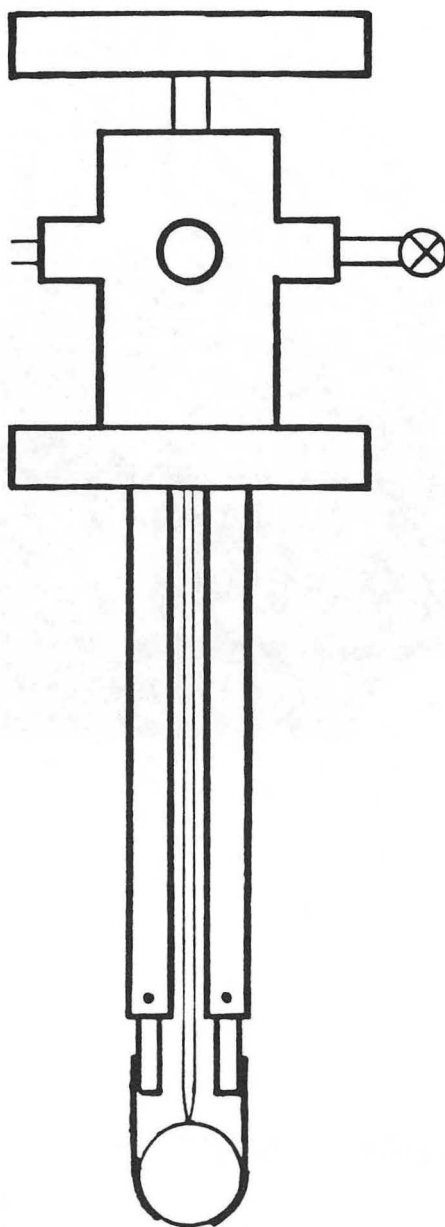
XBL 8610-4146

Fig. 2.4
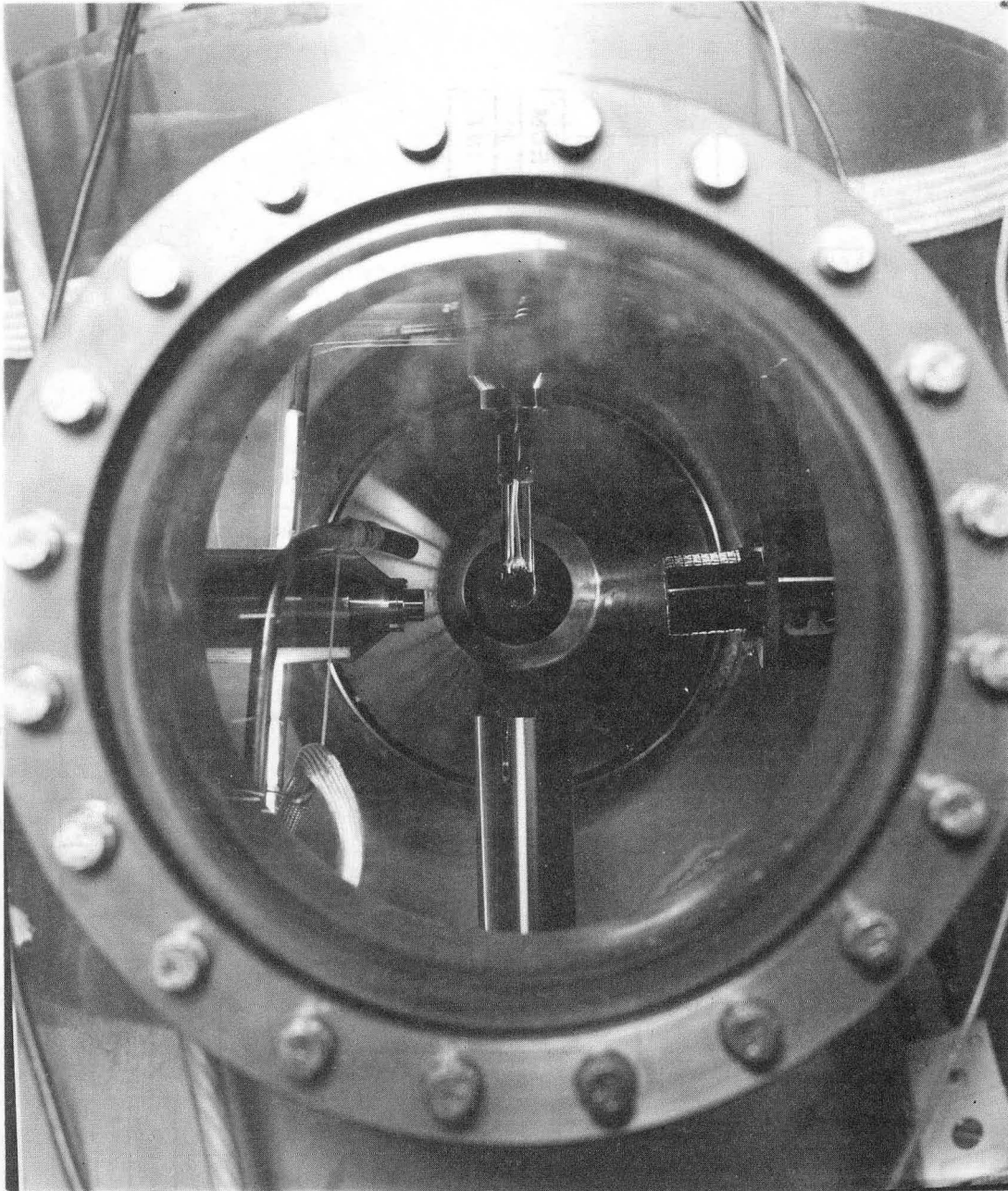
CBB 869-7291

Fig. 2.5

SCHEMATIC DIAGRAM OF REACTION LOOP
AND GAS MANIFOLD
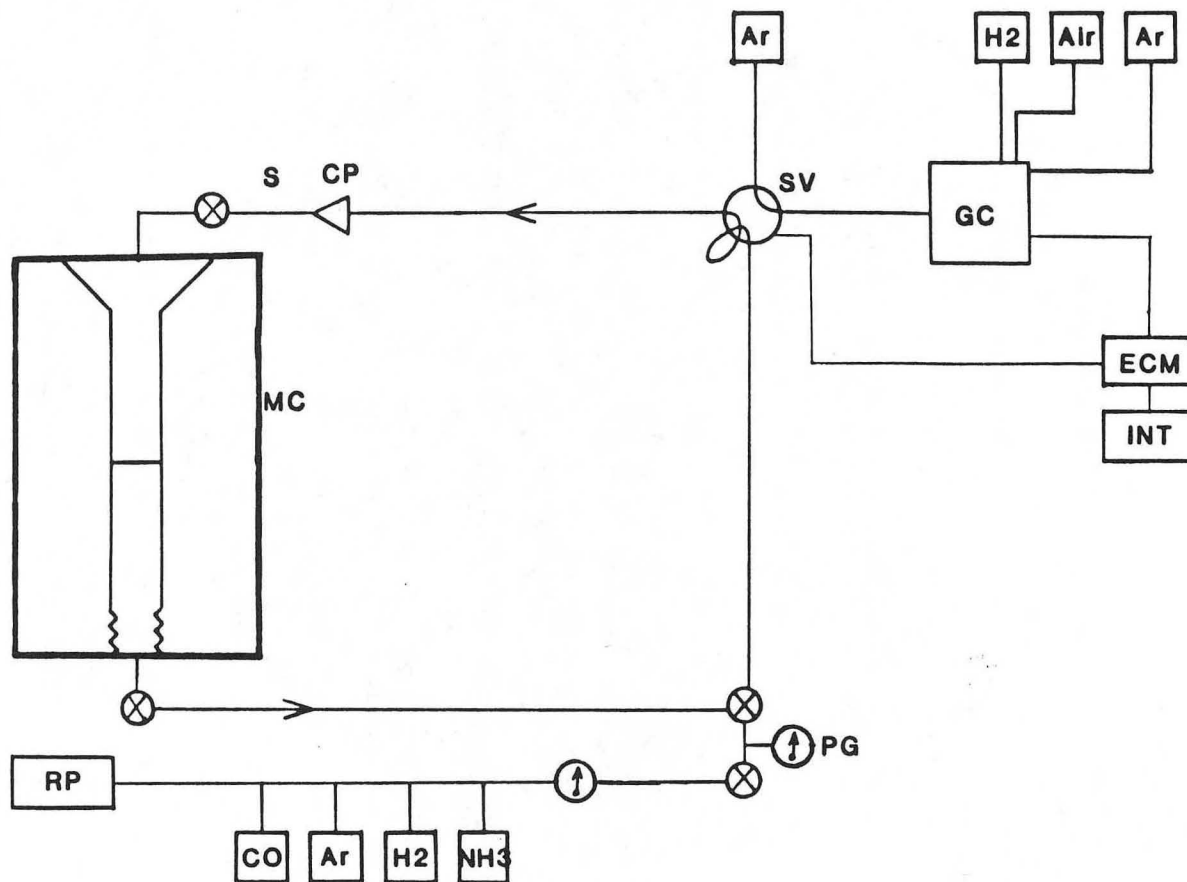
Fig. 2.6

XBL 8610-4145

SCHEMATIC DIAGRAM OF HIGH PRESSURE AUTOCLAVE
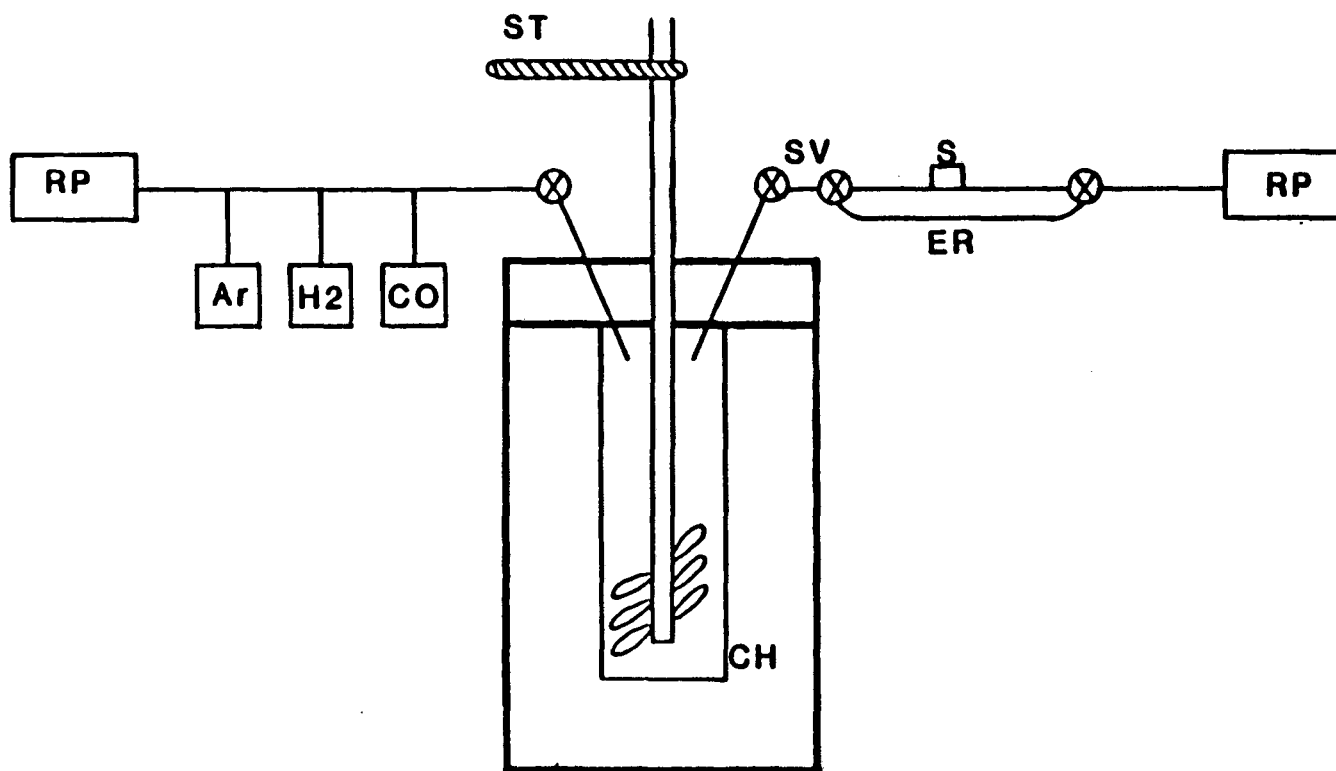
Fig. 2.7

XBL 8610-4144

FACE CENTERED CUBIC SURFACES USED

fcc (III)
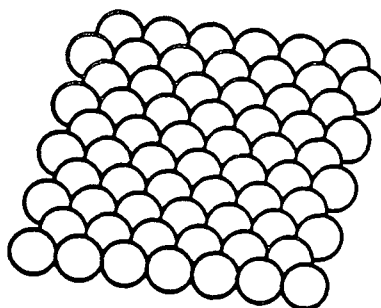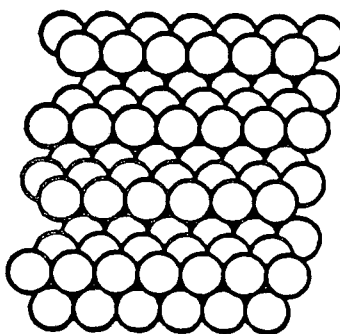
fcc (331)

Fig. 2.8

AUGER ELECTRON EMISSION

(a) EXCITATION   (b) ELECTRON EMISSION
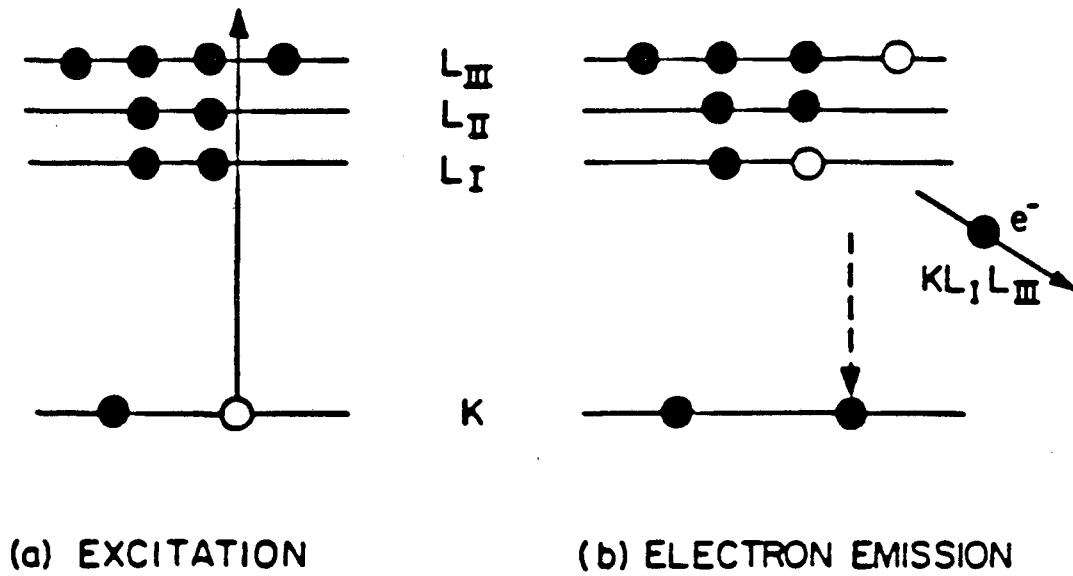
Fig. 2.9   XBL 8610-4143

AUGER ELECTRON EMISSION AND X-RAY FLUORESCENCE YIELDS vs. ATOMIC NUMBER
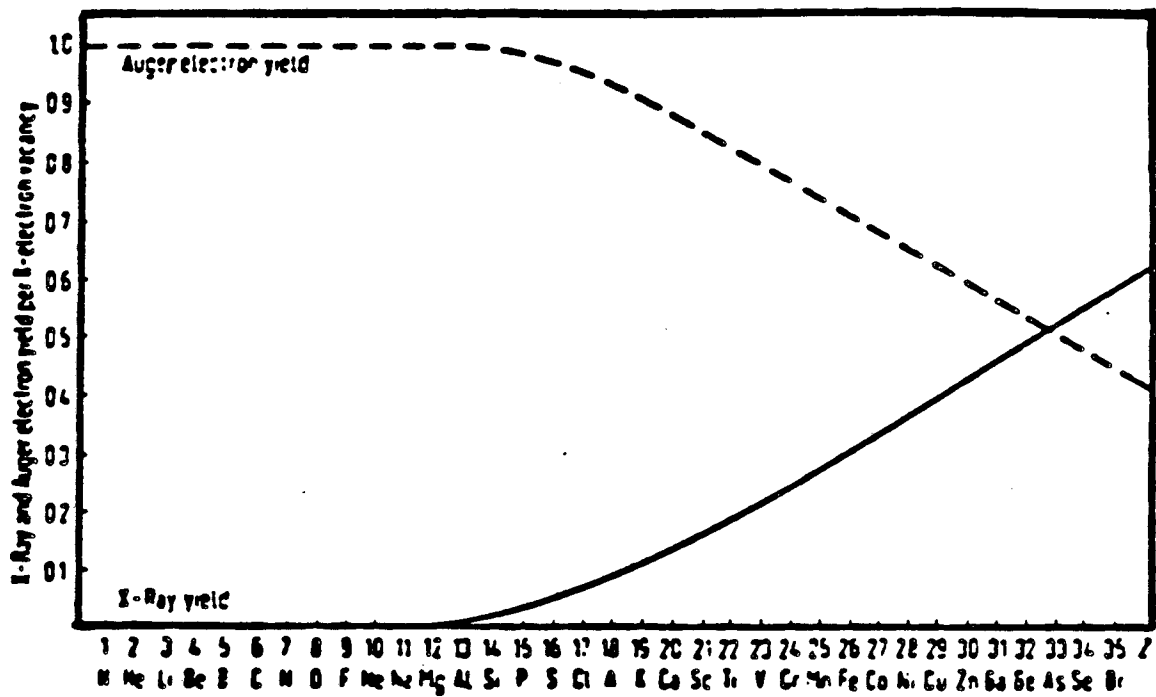
Fig. 2.10   XBL 8610-4142

$$1.70 \times V_6 = \text{ELECTRON ENERGY}$$
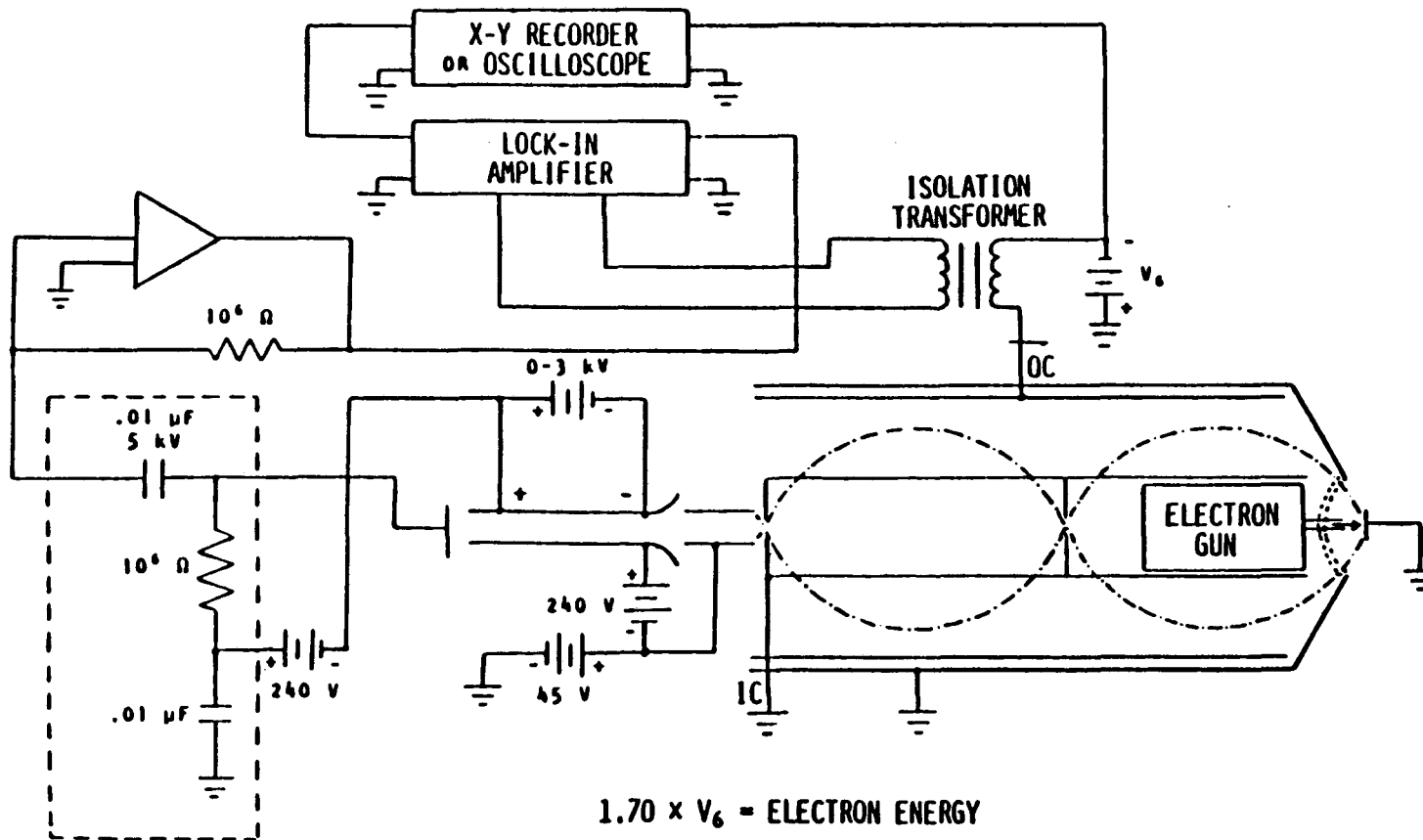
Block diagram of circuitry typically used when in Auger
mode of operation.

Fig. 2.11   XBL 8611-4508

"UNIVERSAL CURVE" FOR ELECTRON MEAN FREE PATH
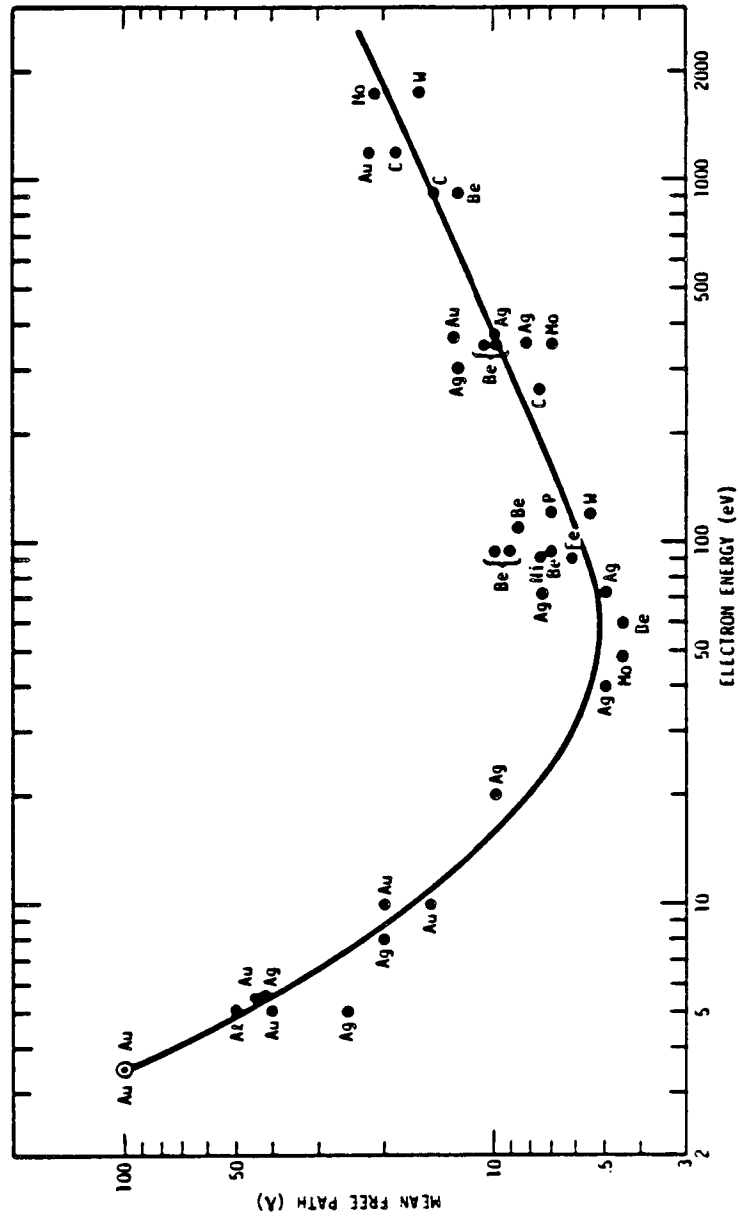
Fig. 2.12

XBL 8610-4141
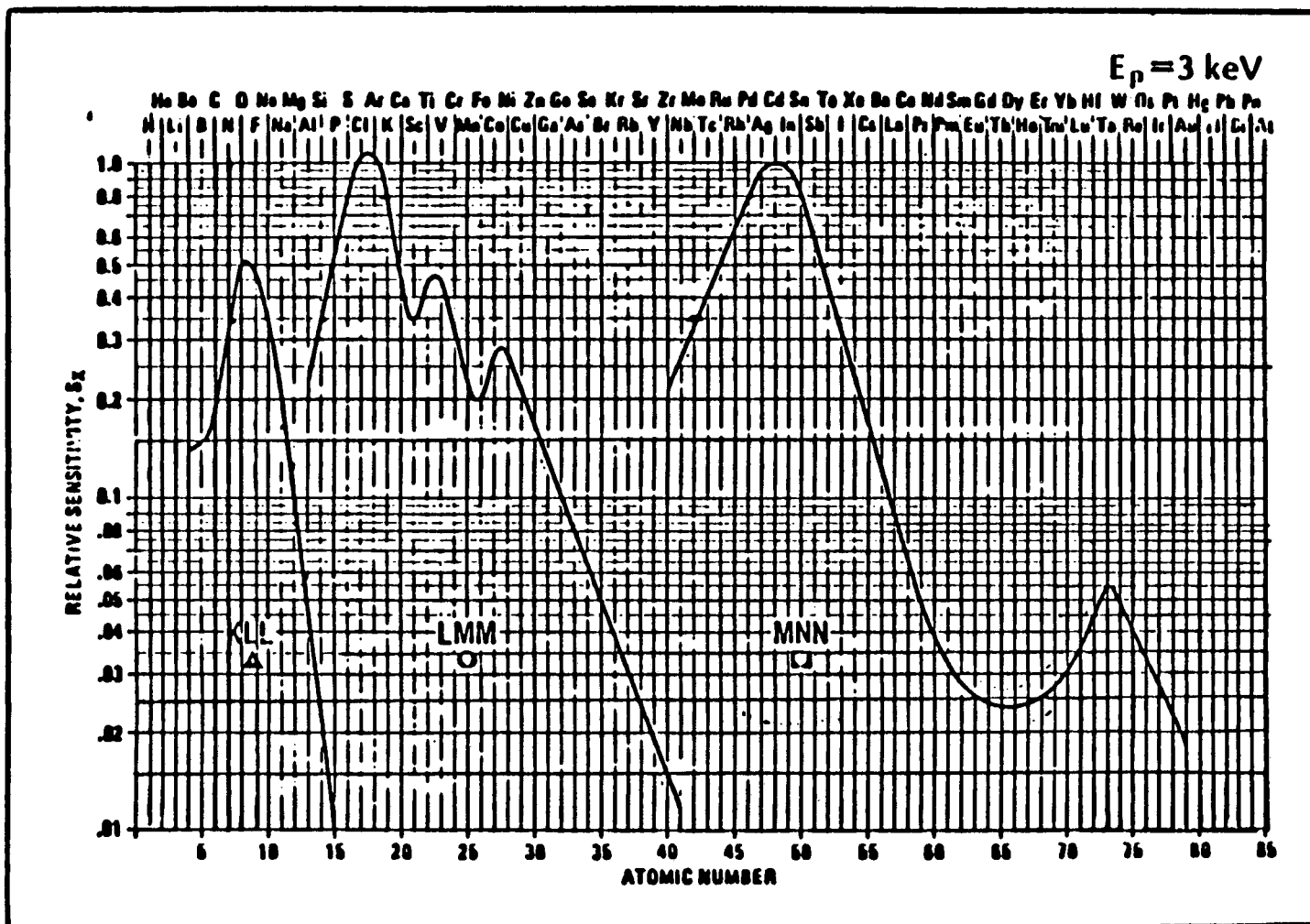
Fig. 2.13

XBL 8610-4140

EXAMPLE AES SPECTRUM
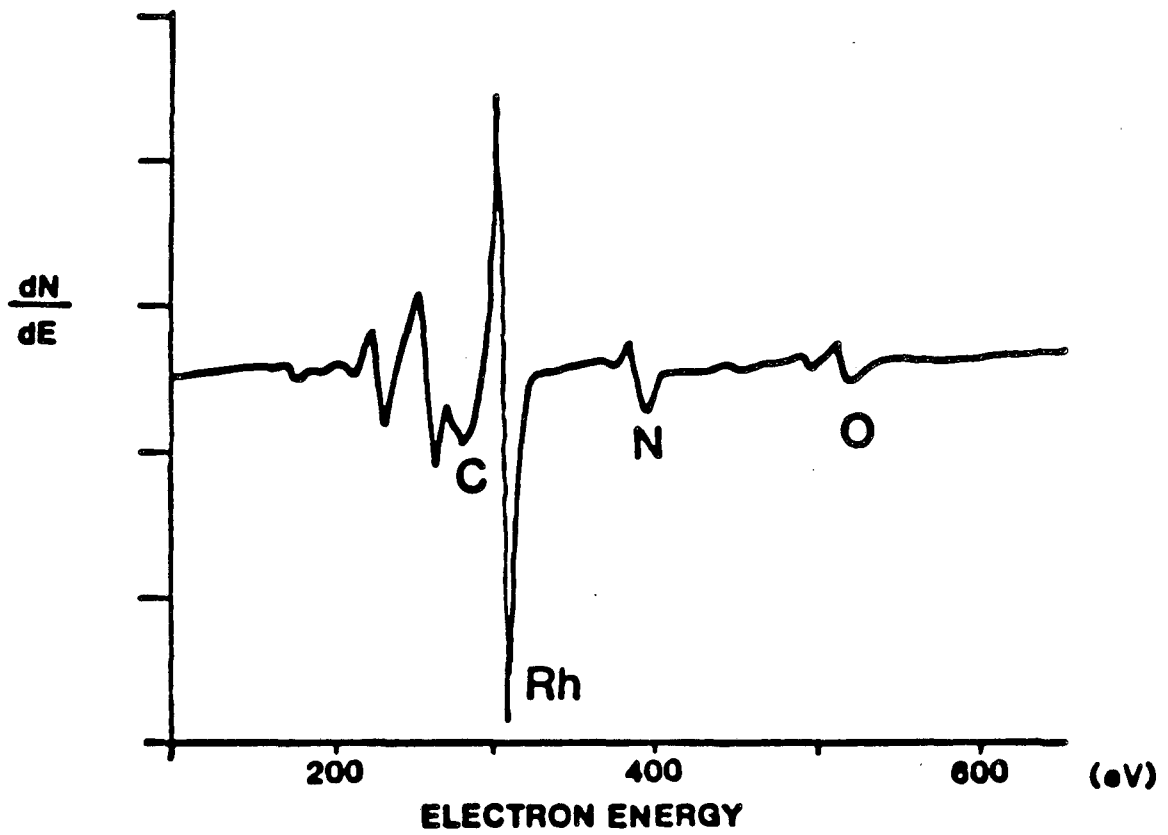
Fig. 2.14   XBL 8611-4507

Double Pass Cylindrical Mirror Analyzer
Retarding Pulse Counting Mode

$V_5 = 1.706 \times V_4 =$ Pass Energy

$eV_6 =$ Electron Energy
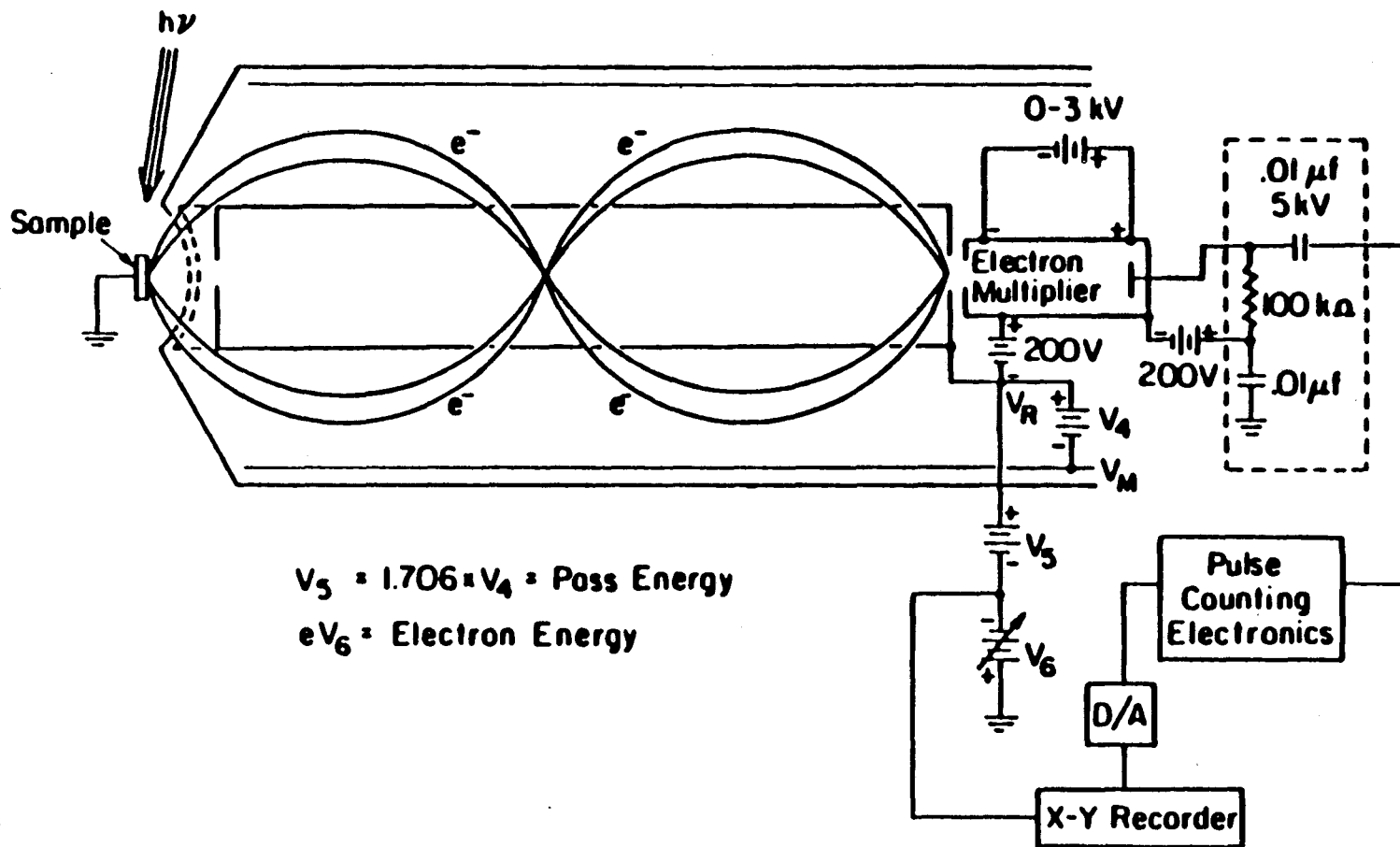
Fig. 2.15

XBL 8610-4138

XPS OF RHENIUM

ELECTRON KINETIC ENERGY
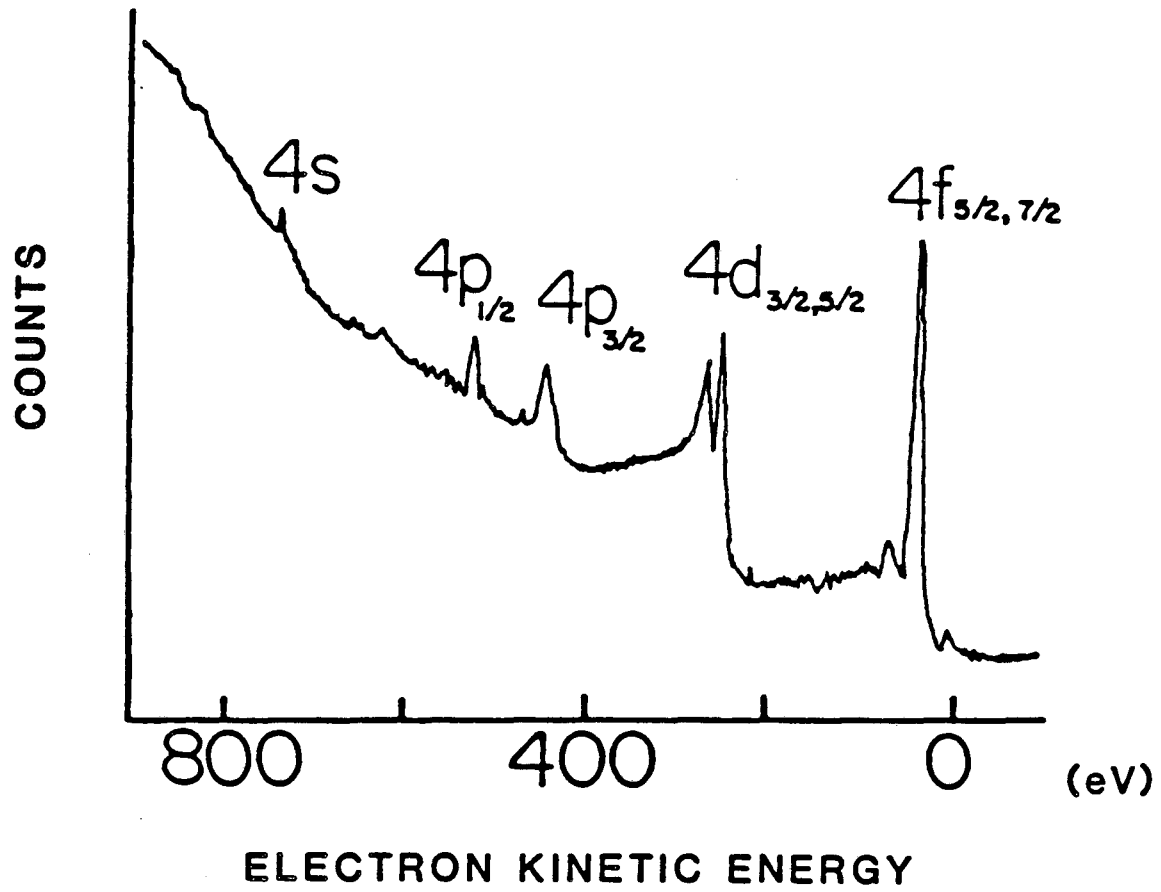
XBL 8610-4137

Fig. 2.16

XPS OF Rh

ELECTRON BINDING ENERGY

XBL 8610-4136

Fig. 2.17

54
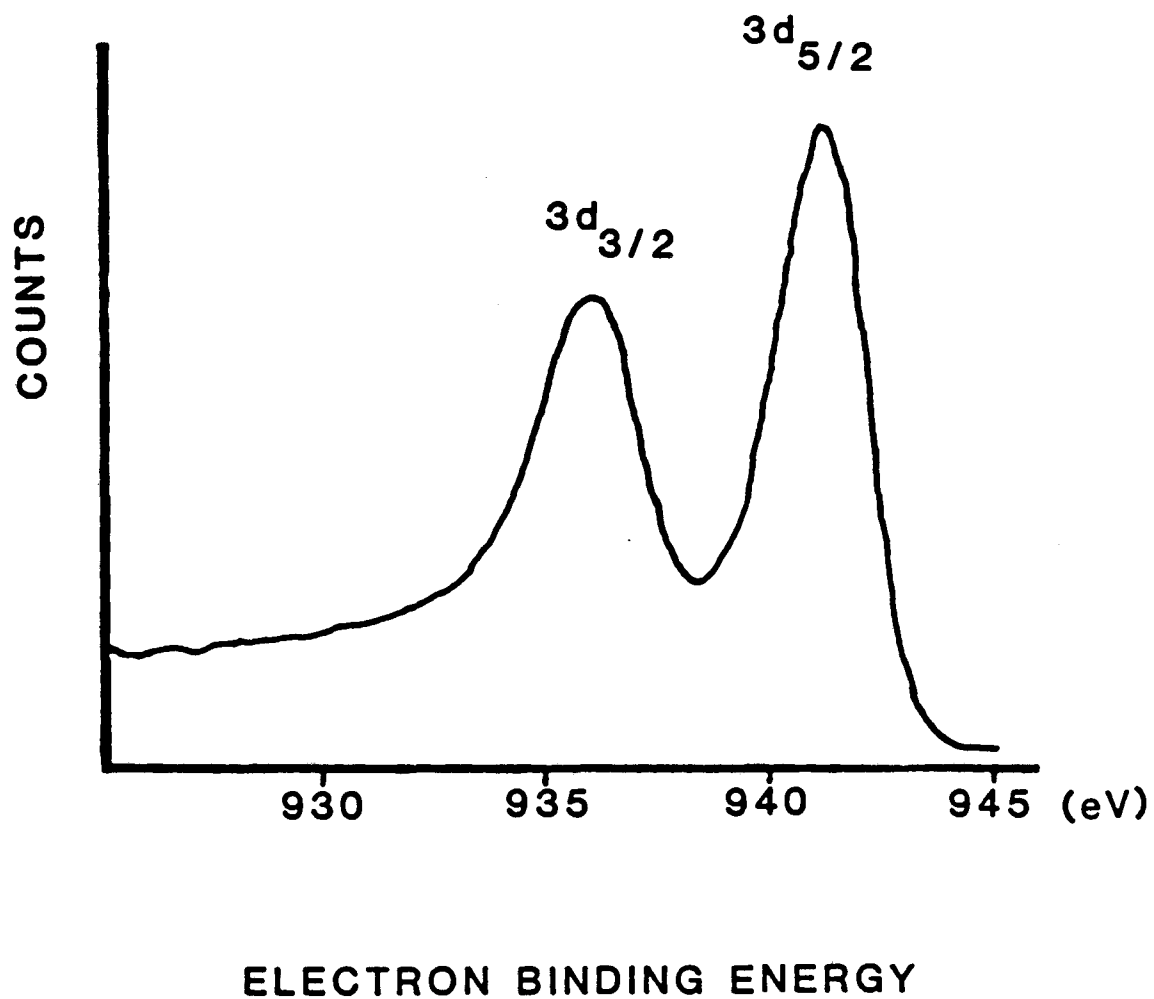
III. THE SYNTHESIS OF BUYTRONITRILE FROM n-BUTANOL and AMMONIA OVER RHODIUM (111) and (331) SINGLE CRYSTAL CATALYSTS

3.1 Introduction

This chapter looks at the reaction of n-butanol and ammonia over single crystal rhodium surfaces. The formation of butyronitrile via this reaction serves as a good model system for the study of ammonolysis reactions. Ammonolysis and ammoxidation are the primary types of C-N bond forming reactions.[1]

These reactions are industrially important and produce amines and nitriles of various types. The catalysts used to form them selectively and at high rates have been described abundantly in the patent literature. They include: a bimetallic catalyst of raney nickel and a rhodium, ruthenium or palladium co-catalyst for the production of amines from alcohols and ammonia;[2] an aluminosilicate catalyst for production of amines via the amination of olefins;[3] a catalytic complex formed by ammonia addition to a copper salt for conversion of unsaturated aldehydes to unsaturated nitriles;[4] a nickel/copper catalyst to form amines from alcohols or aldehydes;[5] and a nickel/rhenium catalyst for amination of alcohols.[6] There are reports for the use of phosphoric acid on alumina, multicomponent cobalt/nickel/copper/silver, nickel/copper/chromium, rhodium/manganese, and molybdenum/bismuth/lead/thallium/iron/arsenic/alkali catalysts.[7-13]

The reaction system of n-butanol and ammonia and the related reaction of benzoyl alcohol to benzonitrile have been studied by Jodra and coworkers.[14-16] The catalyst used for most of their work was zinc oxide. While their work provides an introduction to this system, no surface science has been reported for this reaction. This chapter provides new insight into this ammonolysis reaction using the kinetic and surface science (structure, composition) data provided by a combined high pressure reactor-ultrahigh vacuum surface science system.

In order to explore the elementary surface reaction steps leading to C-N bond formation, the reaction of n-butanol and ammonia over model rhodium (111) and (331) single crystal catalysts was studied. The results show that rhodium can selectively form the nitrile. Also, the formation of butylamine is possible upon the addition of hydrogen to the reaction mixture.

It is shown that the reaction is surface structure sensitive, but that this sensitivity can be eliminated by pretreatment in ammonia. The data shows that the reaction occurs on an overlayer of carbon, nitrogen, and oxygen with only 5% of the metal sites available. The reaction intermediates include butyraldehyde that forms rapidly from the n-butanol and an unstable imine molecule. This imine molecule can react to form either the nitrile or the amine and thus control the selectivity of this catalyst.

3.2 RESULTS

1. Reaction Kinetics

These experiments have shown that both rhodium (111) and (331) crystal surfaces can catalyze the formation of n-butyronitrile from n-butanol and ammonia. The results are displayed in Fig. 1. The open bar graphs show the initial rates for the clean Rh(111) and (331) surfaces. The initial rates of nitrile production for the two surfaces differ by a factor of about three. The (111) surface has a rate of 0.13 molecules/surface site·second and the (331) surface 0.42 molecules/surface·site second. These rates were measured at a reaction temperature of 515 K, an ammonia:alcohol ratio of 10:1, and a total pressure of the reactants of 110 Torr.

The reaction rate figures represent a lower bound for the activities of these catalysts. This arises from an inability to actually determine the number of sites that were catalytically active on the surface. Instead the numbers used were calculated from ideal surface atom densities for the Rh(111) and (331) surfaces.[17] This quite probably leads to an overestimation of the number of active sites as it is not likely that every surface atom is indeed an active site. Surface roughness, especially on the stepped (331) surface could conceivably make this estimate low instead of high. However, CO TPD comparisons between the two surfaces showed close to the expected ratio of CO desorbing, indicating that there is no large difference in surface area other than that predicted by the differences in structures.

In Fig. 2 typical product accumulation curves are shown for the Rh(111) and Rh(331) surfaces. In this typical case, the Rh(111) catalyst maintained its initial rate for over 6 hours at 515 K. Reactions were carried out for over 12 hours, or to about 10% conversion with very little poisoning noted, as judged by decreases in the initial rates. In the case of the Rh(331) catalyst, the lifetime was much shorter and a considerable degree of poisoning was evident after approximately 2 hours reaction time. Thus catalyst deactivation is structure sensitive. These reactions are catalytic, even at the highest rate of poisoning. Even at 1 hour reaction time the total turnover (turnover frequency x reaction time) for the Rh(331) catalyst was in excess of 1000 at 515 K, with a total pressure of 110 Torr, and a 10:1 ammonia to alcohol ratio. Indeed, all reactions mentioned in this work, with the exception of those that included large amounts of water in the reactant mixture, had total turnovers of at least 500. Blank reactions performed by heavily carbiding the catalyst showed negligible activity.

The reaction between n-butanol and ammonia, over the temperature range tested, produced the butyronitrile in Arrhenius fashion over both the basal Rh(111) and stepped Rh(331) surfaces. Figure 3 shows Arrhenius plots for the Rh(111) and the (331) surfaces. The data shown is initial rate vs temperature. The activation energies are 22 ± 3 kcal/mole for the Rh(111) surface and 21 ± 3 kcal/mole for the Rh(331). Within the error of these measurements, these values are

the same, indicating that the rate determining step in the mechanism
for nitrile production is most likely the same on both surfaces.

There is a significant difference in the product distribution for
these two catalysts. The flat surface produced essentially 100% ni-
trile. The stepped catalyst on the other hand had about 10% of CH_4,
C_2H_6, and C_3H_8 present in addition to the nitrile. These product
distributions are listed in Table 1. This observation is consistent
with studies that have previously noted that stepped surfaces are more
active for hydrogenolysis reactions than flat surfaces.[18-19]

More mechanistic data was gained by making pressure dependence
measurements for the reaction of the alcohol and ammonia over the two
catalyst surfaces studied. These results are shown in Figs. 4 and 5
for the Rh(331) surface. The results for the Rh(111) surface are
essentially identical. In these plots of log pressure vs. log rate
of formation of the nitrile, the pressure dependence for the alcohol
is zero, given the error of the measurement. The dependence on the
NH_3 pressure was approximately 2nd order up to a pressure ratio of
about 1:1, ammonia to alcohol, then it became zero order also.

2. Surface Science Studies

Figure 6 shows an AES spectrum of the active surface after a reac-
tion. The active surface was covered with an overlayer of carbon, ni-
trogen, and oxygen. The stochiometry implied from weighting the peak
height ratios with the respective sensitivity factors is approximately
C:N:O, 4:2.5:1. This ratio remained constant within a factor of ± 10%
for both the Rh(111) and (331) steady state active surfaces. For a

poisoned Rh(331) surface the ratio changed to C:N:O, 6:2.5:1 indicating carbon accumulation. The nitrogen to oxygen ratio remained constant in both cases. A higher amount of carbon was also noticed for reactions on the Rh(111) surface that were carried out at higher than 530 K and for reactions in which an ammonia to alcohol ratio of less than 1 was used. In both of these cases poisoning was more rapid.

The thermal desorption spectra of n-butanol, n-butanal, butyronitrile, butylamine, and ammonia on both the rhodium surfaces studied were determined. TPD experiments were performed on both the catalyst surface after reaction and on the clean surface. Molecules were dosed at 300 K in all experiments. None of the molecules listed above produced any molecular desorption features in any of the experiments performed on clean surfaces. Indeed only n-butanol and n-butanal exposure to a clean surface produced any significant desorptions at all for 50 L exposures. Exposures of 10,000 L of ammonia were necessary to produce a small amount of N_2 desorption at 670 K. This indicates rapid decomposition of the oxygenated reactants and poor adsorption of the products on the clean rhodium metal at 300 K. The experimental set up did not allow dosing at a lower temperature.

Both the alcohol and the aldehyde gave very similar desorption spectra when either was adsorbed on the clean catalyst surface. These molecules gave only H_2 and CO desorption. In Fig. 7 the TPD spectra for the alcohol adsorbed on a clean Rh(111) surface are shown. In the (m/e)= 28 desorption one peak, at 455 K, is seen for a 0.5 L exposure. This is indicative of desorption without C-O bond scission,

since it occurs at approximately the same temperature as the molecular desorption noted after CO exposure of the Rh(111) surface (see Discussion). The aldehyde has a similar (m/e)= 28 spectrum with CO desorption at 450 K. The (m/e)= 2 desorptions were also equivalent for both molecules, with the major desorption peak at 385 K followed by a long tailing desorption feature that continued to about 650 K.

The amount of CO that desorbed indicated that the remaining hydrocarbon layer must have a stoichiometry of about C_3H_6. This conclusion was reached by comparing the amount of CO desorbing under these conditions to that which desorbs from a clean surface. The values are very similar indicating loss of just one carbon with its assigned oxygen from these oxygenated molecules. This information is corroborated by an associated decrease in the C AES spectrum, taken following desorption. The amount of H_2 that desorbed was again calibrated to the amount of CO desorbing from a CO monolayer and adjusted for the mass spectral sensitivity. This was necessary because in order to obtain a H_2 monolayer for calibration purposes, cooling the sample is required. This was not possible in this experimental system. Very similar results were obtained on the Rh(331). However, on this surface there were two CO desorption peaks for both the adsorbed alcohol and the aldehyde. One of these was at a high temperature of about 870 K indicating carbon oxygen bond cleavage and recombinant desorption. The other was the same as observed on the Rh(111) surface.

Thermal desorption experiments were performed after a reaction by allowing the sample to cool in the reaction mixture, pumping the gases out of the reaction cell and then returning the catalyst to UHV. A desorption experiment was then carried out. The principle desorbing masses were 2,12,14,27,28,29, and 42 for the alcohol (or aldehyde) – ammonia reaction. No obvious differences between the (331) and (111) surfaces were noted. An example of these desorption peaks from the Rh(331) surface is shown in fig. 8. The desorption peaks at the lowest temperature are at 630 K. These are very small amounts of (m/e)= 29 and 41. This 630 K desorption is closely followed by a much larger peak at (m/e)= 27, a (m/e)= 2 peak, and (m/e)= 28 and 14 peaks. The temperature of all of these desorptions was 670 K. The initial desorptions at (m/e)= 29 and 42 are indicative of the desorption of several of the C_4 molecules used and produced in this reaction. None of these molecules give strong molecular ion peaks and as such identifications were made from the various cracking patterns. Analysis of these cracking patterns allows the alcohol or the amine to be ruled out as possible sources of these desorptions. Characteristic desorptions at (m/e) =31 for the alcohol and (m/e)= 30 for the amine are missing. Thus the only possible sources for the (m/e)= 29 and 41 desorptions are the nitrile, the aldehyde, an imine intermediate or a fragment, all of which could conceivably produce these cracking fragments. As mentioned earlier the nitrile did not adsorb in our TPD experiments. In addition, the aldehyde was shown to decompose on the clean surface and it did not stick to a surface that had been exposed to it after

reaction. Thus neither the nitrile or the aldehyde seem to be the source of these desorptions. It must be noted, however, that the aldehyde cannot be unequivocally ruled out.

Returning to the description of these desorption spectra, the initial desorptions at (m/e)= 29 and 41 are closely followed by a large (m/e)= 27 peak, and (m/e)= 2,28, and 14 peaks. The analysis of these peaks is complicated. For a 2500 L dose of NH_3 at 650 K, Vavere[20] notes a N(380)/Rh(302) AES ratio of 0.06. He argues that this corresponds to a N coverage of somewhat less than 0.5 monolayers. Schmidt[21] for a 5×10^7 L dose at 1400 K shows a N(380)/Rh(252) ratio of 0.17, which should correlate to a N(380)/Rh(302) ratio of about 0.05. For a 18,000 L dose at 500 K a N(380)/Rh(302) ratio of the same 0.05 is found in our work. Our experimental value for a reaction temperature of 507 K at 100 Torr NH_3 pressure is an average of 0.15. This is considerably more N than can be accounted for by what the other data has indicated as a saturation N coverage resulting from NH_3 exposure.

The fact that we see considerably more nitrogen on the surface after a reaction than has been reported for cases of NH_3 exposure to Rh helps us in the assignment of the rest of the TPD spectra. The (m/e)= 28 and 14 desorptions are assigned to N_2 desorbing in a recombination from atomic N on the surface. We note that our temperature of 670 K is higher than the 590 K reported by Schmidt et al., and the 600 K reported by Vavere et al. However the (m/e)= 28/14 ratio is the same as that measured for N_2, so we believe our assignment is correct. However, a lot of desorbing N is unaccounted for in this assignment,

as AES shows no sign of nitrogen after a TPD experiment. We know that only a fraction (~ 1/3) of the N desorbing from the surface can be in the form of N_2, as evidenced by the N/Rh AES saturation ratios for NH_3 adsorption on Rh. The (m/e)= 27 desorption, whose peak shape is sharper than the other desorptions at the same temperature, is the only other significant route for nitrogen desorption possible. This large desorption, the principle desorption product from the surface after a reaction surface, is assigned as HCN. This molecule desorbs at a considerably higher temperature than the 575 K temperature noted by Schmidt et al. in their work. However, given the strength of this peak and the lack of other (m/e) desorptions that suggest a N containing molecule, this assignment makes sense. The (m/e)= 2 desorption is due to hydrogen. This hydrogen must be coming from an organic fragment on the surface as hydrogen bound to Rh would desorb at the much lower temperature of 325 K.[22]

Further TPD experiments were performed to ascertain the amount of bare metal surface available to the reactants under experimental conditions. $C^{13}O$ was used to titrate the bare metal because it will adsorb to the metal surface but not to any of the adsorbate layers present on the surface.[23] The amount of $C^{13}O$ that sticks to the Rh surface after exposure to reaction conditions is indicative of the amount of bare metal surface available. This amount is very small. For experiments carried out on either the Rh(111) or the Rh(331) approximately 5% of the CO adsorption sites were available after a reaction.

3. Studies of Reaction Mechanism

Another interesting comparison between these two catalysts is the effect of catalyst pretreatment in ammonia on the product distribution and rate, shown in Fig. 1 and Table 1. (In reactions where the catalyst was pretreated, ammonia was added with argon as a carrier gas. The catalyst was then heated to reaction temperature for 30 minutes prior to the introduction of the alcohol.) The selectivity and rate of the flat Rh(111) surface was essentially unaffected. However, kinetic parameters were modified by the pretreatment of the stepped Rh(331) surface. The selectivity to nitrile effectively rose to 100%, the same as seen for the flat surface. The rate of formation of the nitrile however, dropped by a factor of eight to 0.05 molecules/site·sec. Both of the effects are likely due to the blocking of the step sites by the strongly adsorbed nitrogen that was deposited during the pretreatment. In addition, the ammonia pretreatment extended the lifetime of the Rh(331) catalyst by at least a factor of 5. Reactions which previously poisoned in 1-2 hours ran for 10-15 hours after pretreatment.

More information was gained about this effect by analyzing the surface after reaction. The AES spectra taken after reactions that occurred on pretreated surfaces did not show an increase in the amount of N present. So the change in reactivity that was noticed was not due simply to a larger than usual buildup in the amount of N on the surface of the catalyst.

One possible source of this effect is an ammonia induced recon-
struction of this surface. This has been reported by Schmidt.[21] To
check this SEM was performed on the Rh(331) catalyst before and after
ammonia pretreatment. We were unable to see any changes in the micro-
graphs. We note that the effect reported by Schmidt was at a much
higher temperature than that used in these experiments. We note that
a reconstruction of a smaller scale, one that would be observable by
LEED experiments is not possible to completely rule out. LEED experi-
ments to confirm or disprove this possibility where not successful,
due to an unbelievable array of experimental problems with the appara-
tus available.

In Tables 1 and 2 product distributions and rates are shown from
several other reactions important to an understanding of the total re-
action scheme in this system. First of all, the reaction of the alde-
hyde with ammonia is compared to that of the alcohol with ammonia.
The resulting rates for the Rh(111) and (331) surfaces are 0.17 and
0.13 molecules/surface·site second, respectively, for the aldehyde –
ammonia reaction, very similar to that of the alcohol – ammonia reac-
tion. Both of these reactions were performed at 515 K, 110 Torr total
reactant pressure, 10:1 ratio of ammonia to alcohol or aldehyde. If
the rate determining step in the overall ammonolysis reaction were the
oxidation of the alcohol to the aldehyde one would expect a consider-
able rate increase due to the large amount of aldehyde available in
this case. This was not observed.

The conversion of alcohol to aldehyde has a rate of 0.44 molecules/site·second for the Rh(111) surface and 0.92 molecules/site·second for the Rh(331) surface. These rates are for a temperature of 515 K and 10 Torr pressure of alcohol. This reaction is then at least a factor of two faster that the overall rate the alcohol to nitrile reaction.

As one possible product of the ammonolysis reaction is an amine, it was of interest to see what, if anything, could be done in these experiments to produce this molecule. The most obvious route is to add H_2 to the reaction mixture. Upon addition of H_2 there were significant changes in the behavior of the catalyst. To begin with, the amine (butylamine < 1% of total products) was formed upon H_2 addition. Determining the actual amount of amine formed is complicated by the fact that the addition of H_2 also produced a high molecular weight molecule that was identified by a very long retention time. This species was tentatively identified via GC/MS as a Schiff base product. A Schiff base is a molecule formed by addition of a amine to an aldehyde. The formula for this molecule is $C_3H_7CHNC_4H_9$. This hypothesis was tested by reacting the amine with the aldehyde, where the same high molecular weight retention time was observed for the product molecule in this reaction, indicating that this molecule was most likely a Schiff base product of the reaction of butyraldehyde with ammonia.

Another effect of H_2 upon the product distribution in the batch reactor was a marked increase in the amount of hydrogenolysis products. These hydrogenolysis products, primarily methane and propane, were observed along with an increase in the rate of production of butyroni-

trile. This data is summarized in Table 1. The magnitude of this effect varied, from about 10% hydrogenolysis products for the aldehyde - ammonia - hydrogen reaction on the Rh(111) surface to 95% for the alcohol - ammonia - hydrogen on the Rh(331) surface. In all cases propane was the most prominent cracking product. The final effect of H_2 addition was that it increased the rate of nitrile formation and decreased the amount of C,N, and O on the post reaction surface.

Reactions to investigate the interaction of the aldehyde and ammonia were performed. Upon addition of ammonia into a mixture of aldehyde and argon, up to 95% of the aldehyde present would disappear as judged by the chromatographic analysis. The rate of this reaction was very fast; 10^3 times faster than the initial rates for nitrile formation. The addition of water reversed this reaction. By adding water up to 30% of the "lost" aldehyde could be recovered. This "equilibrium" process occurred quickly and was not a function of catalyst temperature. Due to the rapid and partially reversible nature of this observation we investigated whether or not a gas phase interaction would cause a reaction between these molecules. FTIR experiments were performed to evaluate this possibility. By doing these experiments we hoped to see either a change in the C=O stretching frequency indicative of a new bond being formed with the carbonyl carbon, or a new feature that could be assigned as a C-N frequency which would also be an indication of a homogeneous reaction.

For the FTIR experiments, a glass cell was prepared using NaCl windows epoxied onto a 25 mm diameter, 12 cm long pyrex tube. A cold finger was attached to allow the introduction of the aldehyde and ammonia via cold trapping. A teflon stopcock was added for evacuation and dosing of the vessel. Several experiments were carried out by freezing the aldehyde and ammonia into the pyrex cell in various ratios, and taking the appropriate spectra. The spectra taken scanned in wavelength from 400 to 4000 cm^{-1}. While deconvolutions of the spectra were difficult due to the rotational fine structure of the ammonia spectrum, it was clear that no major changes in either the aldehyde or the ammonia spectra occurred. Thus it seems that this reaction is not one that occurs readily in the gas phase. It seems then that the interaction between the aldehyde and ammonia and the reverse reaction with water are mediated by either the stainless steel walls of the reactor vessel or by an extraordinarily fast reaction on the Rh surface. It is very unlikely that the Rh surface was catalyzing this reaction as there was no observed difference in the rate or extent of aldehyde disappearance with changes in the temperature of the Rh catalysts or by heavily carbiding this catalyst.

To try and more fully characterize the interaction between aldehyde and NH_3 and H_2O, we added water to the mixture of the aldehyde and ammonia to test its effect upon the resulting reaction to the nitrile. Indeed, it was necessary to add small amounts of water whenever quantification of the amount of aldehyde present was necessary. The results of these experiments are listed also in Table 2. On the Rh(111)

surface the reaction between the aldehyde and ammonia at 240°C with 10 microliters of each aldehyde and water and 100 Torr of ammonia gives a very simple product distribution, essentially 100% nitrile. The rate of this reaction is 0.02 molecules/site·sec, a drop of > 75% from the water free case. Addition of water to this reaction mixture slows the reaction down but does not effect the product distribution.

DISCUSSION

While it would be appropriate and interesting to include in this discussion a comparison of this work with other reactions of this type carried out over single crystal or polycrystalline foil catalysts, this is not possible due to the absence of such studies. A comparison of this work with a model for this reaction suggested by studies on supported catalysts is included later in the discussion. These studies did not, however, include any surface analysis, so complete comparison is difficult. These experiments have shown that both Rh(111) and (331) single crystal surfaces selectively catalyze the formation of butyronitrile from n-butanol and ammonia. The activation energies for both surfaces are the same, with the average being about 21.5 ± 3 kcal/mole. This implies that the rate limiting step does not vary between the two surfaces, and the kinetic and selectivity data seem to support this observation. No extreme differences are noted between the two surfaces that would indicate a change of mechanism.

Rate data leads to the conclusion that both the stepped and flat sites are active in the catalytic production of the nitrile. The basal (111) plane studied showed nearly 100% nitrile production. At 510 K, the (331) surface, which consists of both the stepped and flat sites, produced nitrile at a rate approximately 3 times faster than the flat only surface. From this evidence, and the additional data that the % of cracking products rose from < 1% to about 10% for the ammonolysis reaction on the (331) surface, it can be concluded that the step sites

are more active for the ammonolysis reaction and much more active for the cracking reaction than the flat basal plane sites.

The (111) surface did not poison for long periods of time, reactions were generally run to 10% conversion, although some experiments were run to 25% conversion with only small amounts of poisoning. If the reaction temperature was higher than 530 K or the ammonia to alcohol ratio less than 1:1, poisoning occurred at an accelerated rate. The (331) surface poisoned much more quickly. This behavior could be modified by pretreatment of the catalyst at reaction temperature with ammonia. In reactions where this pretreatment was performed, the catalyst was very stable, with a lifetime at least a factor of five greater than the untreated case. This fact indicates that the pretreatment somehow slows the formation of the carbon deposits on the catalysts that are seen with catalyst deactivation. The correlation between an accumulation of carbon, as determined by a post reaction C:N:O ratio, and catalyst deactivation was clear. The mechanism in which the pretreatment serves to hinder C buildup is not. The data indicates that the step sites are involved in the initiation of poisoning. The reduction in the rate of catalyst deactivation must then involve a modification of these step sites. This modification is most likely the result of NH_3 decomposing and N adatoms blocking the step sites. As mentioned earlier an NH_3 induced reconstruction is also consistent with this result. The reconstruction explanation for this effect is less likely since no changes in the lifetime or selectivity of a non-pretreated Rh(331) catalyst are noted. It is not clear why

the presence of the alcohol would inhibit a reconstruction if one was to occur in the absence of NH_3.

When the stepped surface was pretreated with ammonia, an additional effect was noted; the reactivity of the Rh(331) catalyst was significantly altered. The selectivity became that of the (111) basal plane surface and the rate dropped by about 85%. Hydrogenolysis activity was eliminated, making the product distribution the same as the Rh(111) catalyst. This alteration of activity and selectivity was stable with time. Therefore, the influence of the pretreatment upon the catalyst must be irreversible. Again, we believe this effect was most likely caused by N adatoms formed by ammonia dissociation blocking the step sites. Examples of this type of selective poisoning have been noted in other circumstances.[24-25] In addition this effect is supported by the earlier kinetic data. We note that analysis of the post reaction surface via AES showed no distinction between the composition of the Rh(111) and Rh(331) surfaces. No difference was noted in the TPD either. This is not unexpected; the fraction of the total number of nitrogen atoms on the surface bound to the step sites could be small enough to make the distinction difficult.

The results indicate that in the reaction of the alcohol with ammonia the aldehyde was a likely intermediate. This is shown by the fast rate of the oxidation (alcohol to aldehyde conversion) as compared to the overall rate; the buildup of aldehyde in the reactor as monitored by water addition; and the ability to form the nitrile directly from the aldehyde.

The role of the overlayer is critical in understanding the action of this catalyst. 95% of the metal surface is covered with an overlayer of carbon, nitrogen, and oxygen during the reaction. Poisoned surfaces had a higher amount of carbon. The evidence suggests that this overlayer is composed of a combinations of fragments created by the decomposition of alcohol or aldehyde molecules and some type of molecule or fragment that is formed as a reaction intermediate or product. Specifically the TPD data obtained by dosing the alcohol and the aldehyde on the surface indicate that both of these molecules dissociate on both the clean Rh(331) and (111) surfaces. There was no molecular desorption after room temperature exposures. The only desorption products noted were CO and H_2. TPD indicates that a hydrogen deficient C_3 overlayer is left on the surface after heating to 1000 K. The (m/e)= 28 CO spectra for both molecules on the Rh(111) surface shows a peak at 455 K. This is very similar to the 485 K CO desorption noted by Solymosi et al.[26] for CH_3OH adsorption at 300 K on a Rh(111) crystal. Thus it seems that the alcohol and the aldehyde both undergo alpha-beta carbon-carbon bond breaking. The resulting CO desorption is observed and a C_3 residue is left behind.

If we apply this observed surface science knowledge to what is seen in the catalytic reaction an interesting comparison can be made. When H_2 is added to the reaction mixture a number of shorter hydrocarbons are seen in the product distribution. Propane is the most prominent hydrocarbon product at 80% of the total product in the (331) case. This large amount of C_3 product and the associated reduction seen in the

amount of C on the surface after a reaction using hydrogen, suggest that part of the overlayer on the functioning catalyst is the same hydrogen deficient C_3 fragment that was noted as having been formed by alcohol and aldehyde decomposition. This portion of the overlayer is not involved in the principle reaction to form the nitrile or the amine, as no C_3 product nitriles or amines were formed. However the addition of hydrogen, as well as forming a lot of propane, reduced the amount of carbon on the post reaction surface. It also significantly increased the rate of nitrile production. This fact is consistent with the above interpretation. By the addition of hydrogen, the C_3 fragments which are hydrogen deficient are removed, opening up these surface sites for the desired formation of nitriles or amines. This portion of the overlayer is stable under reaction conditions in the absence of hydrogen.

TPD from the post reaction surface gives information about other components of this active overlayer. The data suggests that it contains a combination of intermediate or product molecules and nitrogen adatoms. This data is however very difficult to interpret. Essentially it is seen that two fragments, $(m/e)= 29$ and 41, desorb and that at almost the same temperature N_2 and HCN are noted to desorb. A key fact in assessing this information as well as explaining the TPD results, is the zero order pressure dependence noted for both the alcohol and NH_3. This dependence indicates that the rate limiting step in the overall reaction might be desorption of the product molecule or some other step very late in the mechanistic pathway. If this were

true, a build up of these species on the surface would be expected. Indeed the results shown here can be interpreted as showing that an intermediate, which can not be unequivocally identified, is present on the surface after the reaction and during the TPD after the reaction. The only indication of this intermediate molecularly desorbing that we see in TPD are these two small (m/e)= 29 and 41 desorptions. We believe that that these are cracking fragments of a desorbing imine intermediate. Note that the imine is an elusive molecule due to its propensity to react with water to reform its parent oxygenate (See references 27-30 for more information about the chemistry of imines). While these fragments could certainly come from this molecule this assignment is in no way conclusive. It makes a great deal of sense however, because the imine is the most logical choice as the adsorbed intermediate whose reaction on desorption is rate limiting. This small amount of (m/e)= 29 and 41 which we assign to the imine desorbing is followed by desorption of N_2, HCN and H_2. We believe the N_2 desorbs from recombination of adsorbed atomic nitrogen. The HCN and H_2 however are hard to unequivocally assign a source. The most compelling explanation is that they are the result of the imine molecule (that just started to desorb) thermally decomposing and desorbing from the surface. Undoubtedly some of the H_2 comes from the other carbonaceous fragments.
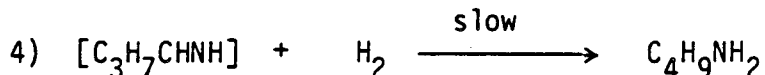
The model for the overlayer develops then as a surface covering that is composed of decomposed aldehyde or alcohol fragments, adsorbed nitrogen adatoms and an adsorbed imine intermediate. It is noted that

some adsorbed HCN would have to be included in this analysis to make the post reaction AES ratios consistent with this model. This is in part speculation. However, it provides a workable picture of the surface to expand and/or improve upon. This model for the overlayer, in addition to being consistent with our kinetic results, fits into a model for nitrile synthesis via an imine intermediate that has been proposed before in both the open literature and in patent disclosures.[6,31]

The model is outlined by:

1) $n- C_4H_9OH \xrightarrow{\text{fast}} C_3H_7CHO + H_2$

2) $C_3H_7CHO + NH_3 \rightleftharpoons [C_3H_7CHNH] + H_2O$

3) $[C_3H_7CHNH] \xrightarrow{\text{slow}} C_3H_7CN + H_2$

and in excess hydrogen,

4) $[C_3H_7CHNH] + H_2 \xrightarrow{\text{slow}} C_4H_9NH_2$
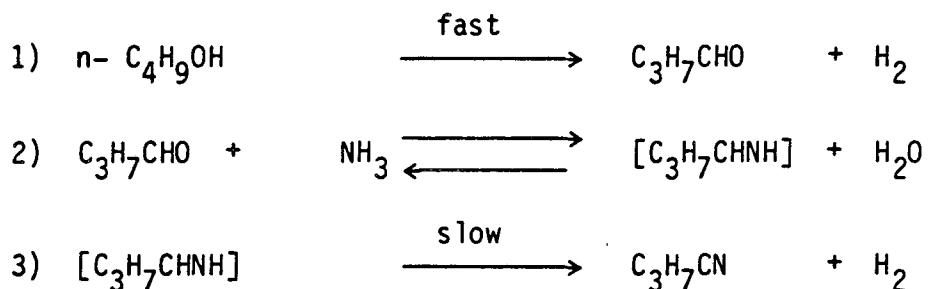
The model proposed consists of a reaction mechanism in which the alcohol is rapidly oxidized to the aldehyde in an initial step. It has been shown that this reaction occurs in our system. The aldehyde then combines with ammonia and loses water to form an imine. This carbon-nitrogen bond forming step is crucial, it is also poorly understood. A likely possibility for this step in our reaction is that it occurs on the walls of the reactor! The addition of water to the reaction increases the amount of aldehyde present, which also is consistent with what is known of the chemistry of imines.

The imine molecule produced can then be dehydrogenated to the nitrile or hydrogenated to the amine. It is possible that this step is the key to understanding many aspects of this reaction. If the overlayer is composed of two primary entities, i.e. the hydrocarbon fragments and the imine intermediate, then this model nicely describes the relative roles of the overlayer and the metal: The metal is needed to dehydrogenate the imine molecule, the organic fragment blocks part of the metal, hydrogen addition removes this blocking species, nitrile production via imine dehydrogenation is increased and amine (and amine by-products) are formed via hydrogenation. Evidence for both of these reaction channels is seen with the route to the nitrile being much preferred over that to the amine on these rhodium catalysts.

Rhodium is at least a fair catalyst for this reaction due to its ability to promote this reaction by initiating the alcohol to aldehyde conversion, dissociate hydrogen, catalyze the imine to amine and the imine to nitrile reactions. The (111) surface also poisons slowly by not coking at a rapid rate.

REFERENCES

3.1 Eds. King, Herrick, Quellette, and Cheremisinoff, Unit Process Series Organic Chemical Industries Vol. 2, "Amination Processes Pollutant Discharges Identification," (Ann Arbor Science Publishers Inc, Ann Arbor, MI 1979).

3.2 U.S. Patent 3,278,598 to Atlas Chemical Ind., K.H. Markiewitz, 7/18/63.

3.3 U.S. Patents 4,375,002 and 4,307,250 to Air Products and Chemicals, J.O.L. Peterson, 2/22/83 and 12/22/81.

3.4 U.S. Patent 4,202,837 to Monsanto Co., A.N. Williamson, 11/16/78.

3.5 U.S. Patent 4,152,353 to Dow Chemical Co., C.E. Haberman, 5/1/79.

3.6 U.S. Patent 4,123,462 to Union Carbide Corp., D.C. Best, 10/31/78.

3.7 U.S. Patent 3,974,432 to Eastman Kodak Co., H.J. Hagemeyer, 9/7/76.

3.8 U.S. Patent 3,347,926 to Atlas Chemical Ind., J.D. Zech, 10/17/67.

3.9 U.S. Patents 3,390,184 and 3,152,998 to Jefferson Chemical Co., P.H. Moss, 6/25/66 and 10/13/64.

3.10 U.S. Patent 3,520,933 to B.A.S.F., K. Adam and E. Haarer, 7/21/70.

3.11 U.S. Patent 3,654,370 to Jefferson Chemical Co., E.L. Yeakey, 4/4/72.

3.12 U.S. Patent 3,128,311 to Jefferson Chemical Co., R.L. Shirley and G.P. Speranza, 4/7/64.

3.13 U.S. Patent 4,244,889 to Union Carbide Corp., W.J. Bartley and G.L. O'Conner, 1/13/81.

3.14 Jodra, L.G., Bayon, A., and Corella, J., Anales de Quimica, 1449 (1972).

3.15 Jodra, L.G., Palancar Montero, M.C., and Romero Salvador, A., Anales de Quimica 79, 228 (1982).

3.16 Jodra, L.G., Bayon,A., and Corella,J., Anales de Quimica, 371 (1980).

3.17 Ph.D. thesis, D. Castner, 1979 University of California, Berkeley.

3.18 Somorjai, G.A., Pure and App. Chem. 50, 963 (1978).

3.19 Blakely, D.W., and Somorjai, G.A., J. Catalysis 42, 131 (1976).

3.20 Vavere, A. and Hansen, R.S., J. Catalysis 69, 158 (1981).

3.21 Hasenberg, D., and Schmidt, L.D., J. Catalysis 91, 116 (1985).

3.22 Castner, D.G., and Somorjai, G.A., Surf. Sci. 83, 60 (1979).

3.23 Levine, M., Salmeron, M., Beu, A.T., and Somorjai, G.A., Surf. Sci. 169, 123 (1986).

3.24 Apesteguia, C.R., and Barbier, J., J. Catalysis 78, 352 (1982).

3.25 Madon, R.J. and Shaw, H., Catal. Rev. Sci. Eng. 15(1), 69 (1977).

3.26 Solymosi, F., Berko, A., and Tarnoczi, T.I., Surface Science 141, 533 (1984).

3.27 Layer, R.W., Chem. Rev. 63, 489 (1963).

3.28 Ogata, Y. and Kawasaki, A., Tetrahedron 20, 855 and 1573 (1964).

3.29 Tolbert, T.L. and Houston, B., J.A.C.S. 28, 695 (1963).

3.30 Patai, S., "The Chemistry of the Carbon-Nitrogen Double Bond," (Interscience 1970).

3.31 Card, R.J., and Schmitt, J.L., J. Organic Chemistry 46, 754 (1981).

Table 1

Product Distributions for the Reactions Studied in This Work

Reactants	Surface	NTRL	ALD	Amine	C_1	C_2	C_3	C_4^+
				Products				
Alcohol and Ammonia	(331)	86	–	–	4	3	3	–
	$(331)^1$	>98	–	–	–	–	–	–
	(111)	>98	–	–	–	–	–	–
Aldehyde and Ammonia	(331)	95	–	–	1	–	4	–
	(111)	>98	–	–	–	–	–	–
Alcohol, Ammonia, and Hydrogen	(331)	4	–	–	10	5	80	–
	(111)	55	–	–	11	1	33	–
Aldehyde, Ammonia, and Hydrogen	(331)	<1	–	<1	5	–	18	75
	(111)	48	–	<1	2	1	7	41
Alcohol, Ammonia, and Water	(331)	>98	–	–	–	–	–	–
	(111)	<98	–	–	–	–	–	–
Aldehyde, Ammonia, and Water	(331)	>98	–	–	1^2	–	1^2	–
	(111)	>98	–	–	1^2	–	1^2	–
Alcohol	(331)	–	48	–	50^3	–	–	–
	(111)	–	90	–	–	–	10	–

All reactions are at 237°, 10:1 NH_3/ BOL or BAL ratio, 200 torr Ar. For H_2 reactions 200 torr of H_2 was used. Most data are the average of several experiments.

[1]This data set was for the pretreated surface.

[2]High uncertainty due to low rate and low selectivity to this product.

[3]These reactions poisoned very quickly.

Table 2

Initial Rates for Reactions Studied in This Work

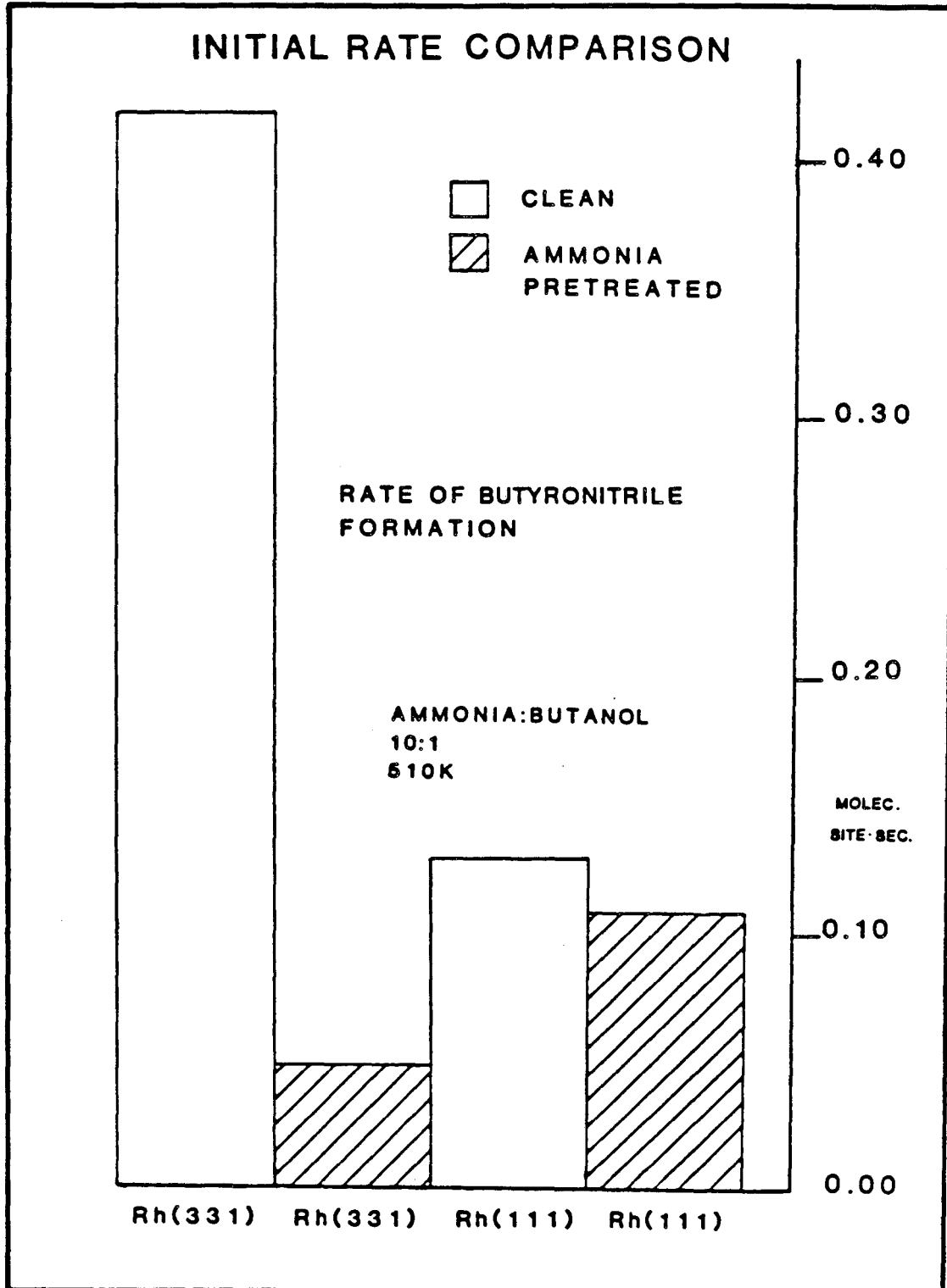| Reactants	Rates for Each Surface Studied	
	Rh(111)	Rh(331)
Alcohol and Ammonia	0.14	0.42
Aldehyde and Ammonia	0.17	0.13
Alcohol	0.44	0.92
Alcohol, Ammonia, and Hydrogen	0.02	0.08
Aldehyde, Ammonia, and Hydrogen	0.5	<0.01
Alcohol, Ammonia, and Water	0.01	0.01
Aldehyde, Ammonia, and Water	0.02	0.01

Rates listed as molecules per surface site per second.

In all reactions the pressure of ammonia was 100 torr. Aldehyde or alcohol pressure was 10 torr. Hydrogen 200 torr, and water 10 torr. Argon was used to make the total pressure 300 torr as necessary. All reaction temperatures were 515 K.

FIGURE CAPTIONS

Fig. 3.1 The rate of formation of butyronitrile from n-butanol and ammonia. A comparison between the initial rate of the clean and ammonia pretreated Rh(111) and Rh(331) surfaces is shown. 510 K, ammonia:butanol 10:1, total pressure reactants 110 torr.

Fig. 3.2 The butyronitrile product accumulation curve for the reaction of n-butanol and ammonia over Rh(111) and Rh(331) catalysts. 510 K, ammonia:butanol 10:1, total pressure reactants 110 torr.

Fig. 3.3 Arrhenius plots for the formation of butyronitrile from n-butanol and ammonia over Rh(111) and Rh(331) catalysts. Ammonia:butanol 10:1, 110 torr total reactant pressure.

Fig. 3.4 The n-butanol pressure dependence of butyronitrile production from n-butanol and ammonia over a Rh(331) catalyst. Ammonia constant = 100 torr, 510 K.

Fig. 3.5 The ammonia pressure dependence of butyronitrile production from n-butanol and ammonia over a Rh(331) catalyst. N-Butanol constant = 10 torr, 510 K.

Fig. 3.6 An AES spectrum of the active Rh(111) catalyst after a reaction of n-butanol and ammonia. Ammonia:butanol 10:1, 510 K, total reactant pressure 110 torr.

Fig. 3.7 TPD from a clean Rh(111) surface dosed at 300 K with n-butanol.

Fig. 3.8 TPD from an active after reaction surface of following the reaction of n-butanol and ammonia over a Rh(331) surface. Ammonia:butanol 10:1, 510 K, total reactant pressure 110 torr.

INITIAL RATE COMPARISON

□ CLEAN

▨ AMMONIA
PRETREATED

RATE OF BUTYRONITRILE
FORMATION

AMMONIA:BUTANOL
10:1
510K

MOLEC.
SITE·SEC.

0.40

0.30

0.20

0.10

0.00

Rh(331)   Rh(331)   Rh(111)   Rh(111)

XBL 8610-4160
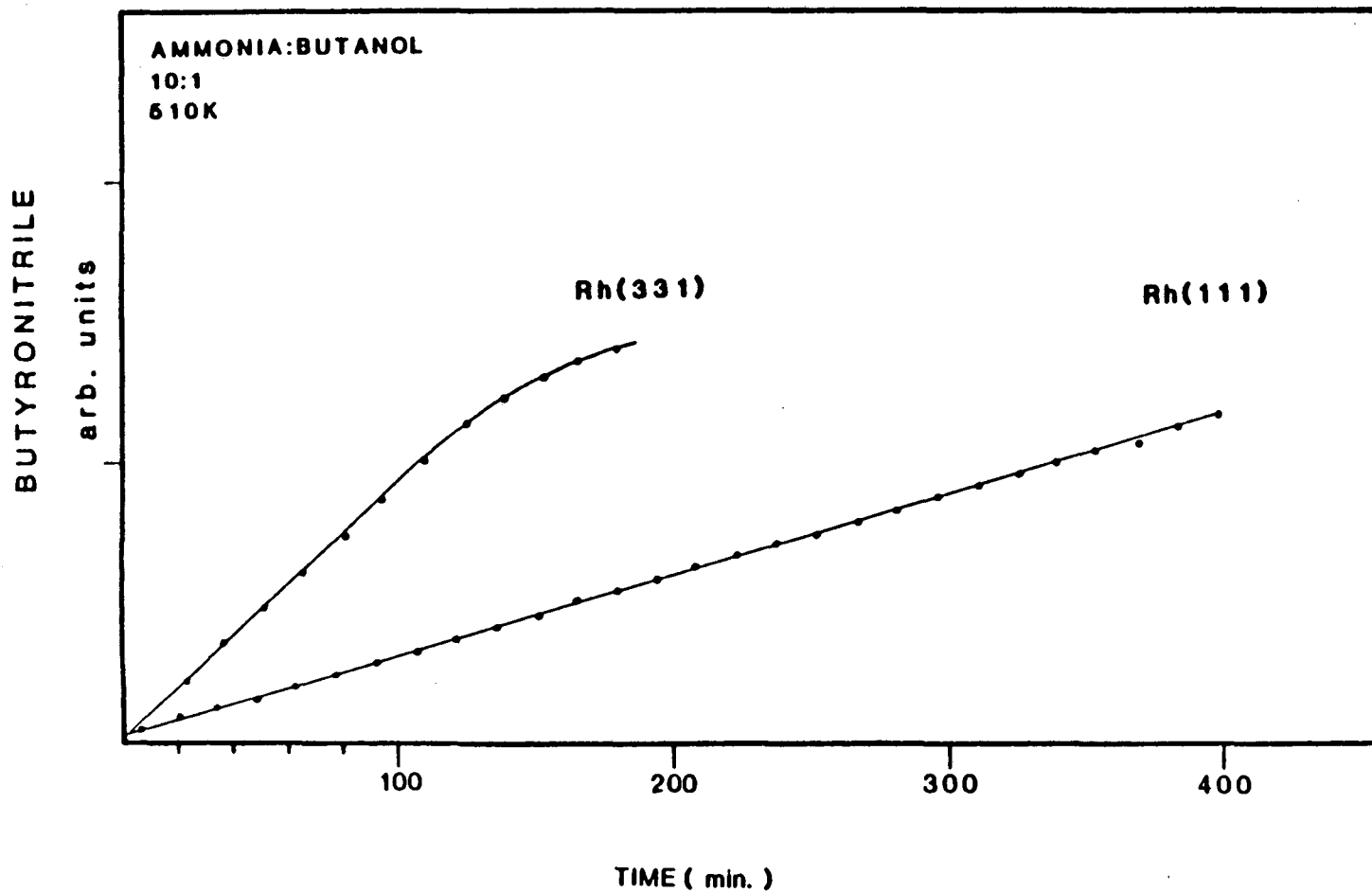
Fig. 3.1

PRODUCT ACCUMULATION

Fig. 3.2

XBL 8610-4159

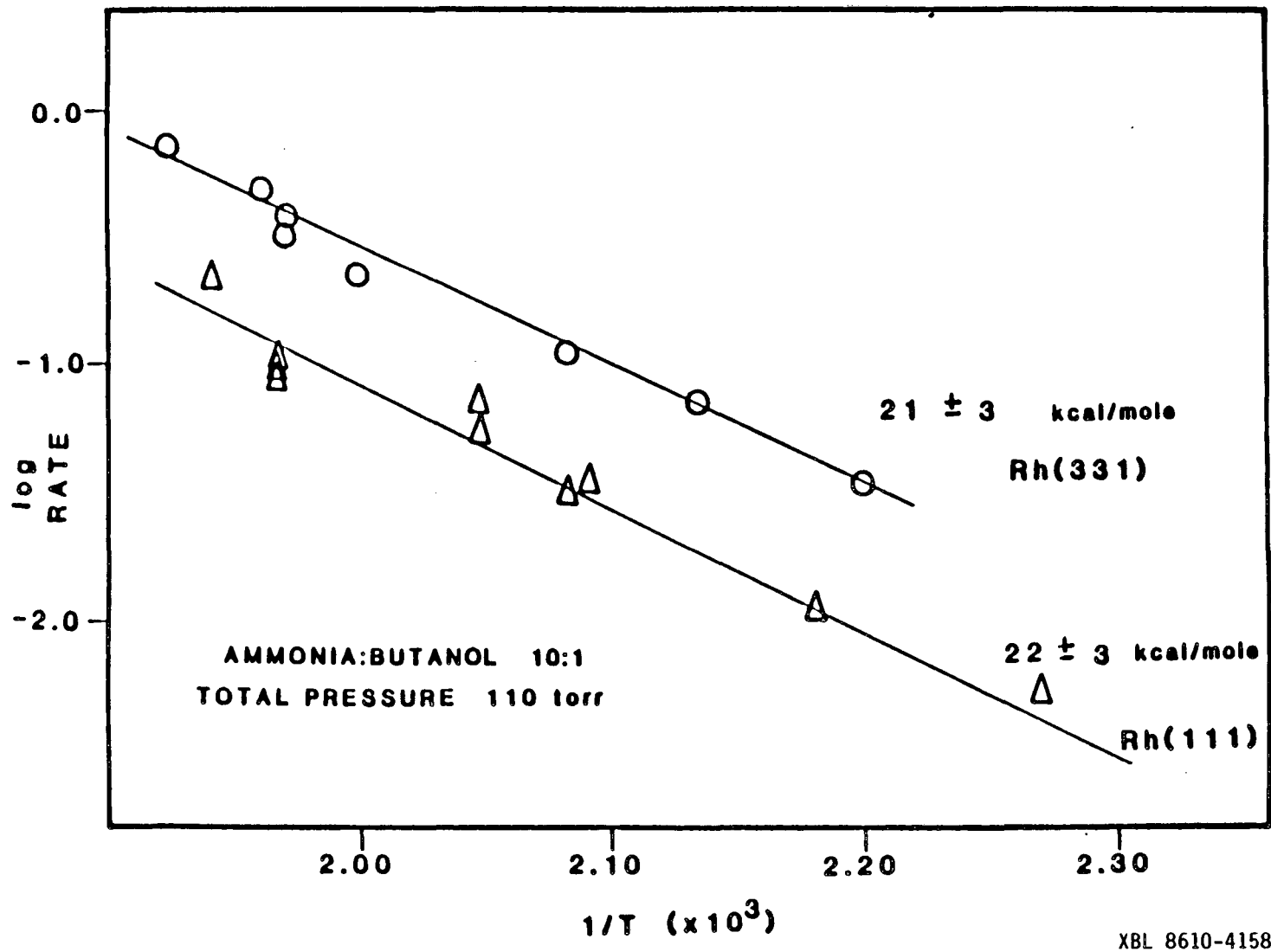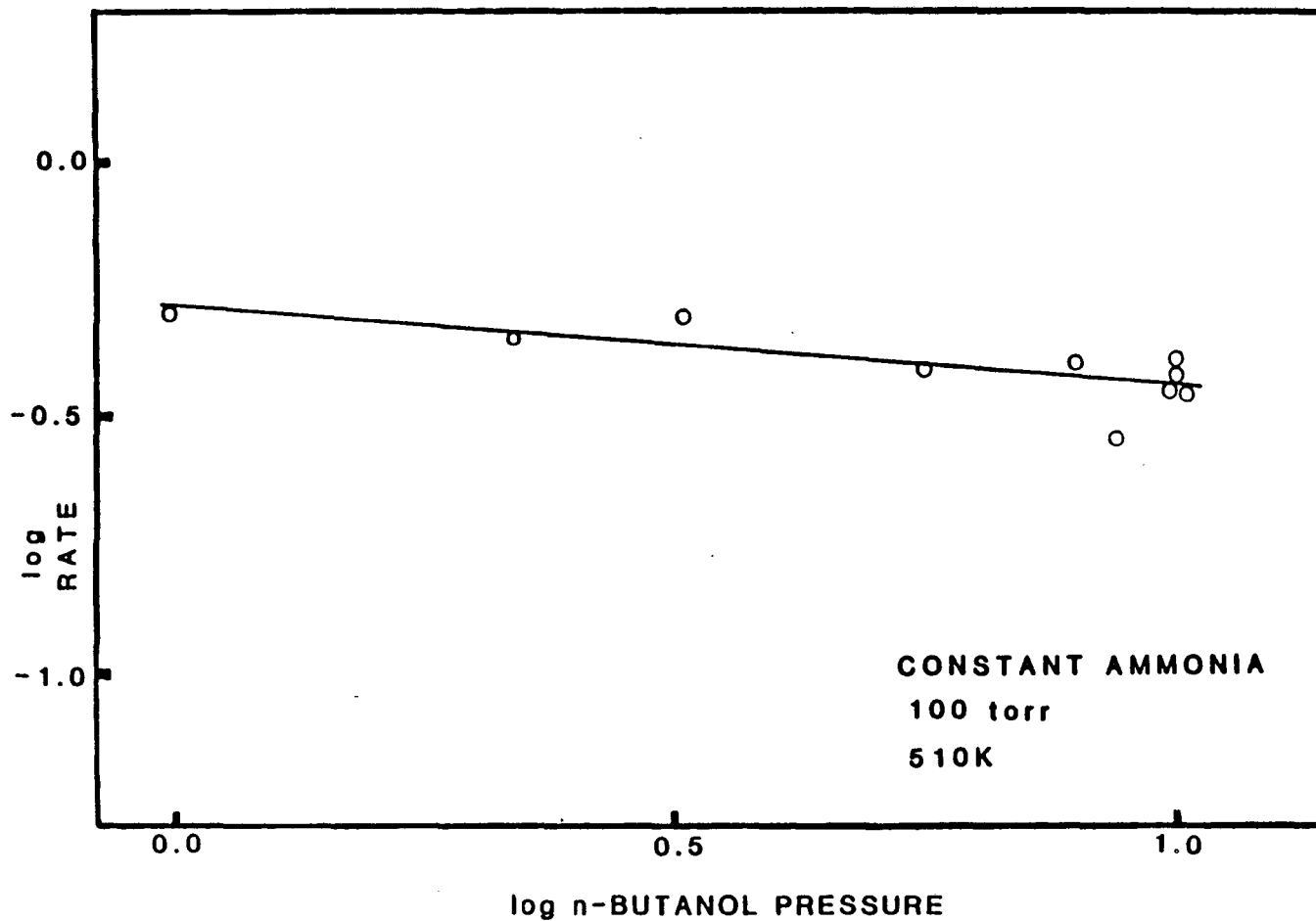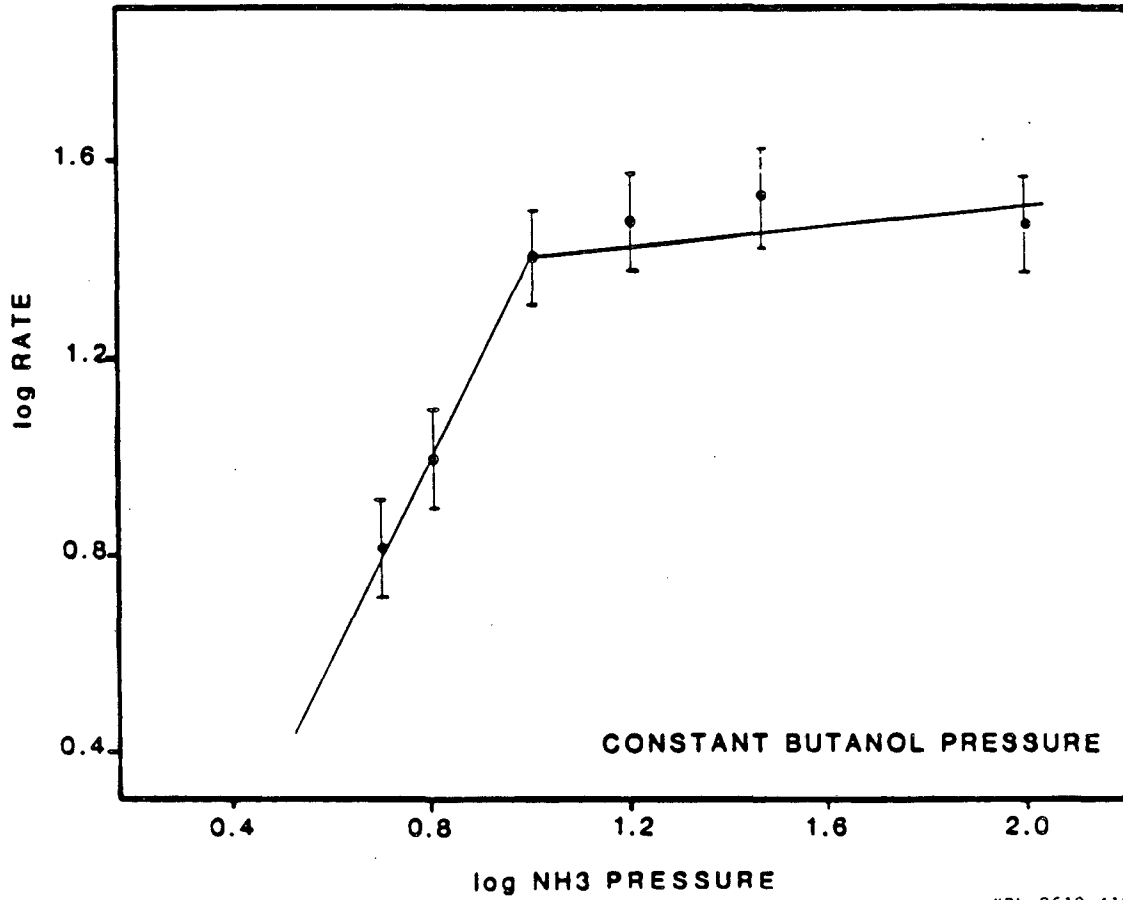# ARRHENIUS PLOTS FOR BUTYRONITRILE PRODUCTION

Fig. 3.3

XBL 8610-4158

BUTANOL PRESSURE DEPENDENCE FOR BUTYRONITRILE
FORMATION OVER Rh(331) CATALYST

Fig. 3.4

XBL 8610-4157

AMMONIA PRESSURE DEPENDENCE FOR BUTYRONITRILE FORMATION OVER Rh(331) CATALYST

CONSTANT BUTANOL PRESSURE

log RATE

log NH3 PRESSURE

XBL 8610-4156

Fig. 3.5

AES OF ACTIVE Rh(111) CATALYST AFTER REACTION

Fig. 3.6

n-BUTANOL TPD FROM Rh(111)

300K dose temperature

m/e 2

25 L

5 L

0.5L

0.05 L

m/e 28

25 L

5.0 L

0.5 L

0.05 L

XBL 8610-4154

Fig. 3.7

TPD FROM AFTER REACTION
Rh(331) SURFACE

NITROGEN

(m/e) 28

(m/e) 14

(m/e) 42   FRAGMENT

(m/e) 29   FRAGMENT

(m/e) 27   HCN

(m/e) 2

HYDROGEN

RELATIVE INTENSITY

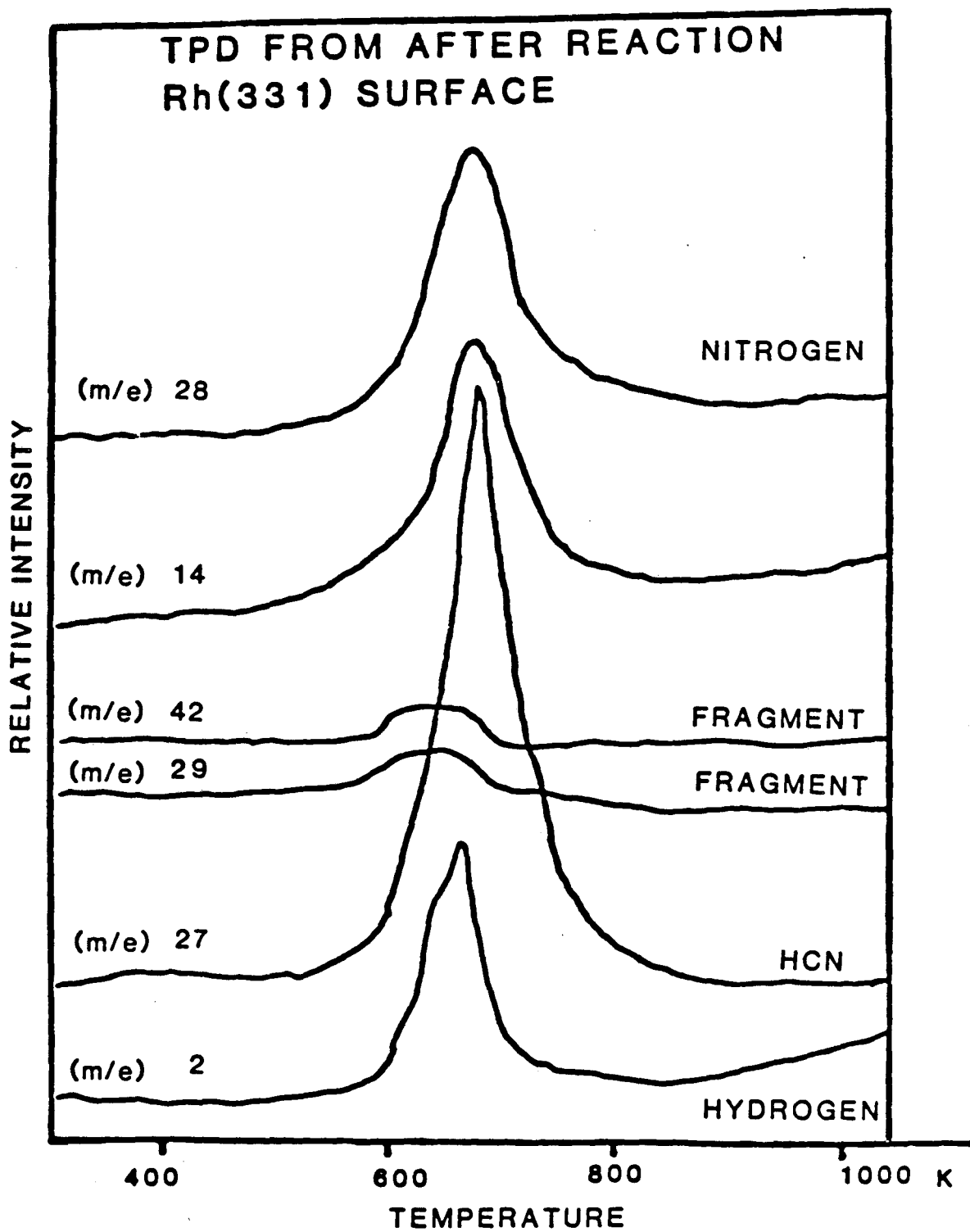400   600   800   1000   K

TEMPERATURE
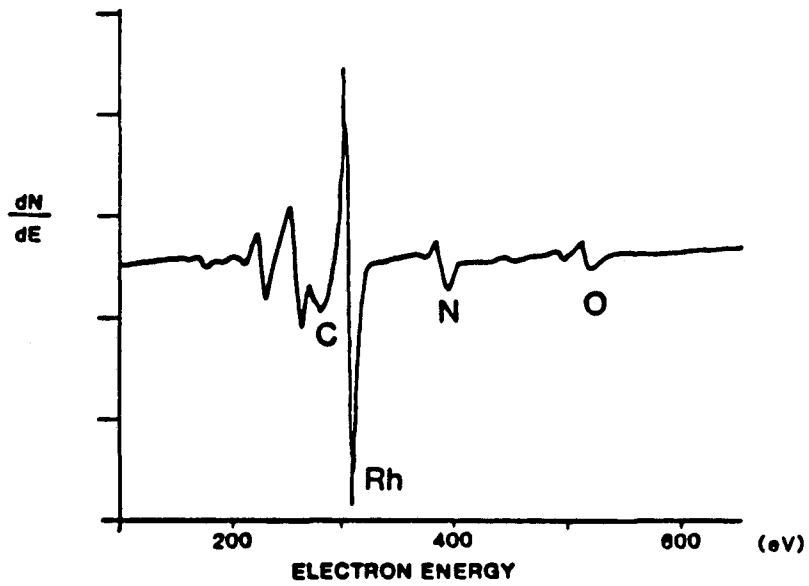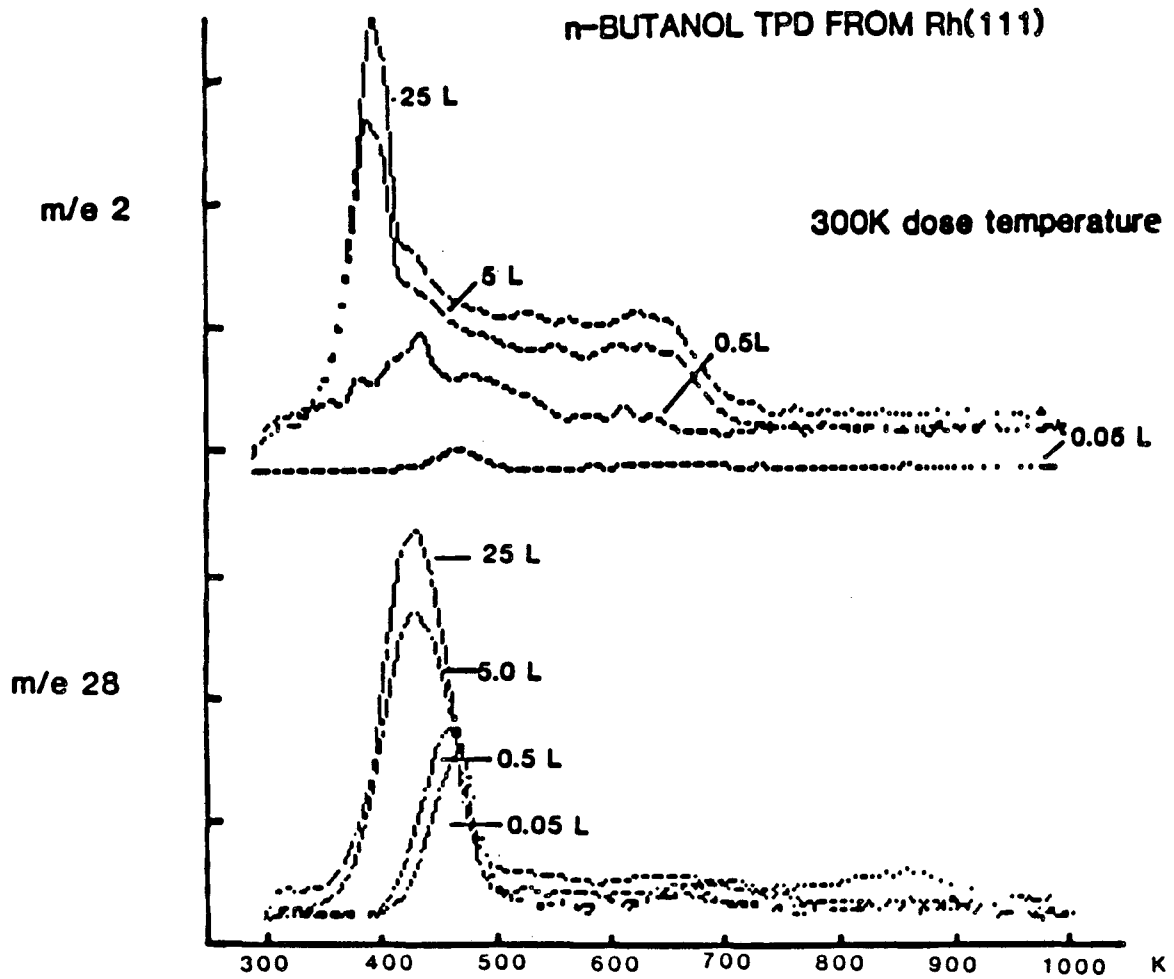
Fig. 3.8

XBL 8610-4153

IV. A COMPARISON OF SINGLE CRYSTAL Cu AND Rh CATALYSTS

FOR n–BUTANOL AMMONOLYSIS

4.1 Introduction

This chapter continues an investigation of the catalytic forma-
tion of n–butyronitrile from n–butanol and ammonia. In Chapter 3 it
was shown that this reaction occurs on a catalyst that is nearly com-
pletely covered with an overlayer of carbon, nitrogen, oxygen and hy-
drogen. In this chapter the same reaction is studied on a Cu(111) cat-
alyst. The motivation for this study is to investigate whether or not
a similar active overlayer would be formed on a different metal surface.

As shown in Chapter 3, this reaction has been reported to occur on
many different catalysts. A number of selective Cu catalysts for am-
monolysis have been studied. These are the copper catalyzed amination
of ethylene glycol,[1] the amination of long chain aliphatic alcohols
over a CuO/CrO catalyst,[2] and several related reactions that have been
disclosed in the patent literature.[3-7] None of these studies were done
on either single crystal or polycrystalline foil catalysts. No surface
analysis was done in any of the works.

In this chapter Cu and Rh(111) surfaces are compared as catalysts for
n–butanol ammonolysis. It is shown that copper behaves very much like Rh
with regard to catalyzing this reaction. The two catalysts have the same
activation energy, similar rates, product distributions and pressure de-
pendences. Both active catalysts form an overlayer composed of carbon, ni-
trogen and oxygen. This layer is qualitatively similar on the two metals.
These results suggest that this overlayer is an integral part of these cat-
alysts.

4.2 Results

In this work it is shown that a Cu(111) single crystal catalyst can selectively form n-butyronitrile from n-butanol and ammonia. The rate of formation of butyronitrile is 0.28 molecules/site·sec at 510 K, 10:1 ammonia:butanol, 110 Torr total pressure of reactants.

This reaction is very selective, with greater than 99% of the total product being butyronitrile. No amines or Schiff base products were observed in the product distribution. Small amounts (<1%) of the hydrogenolysis products methane, ethane and propane were noted.

This reaction exhibited Arrhenius type temperature dependence. Figure 4.1 shows an Arrhenius plot for this reaction. An activation energy of 26 ± 3 kcal/mole was obtained for this catalyst. The reactant conditions were 10:1 ammonia:n-butanol, 110 Torr total reactant pressure.

This catalyst was, in general, stable for a period of approximately 2 hours. A typical product accumulation curve is shown in Fig. 4.2. Even with this relatively short lifetime the total turnover for this catalyst was in all cases greater than 1000.

An additional piece of kinetic information is shown in Fig. 4.3. It shows that the ammonia pressure dependence of this reaction is zero to within the error of this experiment. These reactions were performed with a constant 10 Torr of n-butanol at 513 K.

Additional information concerning this reaction was obtained by surface analysis of the catalyst. Figure 4.4 shows an AES spectrum of the post reaction surface of an active catalyst. The surface of the

catalyst was covered by a layer containing carbon, nitrogen, and oxygen. The relative coverages of these 3 constituents was in this case C:N:O, 4:2:0.25. This value changed for a poisoned surface; the composition of a poisoned catalyst's overlayer was found to be C:N:O 6:2:0.5, indicating the accumulation of C during the poisoning of the catalyst.

To try and gain some idea about the composition of this overlayer TPD experiments were performed after the reaction. Figure 4.5 shows a multi-mass TPD spectrum taken after a reaction from an active catalyst. There are only 3 (m/e) desorptions from this catalyst. These are at (m/e)= 28, 14 and 27. The (m/e)= 28 and 14 desorptions at 700 K are due to N_2 desorption. This is the principle desorbing species. The ratio between the (m/e)= 28 and 14 desorptions is consistent with the observed N_2 cracking pattern. The (m/e)= 27 peak is most likely HCN. This assignment is based on the absence of any other (m/e) desorptions that would indicate the (m/e)= 27 desorption was a cracking fragment of a larger molecule. The (m/e)= 27 desorption which is at a maximum at 705 K has a different peak shape than the (m/e)= 28 and 14 desorptions which desorb at essentially the same temperature. No (m/e)= 2 hydrogen desorption was observed from the sample.

In addition to the above thermal desorption measurements, the clean Cu(111) surface was exposed to n-butanol, ammonia, and butyronitrile. In all cases 50L doses at 300 K produced no AES or TPD features. This indicates that the sticking probability of any of these molecules on Cu(111) at this temperature is very small.

Several other experiments were done in order to obtain additional information about the mechanism for this reaction. As it was known that the aldehyde formed by dehydrogenation of n-butanol was a possible intermediate in this reaction, this reaction was studied independently. The alcohol to aldehyde oxidation reaction was found to be about one order of magnitude faster than the overall conversion of alcohol to nitrile observed. A rate of 3.1 molecules/site·sec of butyraldehyde formation was obtained. The reaction conditions for the oxidation reaction were 10 Torr of n-butanol and a temperature of 513 K.

The effect of hydrogen upon this reaction was also studied. A reaction mixture of 10 Torr n-butanol, 100 Torr ammonia, and 300 Torr hydrogen gave the same product distribution and rate as in the hydrogen-free case.

4.3 Discussion

In this section the results for the ammonolysis of n-butanol over Cu(111) will be discussed and compared with the results of the previous chapter's using a Rh(111) catalyst. Both of these catalysts have been shown to selectively catalyze this reaction.

These experiments have shown that both the Cu(111) and Rh(111) surfaces will form butyronitrile from n-butanol and ammonia. This reaction was shown to have an activation energy of 26 ± 3 kcal/mole on Cu and 22 ± 3 kcal/mole on Rh. These numbers, which are the same within the error of the measurements, indicate that there is probably no difference in the rate limiting step of the mechanism for nitrile formation over these two catalysts. The other kinetic parameters are also consistent with this observation.

The selectivity for both of these catalysts was the same (>99% butyronitrile). The rate on the Cu catalyst was 2-3 times faster than that measured for Rh under similar conditions.

A difference was noted in the lifetime of the two catalysts. The Cu(111) surface poisoned at a significantly faster rate than the Rh(111). The source of poisoning was a build up of carbon.

In both cases the results indicate that the aldehyde is a likely intermediate in the reaction of the alcohol with ammonia. This is inferred by the fast rate of conversion of alcohol to aldehyde on both catalysts. These were 3.1 and 0.44 molecules/site·sec for Cu and Rh respectively, as compared to overall nitrile formation rates of 0.28 and 0.11 molecules/site·sec. In both cases this hypothesis is

supported by a build-up of aldehyde in the reactor (as monitored by water addition) and the ability to form the nitrile directly from the aldehyde.

An integral part of the functioning catalyst on both the Cu and Rh metals was the overlayer that was present. In both cases the overlayer covered much of the catalyst surface (5% of the Rh CO sites were available, no convenient probe molecules like CO adsorb on Cu, making similar estimates for Cu impossible.) The overlayers were qualitatively similar in stochiometry and in the TPD spectra they produced, but there were some differences in the apparent composition of the two overlayers. The Cu catalyst's overlayer had N_2 as its principle desorption product, with the only other (m/e) desorption at 27. This situation was quite different in Rh where (m/e)= 27 was the principle desorption and (m/e)= 2, 29 and 41 desorption were noted. The absence of these other desorptions from the Cu catalyst suggests some differences in the structure of this overlayer; namely a lack of H_2, and an absence of the fragments assigned to molecular imine desorption from Rh. One of these differences could potentially explain the difference in lifetime noted for the two catalysts. On Cu, as on Rh we believe that carbon accumulation is the reason for the poisoning of this catalyst. On Cu there is very little hydrogen present in the overlayer. As a result, most of the carbon present is probably an inactive carbonaceous deposit, that continues to grow and quickly poisons the catalyst. This layer could not be removed upon the addition of hydrogen as on Rh.

Due to the absence of the (m/e)= 29 and 41 desorptions it is difficult to say whether or not an imine intermediate was present on the Cu surface as was hypothesized for the Rh. It is possible that the HCN desorbing is from such a molecule decomposing, but it seems unlikely due to the absence of the hydrogen evolution that would probably accompany this event. Because of this it is difficult to assert that an imine molecule is an actual part of the overlayer on Cu. It seems more likely that the imine is less strongly bound on Cu and as such its surface concentration is much lower.

In addition to the above mentioned carbonaceous deposit that is implied by the carbon AES and lack of H_2 evolution, the rest of the Cu overlayer consists of molecules which produce only (m/e)= 27 (HCN) and N_2 upon desorption. It would be pure speculation to assign these desorptions to any other molecular entity on the surface but these two molecules (HCN and N_2) themselves, and as such the structure of the Cu overlayer remains somewhat vague. As a result it is not possible to hypothesize this overlayer's role in the reaction on copper.

Aside from the differences described in the overlayer the other data comparing the Cu and Rh catalysts suggest the same imine intermediate model. The rates of nitrile formation, the rates of alcohol to aldehyde conversion, the zero order NH_3 pressure dependences, and the rapid interaction of the aldehyde and ammonia are all similar, and all consistent with the model suggested in Chapter 3.

This comparison between Cu and Rh illustrates some of the similarities in their relative abilities to catalyze this reaction. The data just listed shows that both metals can dehydrogenate the alcohol, and quite possibly dehydrogenate an imine molecule. Certainly both catalysts function with an overlayer covering much of their surface, albeit one that is quantitatively different between the two. An interesting difference appears in their apparent ability to hydrogenate the imine and/or the carbonaceous fragments present on the metal. Cu does not strongly chemisorb hydrogen,[8-10] and as such its ability to dissociate H_2 seems limited. This results in the inability to form amines or the related compounds seen on Rh, and also in the inability to hydrogenate fragments under the reaction conditions used to obtain these results on Rh. This also is quite possibly the reason for the increased rate of catalyst deactivation due to carbon accumulation.

REFERENCES

4.1 Runeberg, J., Baiker, A., and Kijenski, J., Applied Catalysis $\underline{17}$, 309 (1985).

4.2 Baiker, A., and Richarz, W., Ind. Eng. Chem. Prod. Res. Rev. $\underline{16}$, 261 (1977).

4.3 U.S. Patent 3,022,349 to to Union Carbide Corp., R.C. Lemon et al., 2/20/67.

4.4 U.S. Patent 3,270,059 to B.A.S.F., S. Winderi et al., 1/15/63.

4.5 U.S. Patent 4,014,933 to B.A.S.F., G. Boettger et al., 8/27/73.

4.6 U.S. Patent 3,520,933 to B.A.S.F., K. Adam and E. Haarer, 10/23/67.

4.7 U.S. Patent 3,151,115 to Jefferson Chemical Co., P.H. Moss and N.B. Godfrey, 5/26/61.

4.8 Balooch, M., Cardillo, N.J., Miller, D.R., and Stickney, R.E., Surf. Sci. $\underline{46}$, 358(1974).

4.9 Cardillo, M.J., Balooch, M., and Stickney, R.E., Surf. Sci. $\underline{50}$, 263(1975).

4.10 Gelb, A. and Cardillo, M.J., Surf. Sci. $\underline{64}$, 197(1977).

FIGURE CAPTIONS

4.1 The Arrhenius plot for the formation of butyronitrile from n-butanol and ammonia over a Cu(111) catalyst. Reaction conditions were 10:1 ammonia:n-butanol, total pressure of reactants 110 torr.

4.2 A product accumulation curve for butyronitrile formed from n-butanol and ammonia. Reaction temperature 513 K, total pressure reactants 110 torr, ammonia:n-butanol, 10:1.

4.3 The ammonia pressure dependence of the reaction of n-butanol and ammonia to form butyronitrile over a Cu(111) catalyst. Reaction conditions were a constant 10 torr of n-butanol and a temperature of 513 K.

4.4 Auger spectrum of a post reaction active Cu(111) catalyst surface. Taken after a reaction of n-butanol with ammonia.

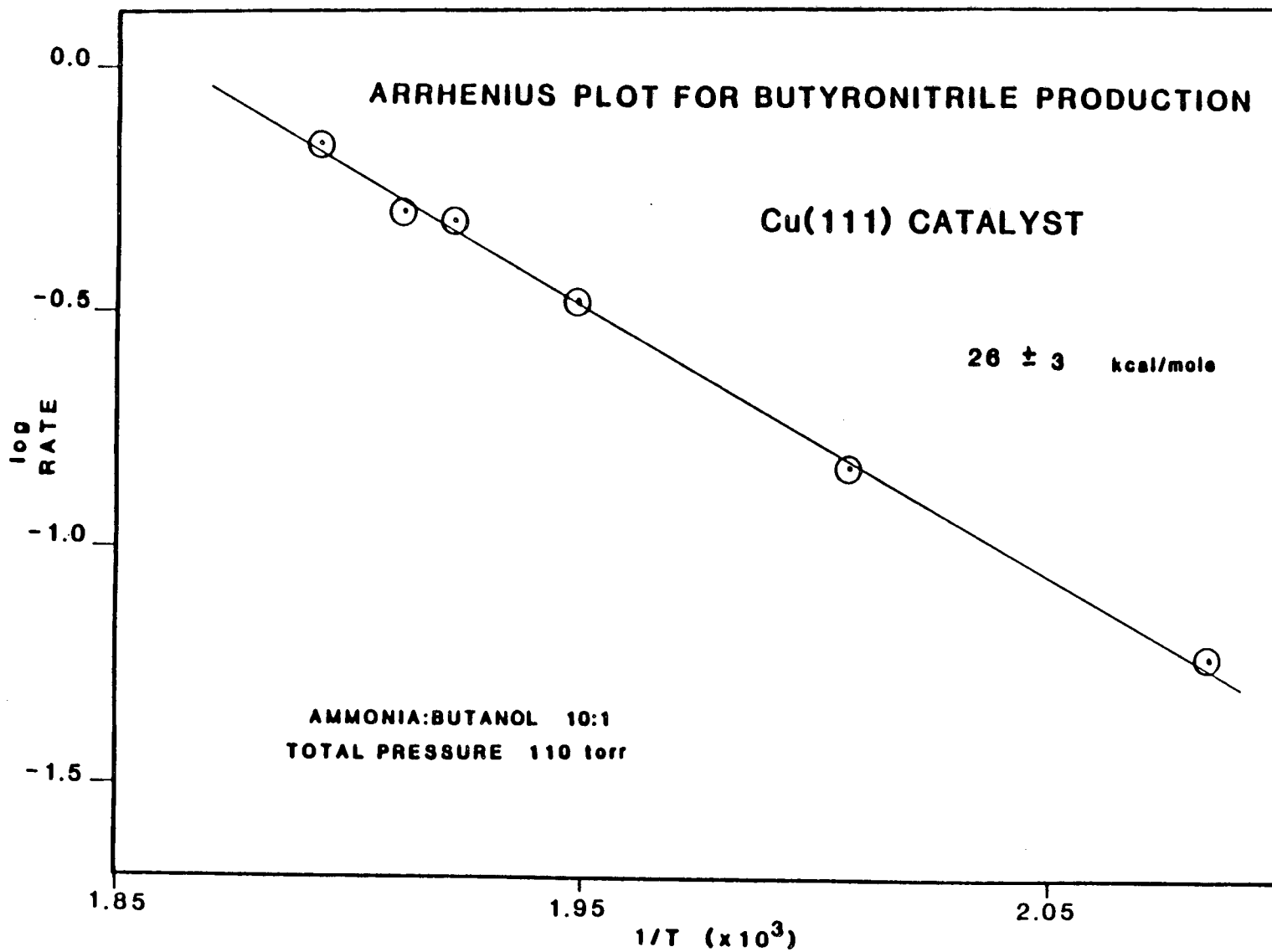4.5 TPD of the active after reaction Cu(111) catalyst surface. Taken following a reaction of n-butanol with ammonia.

ARRHENIUS PLOT FOR BUTYRONITRILE PRODUCTION

Cu(111) CATALYST

26 ± 3 kcal/mole

AMMONIA:BUTANOL 10:1
TOTAL PRESSURE 110 torr

1/T (x10³)

XBL 8610-4148

Fig. 4.1

PRODUCT ACCUMULATION

AMMONIA:BUTANOL
10:1
610K

BUTYRONITRILE arb. units
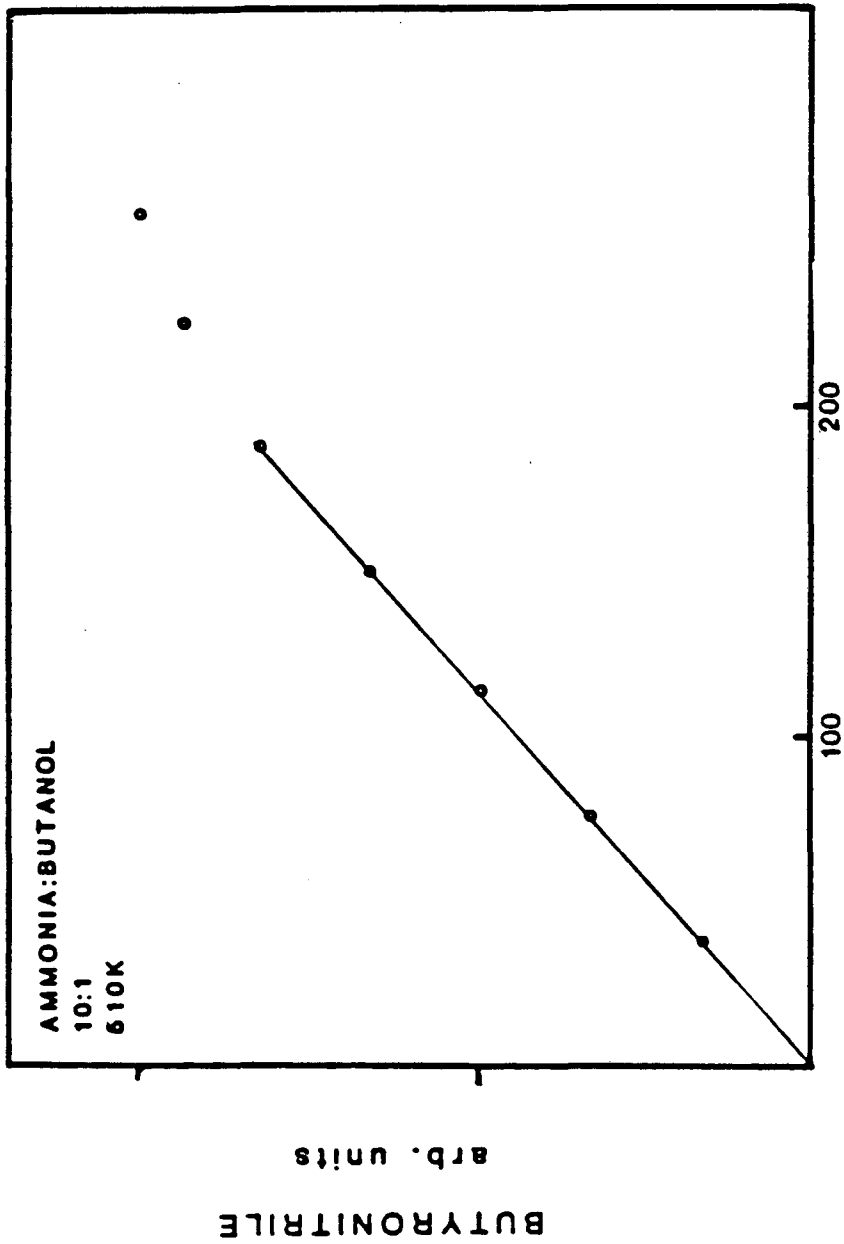
TIME (min.)

200

100

XBL 8610-4152

Fig. 4.2

AMMONIA PRESSURE DEPENDENCE FOR BUTYRONITRILE FORMATION OVER Cu(111) CATALYST
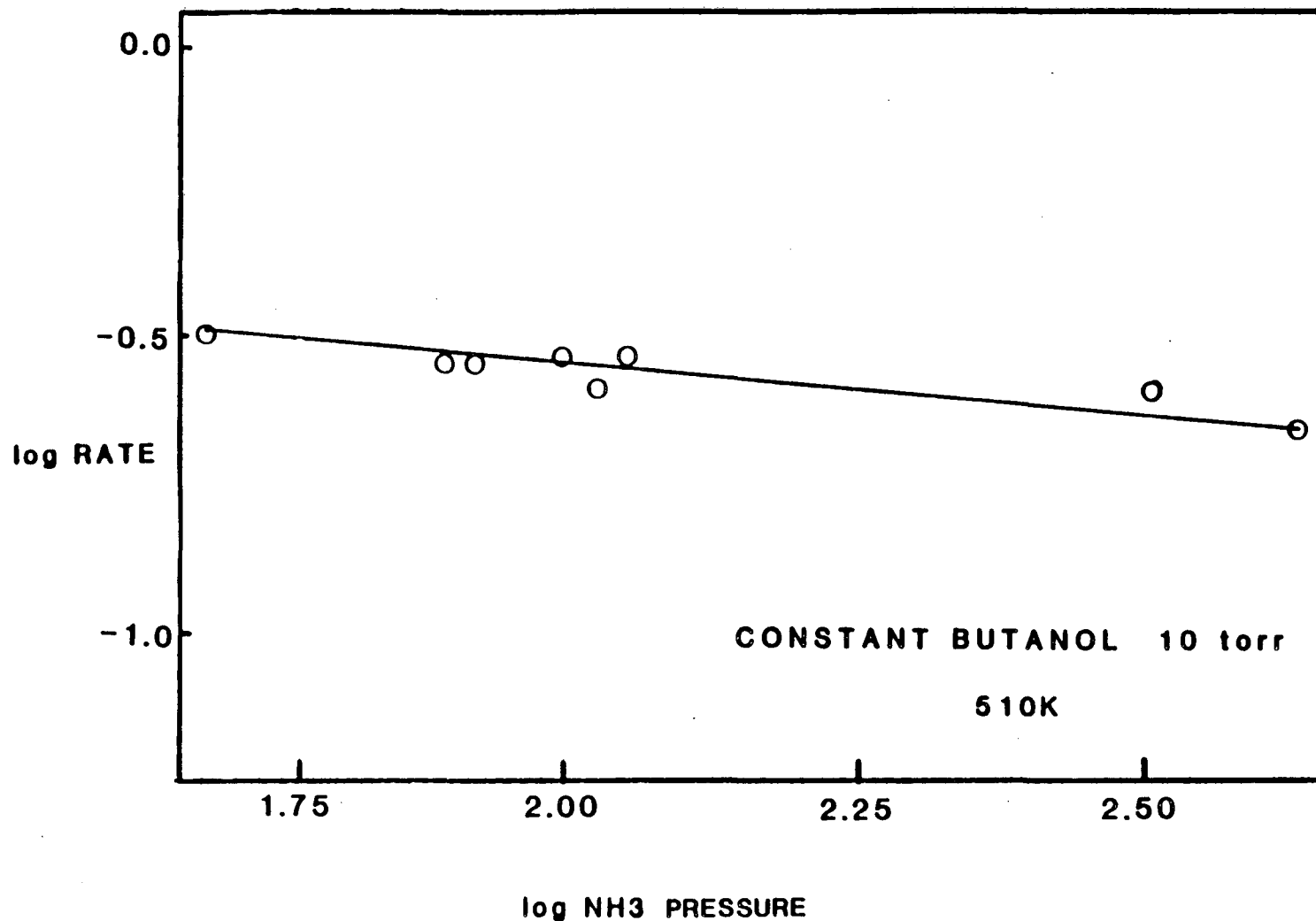
Fig. 4.3

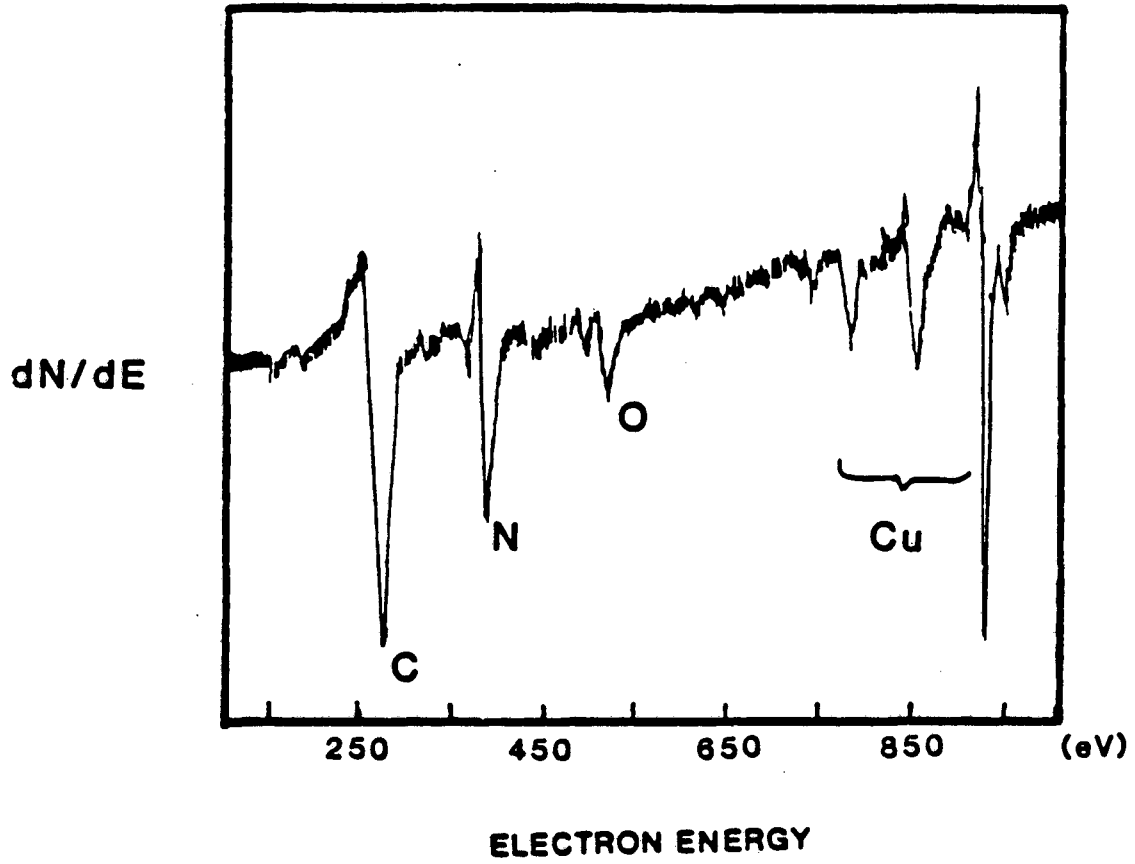XBL 8610-4149

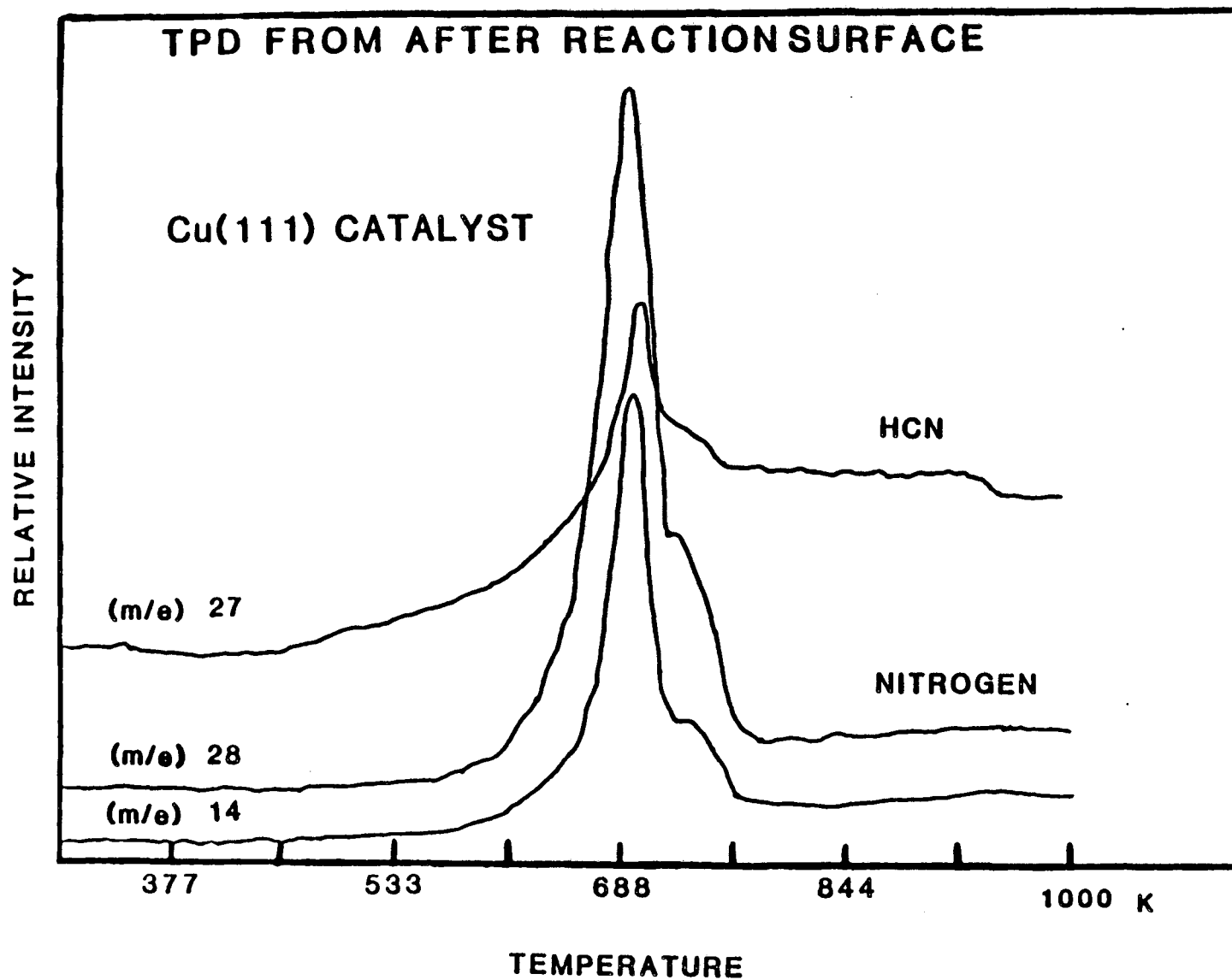# AFTER REACTION SURFACE ANALYSIS VIA AUGER

Cu(111) CATALYST

ELECTRON ENERGY

Fig. 4.4

XBL 8610-4150

TPD FROM AFTER REACTION SURFACE

Cu(111) CATALYST

HCN

NITROGEN

(m/e) 27

(m/e) 28

(m/e) 14

RELATIVE INTENSITY

377   533   688   844   1000 K

TEMPERATURE

XBL 8610-4151

Fig. 4.5

V. THE HYDROGENATION OF CARBON MONOXIDE OVER MODEL RHENIUM CATALYSTS: ADDITIVE EFFECTS AND A COMPARISON WITH IRON

5.1 Introduction

The hydrogenation of carbon monoxide to produce hydrocarbons at a high rate and selectivity is under intensive study in many laboratories. Many different transition metals and transition metal compounds have been identified as good catalysts to produce C_1 molecules (methane, methanol),[1] high molecular weight liquid fuels[2] or oxygenated molecules (acetaldehyde and higher alcohols).[3] Often promotion by alkali yields increased molecular weight products and a lower concentration of ethane,[4,5] while transition metal oxide catalysts produced more of the oxygenated species.[3,6,7]

Rhenium has received relatively little attention as a catalyst in comparison with other transition metals. Nevertheless, rhenium has recently been shown to be a very active catalyst for ammonia synthesis.[8] CO and N_2 bond scission are thought to be prerequisites for both ammonia synthesis (N_2/H_2) and CO hydrogenation (CO/H_2). Since iron is known to be active in both reactions and rhenium is active for the ammonia synthesis, it can be inferred that rhenium might also display good catalytic behavior for CO hydrogenation. In one survey study, promoted rhenium oxides on silica support were reported to have high selectivity for alcohol production.[9]

The purpose of this work is to explore the catalytic activity of rhenium metal foil for the hydrogenation of CO when clean and in the presence of alkali and oxygen and to compare its activity and selectivity with that of iron.

5.2 Results

Figure 5.1 shows an example of the results of methane accumulation versus time for a rhenium foil. The experimental conditions were $H_2/CO=4/1$, 32 psig total pressure, and a reaction temperature of 260°C. The runs were characterized by a long stable period of constant reaction rate, which would eventually decay after several hours. As will be discussed below, this decline in the rate of methane formation is attributable to the slow build-up of a carbonaceous layer which poisoned the surface.

From the rate of methane production at various temperatures, Arrhenius plots were constructed. Figures 5.2 and 5.3 show Arrhenius plots for various runs on rhenium and iron foils. The slope of the plots allowed determination of the activation energies of the reactions. In addition, by looking at the temperature at which the linear plot started to bend over it can be see where rapid surface poisoning began, primarily due to carbon accumulation.[11] Methane was the dominant product on the initially clean rhenium samples that were studied.

The activation energies and the selectivities of rhenium and iron foils are displayed in Fig. 5.4. The turnover frequencies (molecules/site·sec) reported were the maximum values reached by the catalyst following an induction period (usually less than 20 minutes after initiation of the reaction). The turnover frequency listed assumed an active number of surface sites of 10^{15}.

Figure 5.5 shows how the selectivities changed as a function of temperature. As noted in Fig. 5.4, the activation energy for ethylene formation was lower than that for methane. Thus methane production should be favored by higher temperatures, as was observed.

The amount of carbon on the surface after a given run was a function of catalyst pretreatment, reaction temperature, and reaction time.

Figure 5.7 shows the product distributions over the rhenium and iron surfaces following alkali and oxygen promotion. The general pattern observed with the alkali promoter was a change in selectivity towards higher molecular weight products as well as a decrease in the rate of methanation. The effect was more marked with rhenium than with iron, as clean iron already produces a large fraction of higher molecular weight species.

Preoxidation of the surface caused an opposite effect to what was observed with the addition of sodium, a higher selectivity towards methane. A problem occurred here concerning the number of active sites to be used in calculating turnover frequencies (in Fig. 5.2). Oxidation tends to increase the surface area of the catalyst. In addition, the degree of oxidation changes throughout the reaction as a function of catalyst temperature, reaction time, and partial pressure. It seems however that the values reported here are correct to within 50 percent as these results are in good agreement with the behavior of industrial iron Fischer-Tropsch catalysts.[6]

5.3 Discussion

Rhenium metal appears to be a methanation catalyst that produces CH_4 at lower rates than either nickel or iron but with an activation energy that is similar to these two more active metals. Thus, the mechanism for producing methane is likely to be similar, i.e. CO dissociation followed by sequential hydrogenation of the carbon and the CH_x fragments. The large carbon build-up on the rhenium surface indicates that CO dissociation is facile and also that the hydrogenation step is likely to be rate determining.

The degree of carbon build-up on the samples was measured by AES. It was thus possible to distinguish between an active "carbidic" carbon, and an inactive "graphitic" one. This classification has been discussed extensively by other authors and results either from a comparison of the post reaction carbon AES peak shape with known peak shapes of metal-carbide and graphite surfaces,[5,11] or with corresponding XPS studies.[5] The overlayers also contained large amounts of adsorbed (or trapped) oxygen, hydrogen and hydrocarbons, as was noticed in thermal thermal desorption following the reaction. Therefore, the carbidic overlayer should not be considered as simply a surface or bulk metal carbide, but as a complex overlayer consisting of species where metal-carbon, carbon-hydrogen, and carbon-oxygen bonds exist. "Carbidic" carbon was the dominant surface species observed following low temperature, short reaction time experiments. "Graphitic" carbon was dominant following high temperature experiments,

or after flashing any post-reaction surface to >700 K. At this temperature, carbon-carbon bonding in graphitic layers covers much of the surface.

On the iron catalyst the oxidation of the surface caused a significant change in the activation energy, as shown in Fig. 5.2. This means that hydrogenation on this oxycarbide surface has a higher activation energy than on a metal surface. This may be expected since H addition is thought to be the rate limiting step and metal, in general, dissociates and transfers H easier than carbon and oxygen.

In general, the presence of alkali on the surface accelerated the rate of carbon build-up. A commonly invoked model states that by lowering the dipole field at the surface, potassium allows the metal to more easily backdonate into the CO $2\pi^*$ antibonding orbitals[10,12,13] then can readily dissociate at reaction temperatures. This results in increased atomic carbon on the surface and hence an increase in the carbon to hydrogen ratio. Consequently, the decreased overall reaction rates in the presence of the sodium can be explained by the change in carbon to hydrogen ratio. Assuming that hydrogenation is the slow step.[11] If CO dissociation were the rate determining step, the presence of the alkali would likely result in an increased reaction rate. The altered surface carbon to hydrogen ratio can also explain the change in selectivity towards high molecular weight species. This should occur since the rate of carbon-carbon bond formation will be increased relative to the rate of carbon-hydrogen bond formation.

In studies by Dwyer and Hardenbergh on iron foils and powders[14,15] it was shown that the poisoning of iron foils by carbon deposition was not observed for iron powders. Although the turnover frequencies on powders were lower than those observed on foils, they showed that even the bulk iron carbide (Fe_5C_2) powder created during a reaction displayed behavior on both unpromoted and alkali promoted sample which was similar to known industrial reactivity (and that described in this work). In addition, they showed that the carbonaceous layers on iron powders contained more and longer hydrocarbon chains when alkali was used as a promoter.

Another interesting observation was that only sodium, oxygen, and carbon (i.e., not rhenium or iron) were visible in the Auger spectra following several reactions (see Fig. 5.7). This was also observed by Bonzel and Krebs,[16] and they suggested that a potassium oxide layer was floating on top of a carbonaceous layer. We would further suggest that the alkali oxide (or suboxide) layer can itself play an important role in the catalytic reaction. Alkalis have long been useful as catalysts in the steam gasification of carbon sources. The possibility that the build-up of the carbonaceous layer is being hindered by the ability of alkalis to catalyze the reaction of water with carbon must be considered.[17] Within this framework, alkali increases both the rate of CO dissociation (hence carbon build-up) and the rate of removal of the carbonaceous layer, once formed.

The effect of pre-oxidation of the rhenium and iron surfaces depended upon the degree to which the surface was pre-oxidized and the temperature and time of the reaction. The extent of catalyst oxidation grew when water was introduced into the gas-phase, allowing the surface to better resist the carbon build-up so apparent in most of the experiments. Although the initial reaction rates did not increase the rate of poisoning was slower for oxidized surfaces.

Another significant change induced by oxidation was the change in selectivity towards lower molecular weight species. By reducing both the amount of surface carbon and the number of adjacent metal atoms, the oxide surface does not permit extensive C-C bond formation. No significant amounts of oxygenates were detected over our low surface area rhenium and iron foils, in contrast to high surface area promoted industrial catalysts.[4,6,7]

Conclusion

Rhenium metal has been shown to be less active than iron and to have a relatively low selectivity towards higher molecular weight hydrocarbons. Thus rhenium acts more like nickel than iron in its CO hydrogenation behavior. Alkali monolayers decreased the reaction rates and changed the selectivity towards higher molecular weight species. These effects result from a higher carbon to hydrogen ratio on the surface. These results are consistent with both the known industrial behavior[4,6,7] and recent UHV experiments showing an increased tendency for CO to dissociate when alkali is coadsorbed.[5,18,19,20] The oxidation of the surface caused selectivity changes to lower molecular weight products.

116

5.4 References

5.1 Somorjai, G.A., in: Catalysis Rev. Sci. Eng. (1981).

5.2 Bell, A.T., in: Catalysts Rev. Sci. Eng. (1981).

5.3 Watson, P.R., and Somorjai, G.A., J. Catal. 74, 282 (1982).

5.4 Anderson, R.B., J. Catal. 4, 56 (1965).

5.5 Wesner, D.A., Coener, F.P., and Bonzel, H.D., Lang. Vol. 1 (4), 478 (1985).

5.6 Vannice, M.A., Cat. Rev. Sci. Eng. 14(2), 153 (1976).

5.7 Natta, G., in: Catalysis, Vol. 3 and 5, (P.H. Emmett, ed.) Reinhold, New York (1955).

5.8 Spencer, N.D., and Somorjai, G.A., J. Catal. 78, 142 (1982).

5.9 Tsunda, Chem. Lett., Chem. Soc. Japan, 819 (1981).

5.10 Garfunkel, E.L., Ph.D. thesis, Univ. California Berkeley (1983).

5.11 a. Goodman, D.W., Kelley, R.D., Madey, J.E., and Yates, J.T., J. Catal. 63, 226 (1980).

b. Campbell, G.T., and Goodman, D.W., Surf. Sci. 123, 413 (1982).

5.12 Nieuwenhuys, B.E., Surf. Sci. 105, 505 (1981).

5.13 Luftman, H., Sun, Y.M., and White, J.M., Surf. Sci. 139 369 (1984).

5.14 Dwyer, D.J., and Hardenbergh, J.H., Appl. Surf. Sci., in press.

5.15 Dwyer, D.J., and Hardenbergh, J.H., J. Catal. 87, 66 (1984).

5.16 Bonzel, H.D., and Krebs, H.J., Surf. Sci. 109, L527 (1981).

5.17 Wen, W.Y., Cat. Rev. Sci. Eng. 22, 1 (1980).

5.18 Kiskanova, M., Surf. Sci. 111, 584 (1981).

5.19 Benziger, J., and Madix, R.J., Surf. Sci. <u>94</u>, 119 (1980).

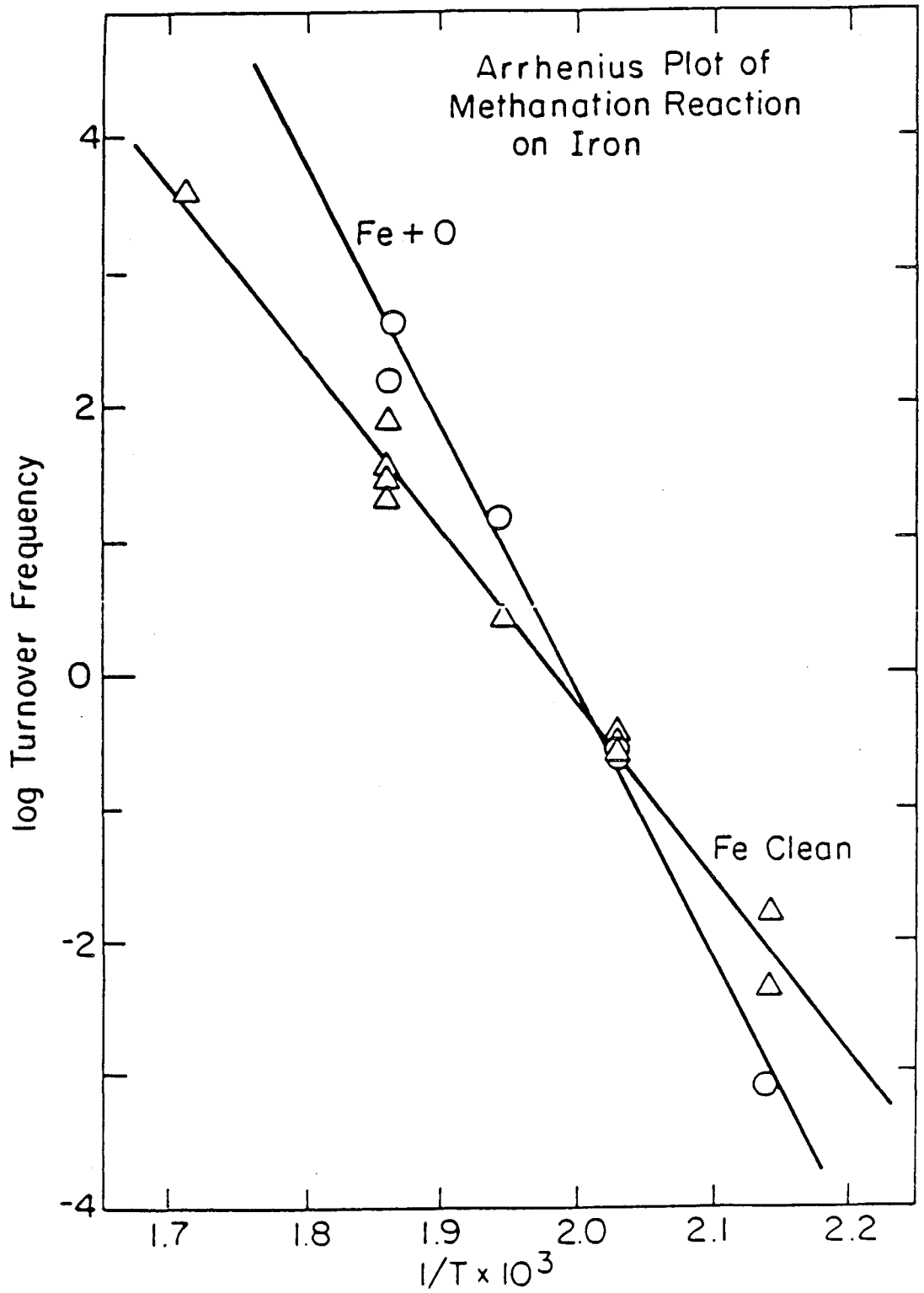5.20 Crowell, J.E., Garfunkel, E.L., and Somorjai, G.A., Surf. Sci. <u>121</u>, 301 (1982).

FIGURE CAPTIONS

Fig. 5.1 Product accumulation curve for CO hydrogenation over rhenium foil. $H_2/CO = 4/1$; 1 atm.

Fig. 5.2 Arrhenius plot of methanation reaction on iron. $CO/H_2 = 1/4$, 32 psi.

Fig. 5.3 Arrhenius plot of methanation reaction on rhenium. $CO/H_2 = 1/4$, 32 psi.

Fig. 5.4 A comparison of the selectivities for C_1 and C_2 species at 540 K, $CO/H_2 = 1/4$, 32 psi, over iron and rhenium foils.

Fig. 5.5 Temperature dependence of the product selectivity for CO hydrogenation on rhenium foil, $CO/H_2 = 1/4$, 32 psi.

Fig. 5.6 The effect of oxidation and alkali addition on product selectivity.

Fig. 5.7 Auger spectra of a sodium oxide promoted sample prior to (B) and following (A) a catalytic reaction.

CO Hydrogenation over Re foil
$H_2/CO = 4/1$; 32 psi

Fig. 5.1

XBL 85 2-5827

Arrhenius Plot of
Methanation Reaction
on Iron

Fe + O

Fe Clean

log Turnover Frequency

$1/T \times 10^3$
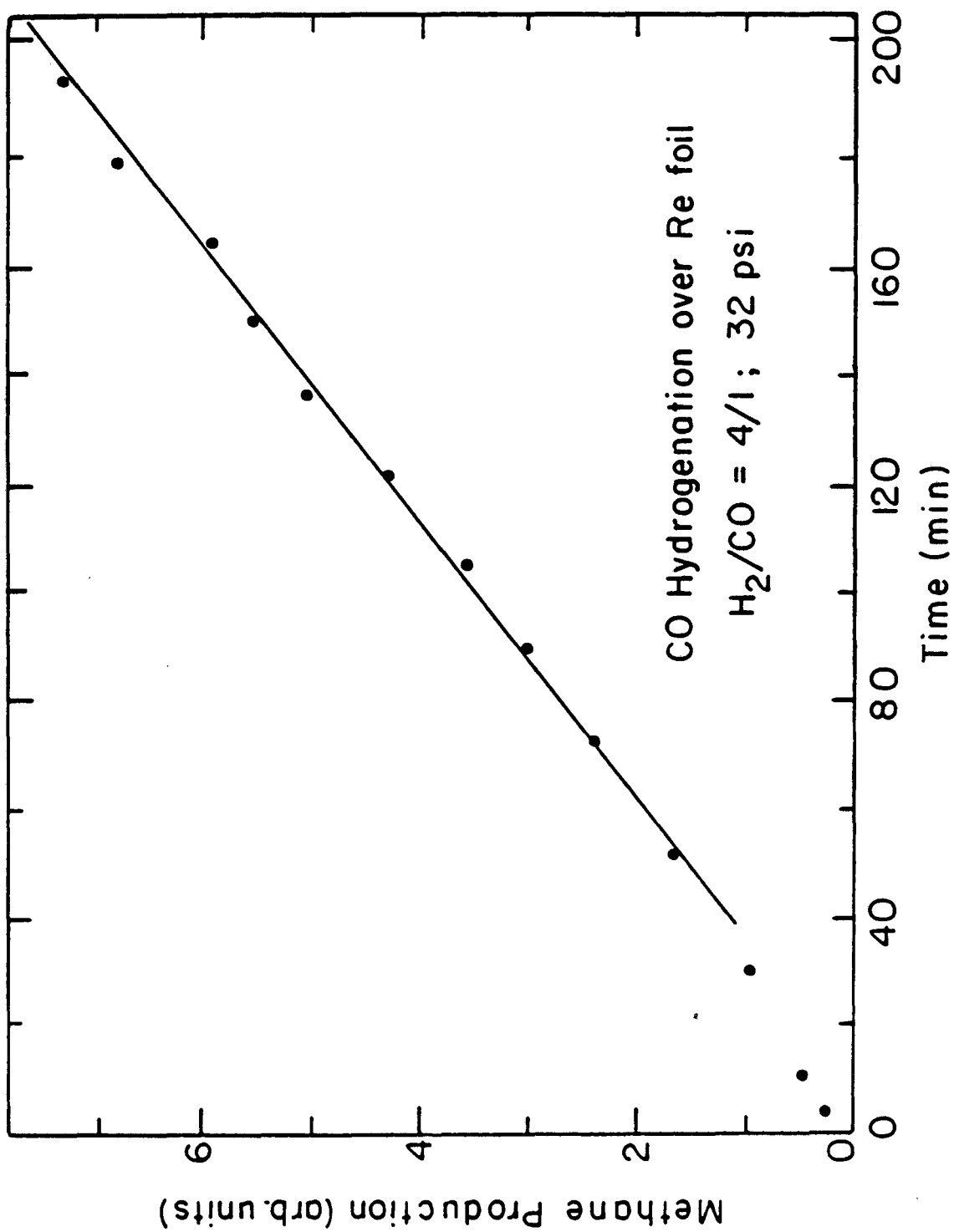
XBL 8310-6566

Fig. 5.2

Fig. 5.3

XBL 837-6025

Fig. 5.4

XBL 837-6026

Product Selectivity

Temperature Dependence for CO Hydrogenation on Rhenium Foil
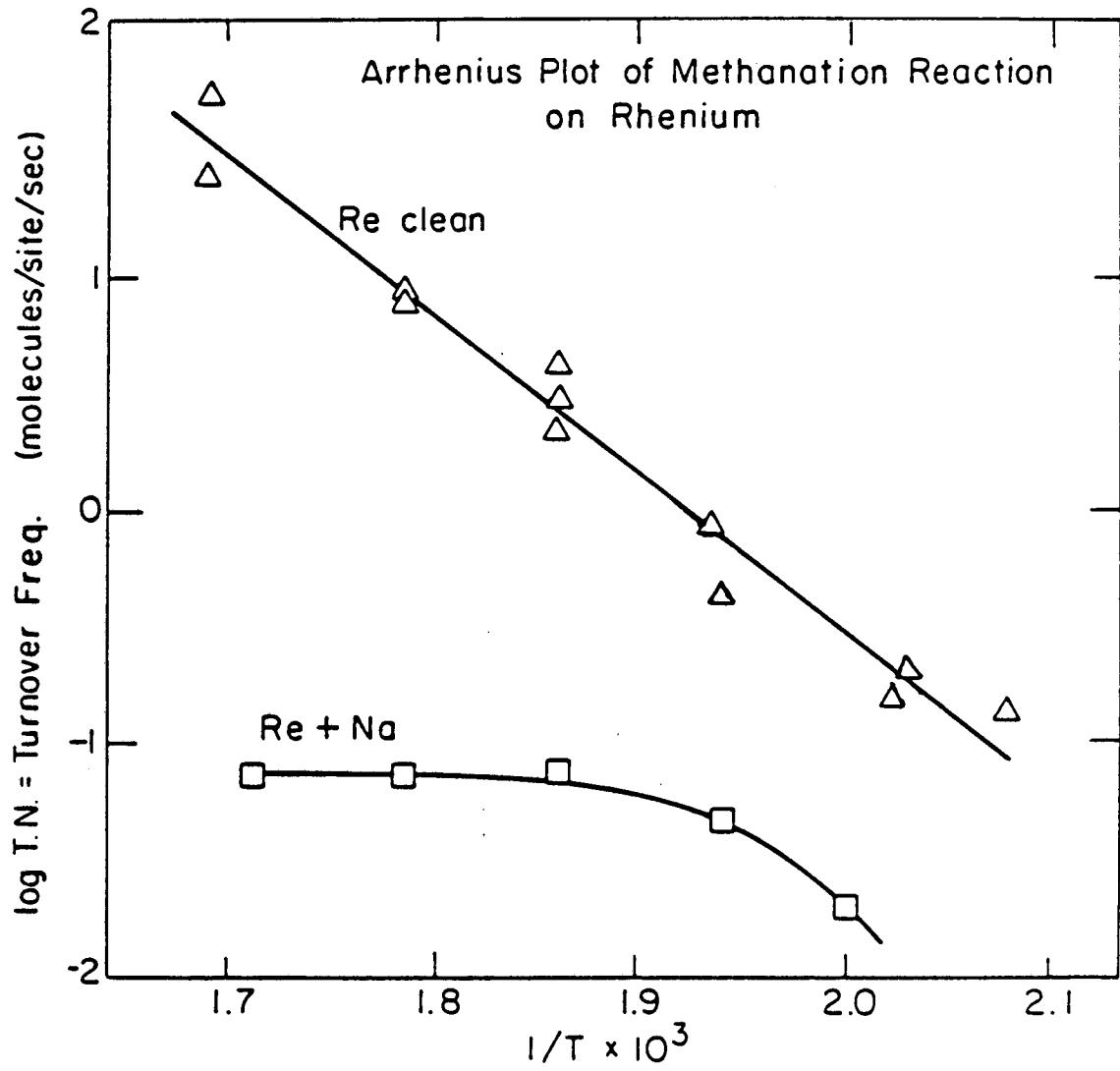
$CO/H_2 = 1/4$; 32 psi
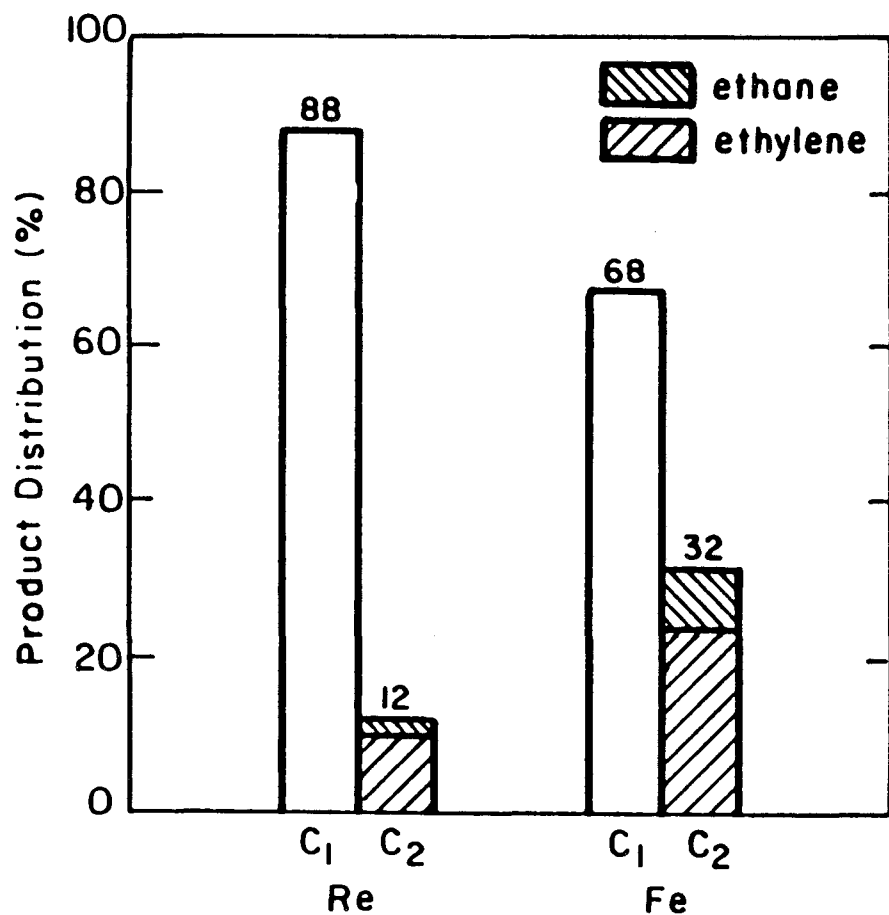
Fig. 5.5

XBL837-6029

CO Hydrogenation
540 K; CO/H$_2$= 1/4; 32 psi
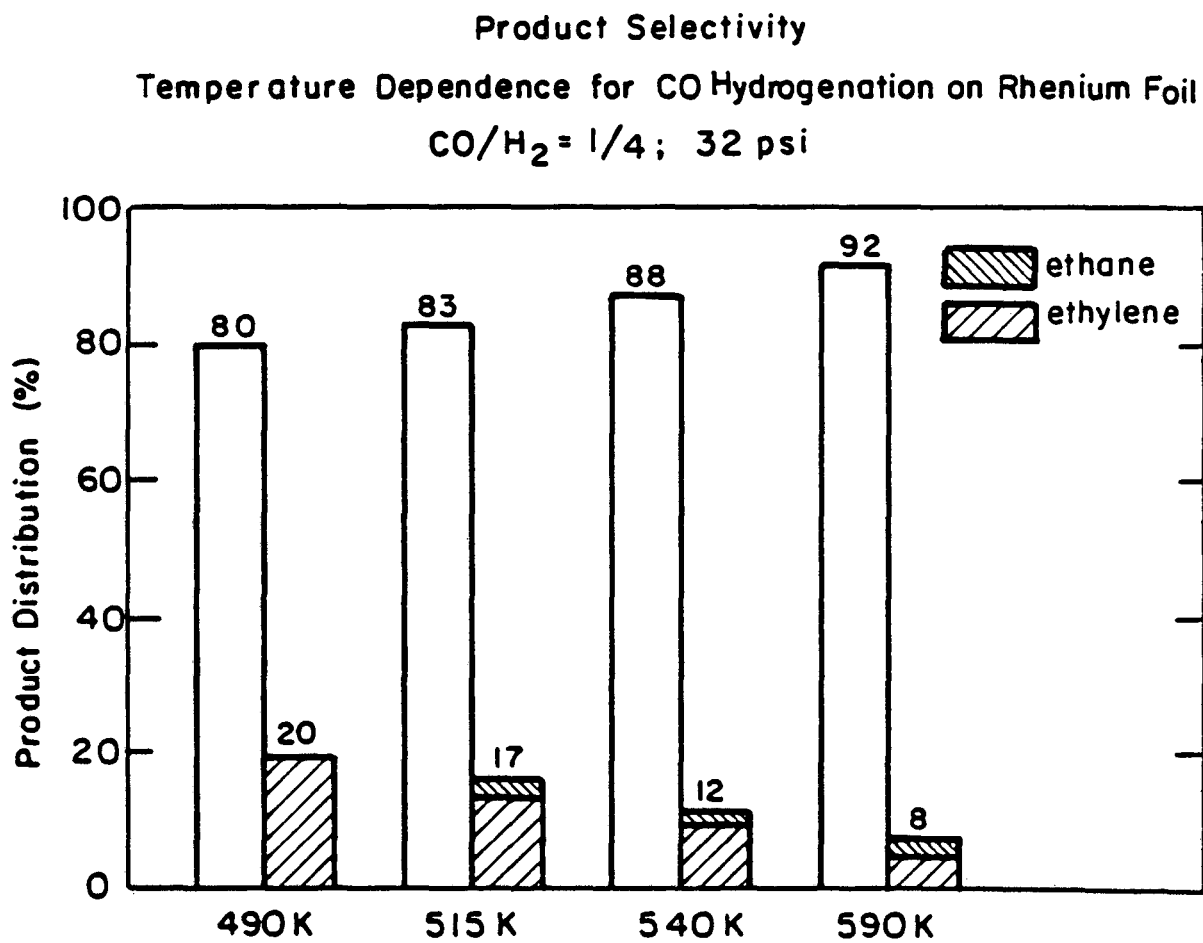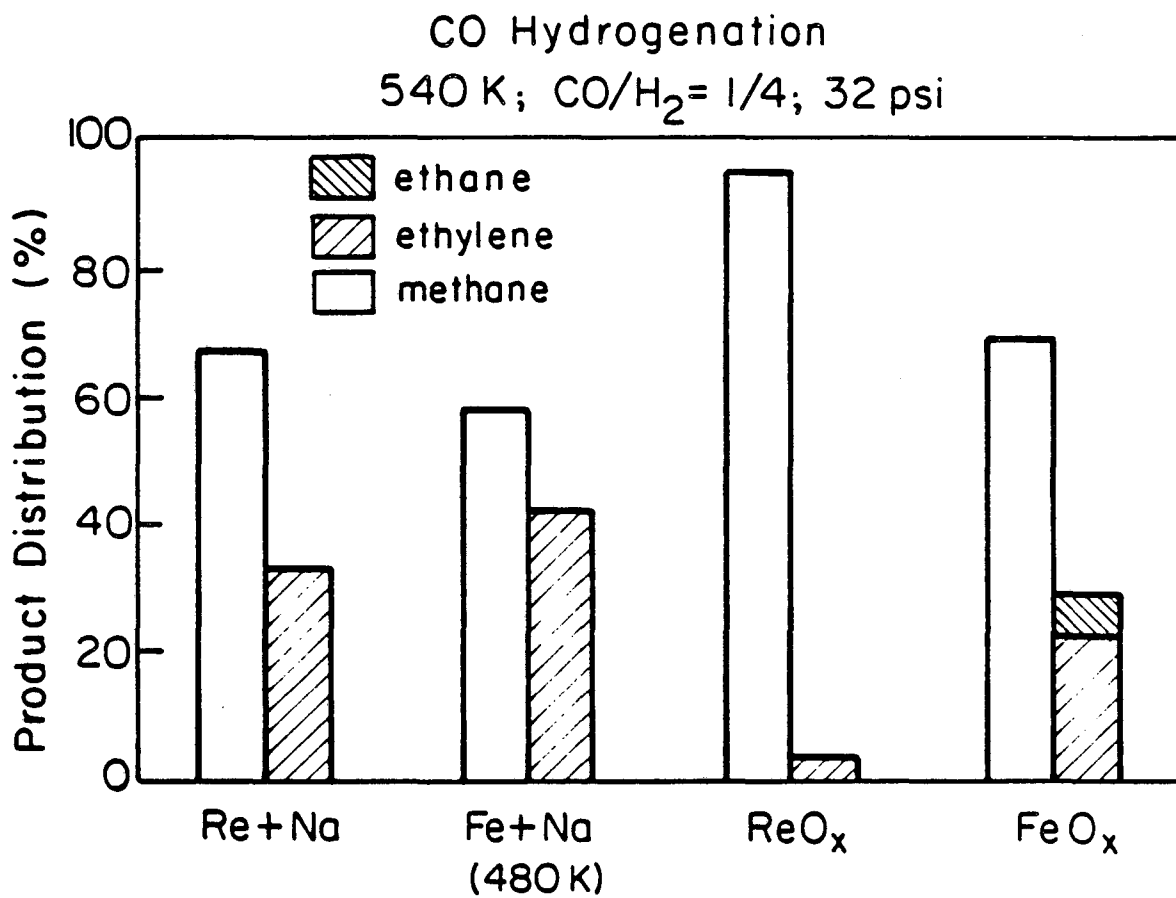
Fig. 5.6

XBL 856-6366
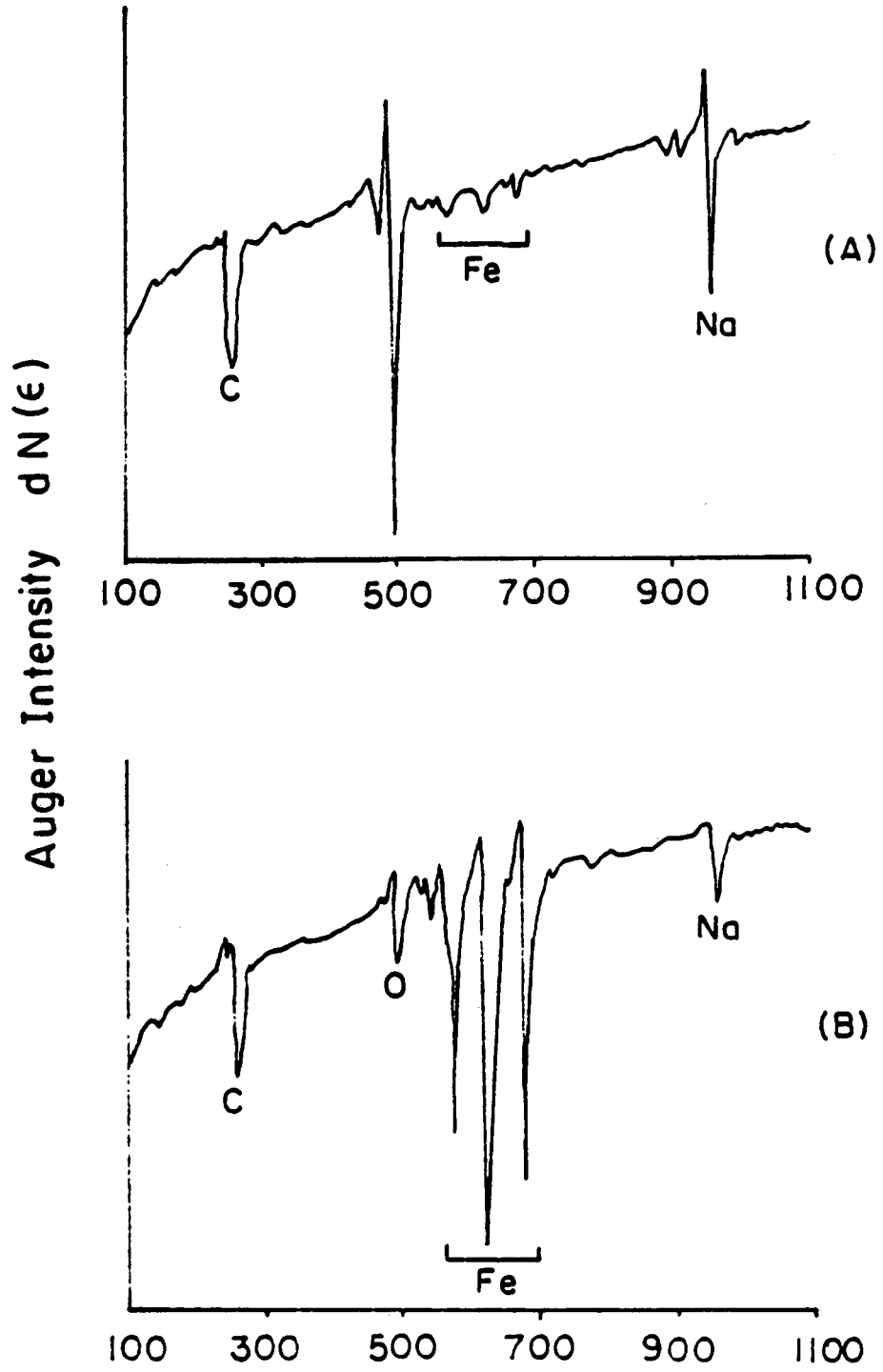
Fig. 5.7

XBL 838-11132

VI. ALCOHOL SYNTHESIS FROM CARBON MONOXIDE AND HYDROGEN
OVER MOLYBDENUM DISULFIDE. THE EFFECT OF PRESSURE
AND PROMOTION BY POTASSIUM CARBONATE

6.1 Introduction

Recently, molybdenum sulfides have been reported to produce methane, other alkanes,[1-2] and alcohols[3] under a variety of experimental conditions. The purpose of this investigation was to explore the catalytic behavior of molybdenum sulfide for this important reaction using well characterized catalysts. Compounds of the early transition metals Mo,W, V,Nb and Cr have not been explored as possible catalysts for the selective production of hydrocarbons from CO and H_2 to the same extent as the late transition metals Cu,Zn,Ni,Ru,Pd,and Rh. References 4-17 provide an overview of the large volume of work that has been done on the latter metals and their compounds.

In this chapter the preparation and characterization of a K_2CO_3 promoted MoS_2 catalyst for alcohol formation from CO and H_2 is described. In addition to the K_2CO_3 promotion, the dependence of this catalyst's selectivity upon pressure is demonstrated. It is shown the alcohol selectivity is very sensitive to both K_2CO_3 promotion and total pressure. Increases in either K_2CO_3 concentration or total pressure greatly increase the alcohol selectivity.

6.2 Results and Discussion

The catalysts used in these experiments were initially characterized via X-ray diffraction and XPS. X-ray diffraction patterns of the material prepared in our lab give the same peak positions as that of a commercially obtained MoS_2, but the peaks were much broader, as shown in Figure 6.1. The lack of sharp diffraction features indicates that either our product is MoS_2 with small particle size or that it lacks uniform composition. Further studies are needed to better characterize the catalyst's bulk properties. It is clear, however, that the near surface region of this catalyst is actually MoS_2. This is shown by the Mo 3d and S 2p XPS spectra that are displayed in Figures 6.2 and 6.3. In both cases the spectra the MoS_2 prepared by this method agree with those of commercial MoS_2. B.E.T. measurements indicate that the catalyst has a surface area of 6.9 m^2/g.

Experiments using our catalysts indicate that MoS_2 has a high catalytic activity for CO hydrogenation to hydrocarbons, but very little alcohol formation is apparent. The total selectivity to alcohol for the unpromoted MoS_2 is less than 5%. Note that all selectivities quoted in this work refer to those at one hour reaction time, unless otherwise noted. The conversion at one hour was very low (< 0.01) which allowed thermodynamic equilibrium considerations in this system to be neglected.

The turnover rate of methane production of the MoS_2 catalyst is approximately 10^{-3} sec^{-1}, at 250°C, 1000 psi, and $CO:H_2$ 1:1. This in the same range as reported for the more common Group VIII Ru, Ni, and

Fe catalysts by Vannice.[18] This number also falls within the range reported for supported MoS_2 and Mo-C catalysts.[19]

After adding K_2CO_3 to MoS_2 the product distribution shifts dramatically to selective alcohol formation. In Figure 6.4 the selectivity of MoS_2 and a K_2CO_3 promoted MoS_2 are compared. The experimental conditions were 250°C, $CO:H_2$ ratio of 1:1, reaction time 1 hour, and a total pressure of 1000 psi. The addition of K_2CO_3 promoted both the production of CH_3OH and C_2H_5OH, with CH_3OH selectivity peaking at about 55% and C_2H_5OH at about 10%. The CH_4 selectivity drops from about 50% to 35%, C_2H_6 and C_3H_8 selectivities decline from 25% and 15% respectively to essentially zero. Note that the promoted catalyst has a total of only 10% C_2^+ products as opposed to about 40% for the unpromoted catalyst.

By K_2CO_3 promotion alone the selectivity to alcohol for this catalyst has increased from about 2% to 65%. This effect appears to level off at a loading of approximately 0.3g K_2CO_3/g MoS_2 catalyst. It should be noted here that the addition of K_2CO_3 does not change the conversion significantly, only the selectivity is shifted greatly.

In addition to K_2CO_3, other alkaline compounds can also promote MoS_2 to increase the selectivity of CO hydrogenation to alcohol. Table 6.1 gives a comparison of the effects for several promoters. The results show that KOH has a promotion effect similar to K_2CO_3. NaOH, Na_2CO_3 also show promoter effect but not to the extent of either K_2CO_3 or KOH. A detailed study of the behavior of these different promoters has not yet been completed.

The effect of alkali promoters on this catalyst is to increase the selectivity to alcohols. This behavior was also reported by Quarderer and Cochran.[3] Their catalyst was supported MoS_2/K_2CO_3 with about 10% K_2CO_3 loading by weight. Their results are in qualitative agreement with these introduced here. Similar catalysts were also used by Murchison and Murdick.[20] In their experiments a catalyst with a much lighter loading of K_2CO_3 gave no alcohol. The result was an enhancement of C_2–C_5 yield.

The addition of high concentrations of alkali compounds to MoS_2 is necessary to promote alcohol formation. The reasons for this have yet to be determined. The high levels necessary to achieve this effect suggest the formation of an alkali overlayer or compound with MoS_2. Perhaps with this amount of alkali carbonate on the surface weaker interactions of molecular CO with the overlayer, that lead to its direct hydrogenation, dominate other reaction channels and the catalysis no longer occurs on the MoS_2. Much more work is necessary to determine the nature of this effect.

The alcohol selectivity could also be greatly increased by increasing the pressure. Increases in either the total pressure or of the H_2 pressure led to significant increases in the alcohol selectivity of the K_2CO_3 promoted MoS_2 catalyst. In Figure 6.5 we the effect of increasing the H_2 pressure upon alcohol selectivity is shown. The figure illustrates that the selectivity to alcohol increases from 65% to 90% for a catalyst that is 0.6g K_2CO_3/g MoS_2. These experiments covered a pressure range of 500 to 1500 psi H_2, with a constant CO

pressure of 500 psi. This increase is entirely due to the increased production of CH_3OH. As a result of this and a lack of a concommitant increase in the production of C_2H_5OH, the C_2H_5OH selectivity decreases. Note that the increase in CH_3OH production was continuous for the pressure range tested. In contrast, note Figure 6.6 where the fact that the pressure has very little influence on the selectivity of the unpromoted MoS_2 catalyst is depicted.

Figure 6.7 shows that the selectivity to alcohols can also be increased by increasing the total pressure and keeping the $CO:H_2$ ratio constant. This is also accompanied by a decrease in CH_4 formation. At a total pressure of 500 psi, CH_4 is favored over CH_3OH by a margin of 60% to 28% of the total products. At 2000 psi this has reversed to 75% CH_3OH to 15% CH_4. In both the aforementioned experiments the amount of C_2H_5OH stayed relatively constant and equal to 10%.

Experiments that monitored the selectivity as a function of the CO pressure were performed. The results showed that again higher pressures led to increased alcohol production. However, severe catalyst deactivation during these experiments did not allow quantification of this trend.

These studies show the alcohol selectivity of the promoted catalyst is increasing with pressure. The unpromoted catalyst was insensitive to pressure. This variation with pressure could be due to the enhancement of a reaction pathway that exists only on the promoted catalyst. As mentioned earlier, the reaction to form the alcohol might occur on the alkali overlayer. Possibly this layer stabilizes an intermediate

to alcohol formation. This species, possibly a weakly bound formate, would be present in much higher concentrations at high pressures.

The residence time of the products in this batch reactor can also influence the selectivity of the K_2CO_3/MoS_2 catalyst. Figure 6.8 shows the effect of increasing reaction time. The selectivity shifts away from CH_3OH to CH_4. The selectivity to CH_3OH shifted from 58% at 60 minutes to 30% at 300 minutes. Correspondingly, the selectivity to CH_4 increased from 35% to 60%. The production of C_2H_5OH also dropped, however less than 1% of the final products were C_2H_6. These changes are due, as shown in Figure 6.9, to a secondary reaction of CH_3OH that produces the decomposition products of CH_4, H_2O, and CO_2. In this experiment the decomposition of CH_3OH was monitored in Ar at 250°C, and 1000 psi total pressure.

6.3 Conclusions

This work shows the effects of K_2CO_3 promotion and increased pressure upon alcohol synthesis from carbon monoxide and hydrogen over a molybdenum disulfide catalyst. Increasing K_2CO_3 concentrations greatly enhances the selectivity of the reaction to methanol.

Similar results from experiments with other oxygenated promoters Na_2CO_3, NaOH, and KOH suggest an alkali oxide or alkali/oxygen compound with MoS_2 is the surface site responsible for the formation of the alcohol.

The other major conclusion of this work is that K_2CO_3 promotion makes the product distribution pressure dependent. The product distribution of the CO/H_2 reaction over the MoS_2 catalyst did not show any dependence on either total or hydrogen partial pressure. However, when the catalyst is promoted with K_2CO_3 we see a large pressure dependence; increased total total pressure yields increased selectivity to methanol.

Finally, it has been shown that CH_3OH decomposes on the catalyst. This reaction becomes more significant with increased reaction time, as the concentration of the alcohol increases in the batch reactor.

6.4 <u>References</u>

6.1 Concha, B.E., Bartholomew, G.L., and Bartholomew, C.H., J. Catal. <u>89</u>, 536-541 (1984).

6.2 Happel, J. and Hnatow, M.A., U.S. Patent: 4,320,030, (March 1982).

6.3 Quarderer, G.J., and Cochran, G.A., European Patent Application: 0119609 (September 1984), and references cited therein.

6.4 Klier, K., in <u>Advances in Catalysis</u> Vol.31, 243, Academic Press NY, 1982, and references cited therein.

6.5 Herman, R.G., Klier, K., Simmons, G.W., Finn, B.P., Bulko, J.P., and Kohylinski, P.D., J. Catal. <u>56</u>, 407 (1979).

6.6 Bowker, M., Vacuum, <u>33</u> No. 10-12, 669-685 (1983).

6.7 Loktev, S.M., J. Mol. Catal. <u>17</u>, 225 (1982).

6.8 Kellner, C.S., and Bell, A.T., J. Catal. <u>71</u>, 288-95 (1981).

6.9 Hicks, R., and Bell, A.T., J. Catal. <u>91</u>, 104-115 (1985).

6.10 Poutsma, M.L., Elek, L.F., Ibarbia, P.A., Risch, A.P., and Rabo, J.A., J. Catal. <u>52</u>, 157-168 (1978).

6.11 Ryndin, Y.A., Hicks, R.F., and Bell, A.T., with Yermakov, Y.I., J. Catal. <u>70</u>, 287-297 (1981).

6.12 Poels, E.K., Koolstra, R., Geus, J.W., and Ponec, U., Imelik, B., et al. (editors), <u>Metal-Support and Metal-Additive Effects in Ca-</u><u>talysis.</u> 1982, Elsevier Scientific Publishing Comp., Amsterdam.

6.13 Orita, H., Naito, S., and Tamaru, K., J. Catal. <u>90</u>, 183-193 (1984).

6.14 Conesa, J.C., Sainz, M.T., Soria, J., Munuera, G., Rives-Arnau, V., and Munoz, A., J. Mol. Catal. <u>17</u>, 231-240 (1982).

6.15 Ichikawa, M., Bull. Chem. Soc. Jpn. <u>51</u>, 2268 (1978).

6.16 Ellgen, P.C., and Bhasin, M.M., U.S. Patents: 4,014,913 (March 1977); 4,096,164 (June 1978); and 4,162,262 (July 1979).

6.17 Happel, J., and Hnatow, M.A., U.S. Patent: 4,151,191 (April 1979).

6.18 Vannice, M.A., J. Catal. 37, 449 (1975).

6.19 Bridgewater, A.J., Burch, R., and Mitchell, R.C.H., J. Catal. 78, 116-125 (1982).

6.20 Murchison, C.B., and Murdick, D.A., Hydro. Proc. 1, 159 (1981).

TABLE 6.1
A COMPARISON OF ALCOHOL SELECTIVITIES FOR DIFFERENT PROMOTED CATALYSTS
(250°C, 1000 psi, CO:H_2 = 1:1, 1 hour)

CATALYST	WT. MoS_2:WT. PROMOTER	ALCOHOL
MoS_2		2.7
MoS_2/K_2CO_3	1:0.6	65.0
MoS_2/KOH	1:0.6	64.8
$MoS_2/NaOH$	1:1	61.8
MoS_2/Na_2CO_3	1:1	29.7

FIGURE CAPTIONS

Fig. 6.1 X-ray diffraction patterns of MoS_2 prepared from thermal decomposition of MoS_2 and of Alfa Co. MoS_2.

Fig. 6.2 Mo 3d x-ray photoelectron spectra of Alfa Co. MoS_2, and of MoS_2 prepared in our lab before and after reaction.

Fig. 6.3 S 2p x-ray photoelectron spectra of Alfa Co. MoS_2, and of MoS_2 prepared in our lab before and after reaction.

Fig. 6.4 The product distribution of the MoS_2 catalyst as a function of K_2CO_3 loading.

Fig. 6.5 The H_2 pressure dependence of the K_2CO_3/MoS_2 catalyst's selectivity.

Fig. 6.6 The H_2 pressure dependence of the MoS_2 catalyst's selectivity.

Fig. 6.7 The total pressure dependence of the K_2CO_3/MoS_2 catalyst's selectivity.

Fig. 6.8 The effect of increasing the reaction time upon the selectivity of the K_2CO_3/MoS_2 catalyst.

Fig. 6.9 The decomposition of CH_3OH as a function of reaction time over K_2CO_3/MoS_2 catalyst.

MoS$_2$ (commercial)

MoS$_2$ (thermodecomposition)

2θ
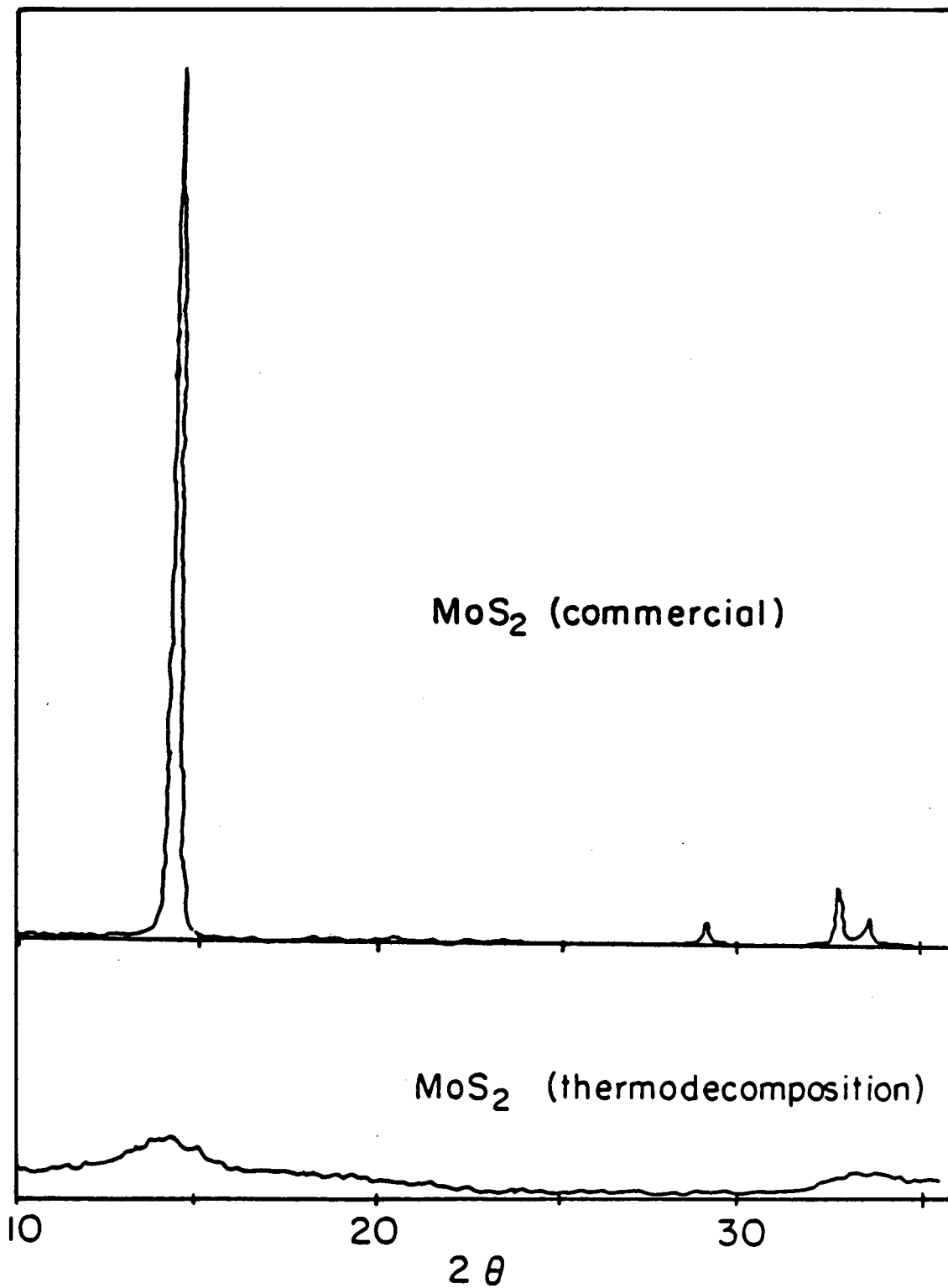
X-Ray Diffraction Patterns

Fig. 6.1

XBL 858-6527
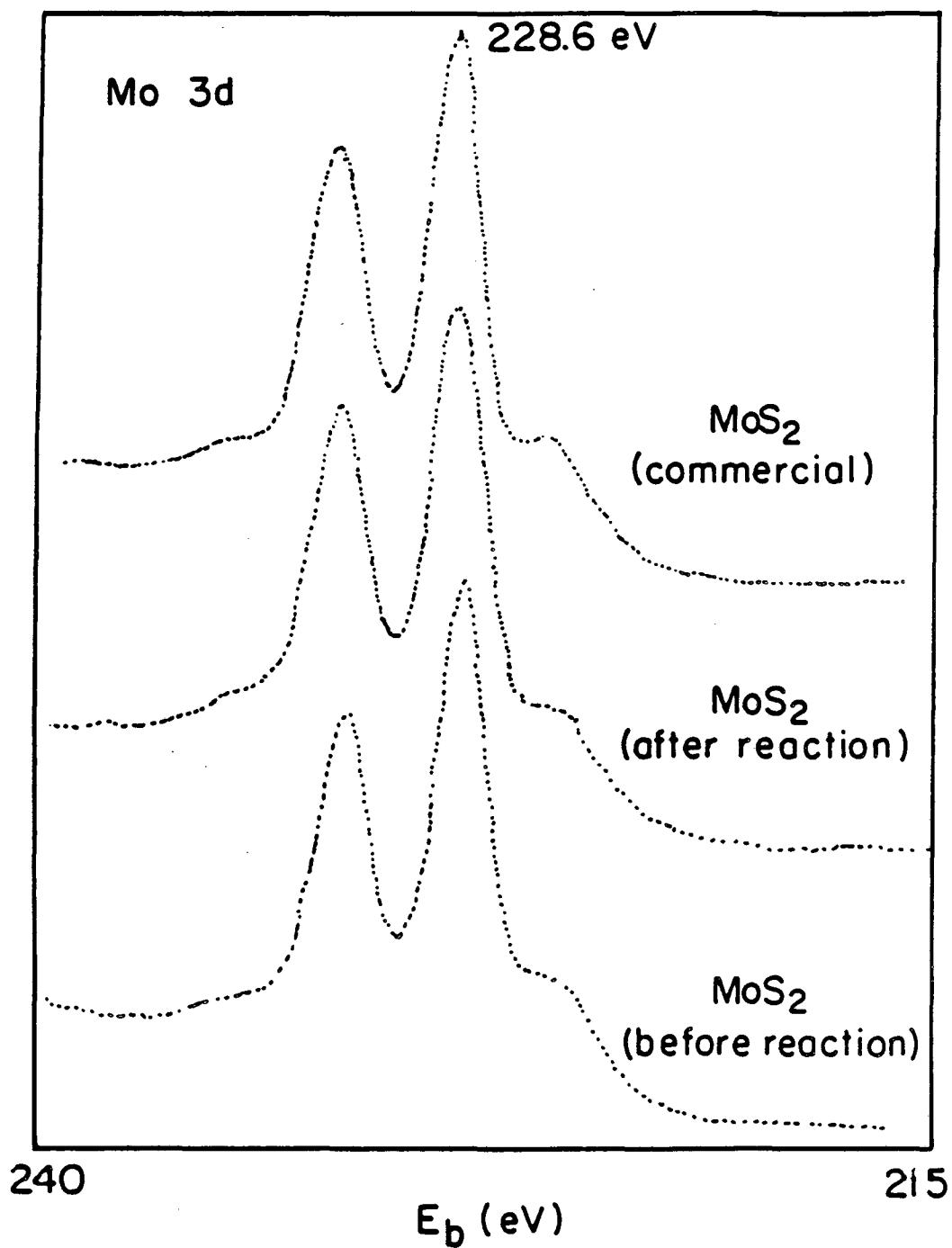
XPS Spectra of MoS$_2$

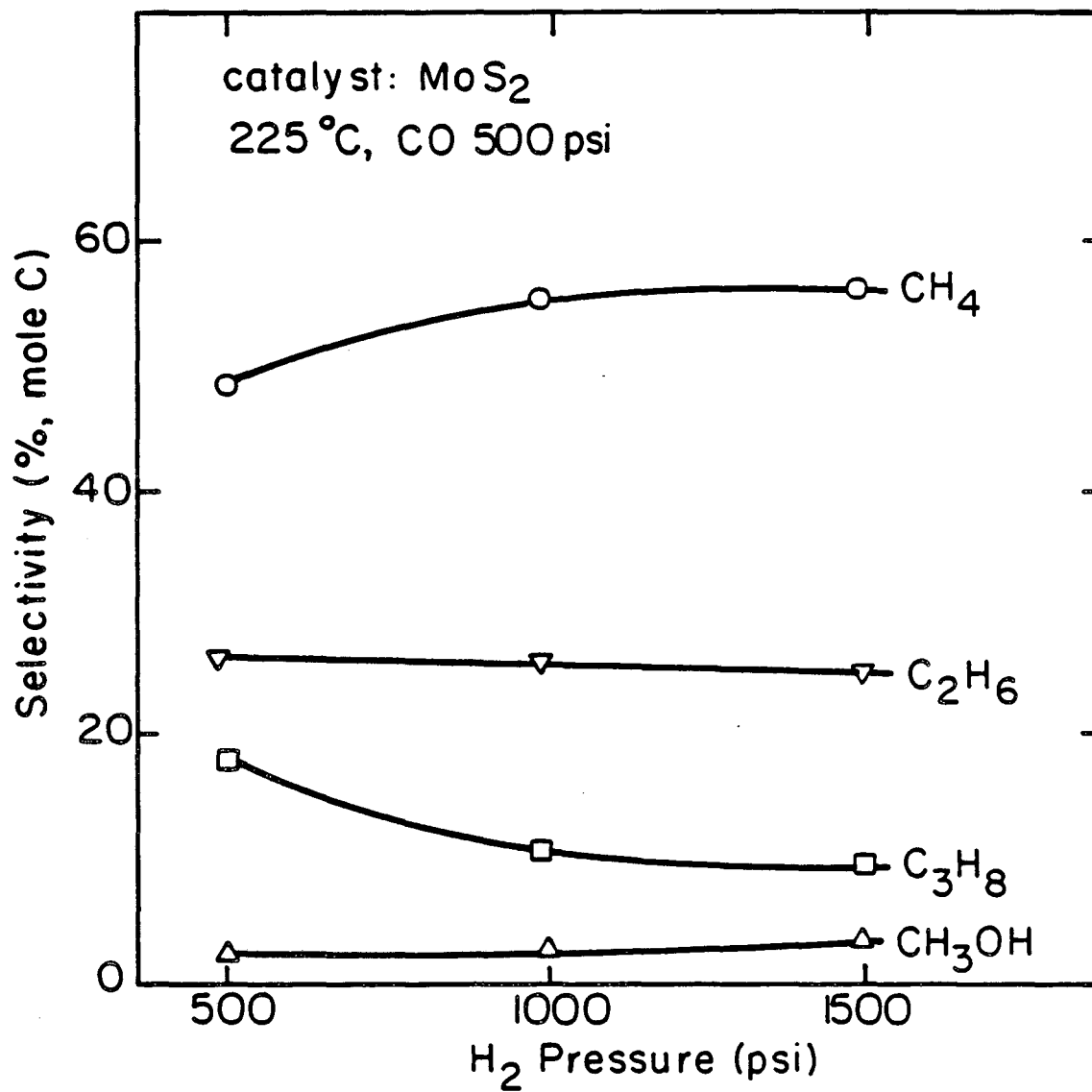Fig. 6.2   XBL858-6526
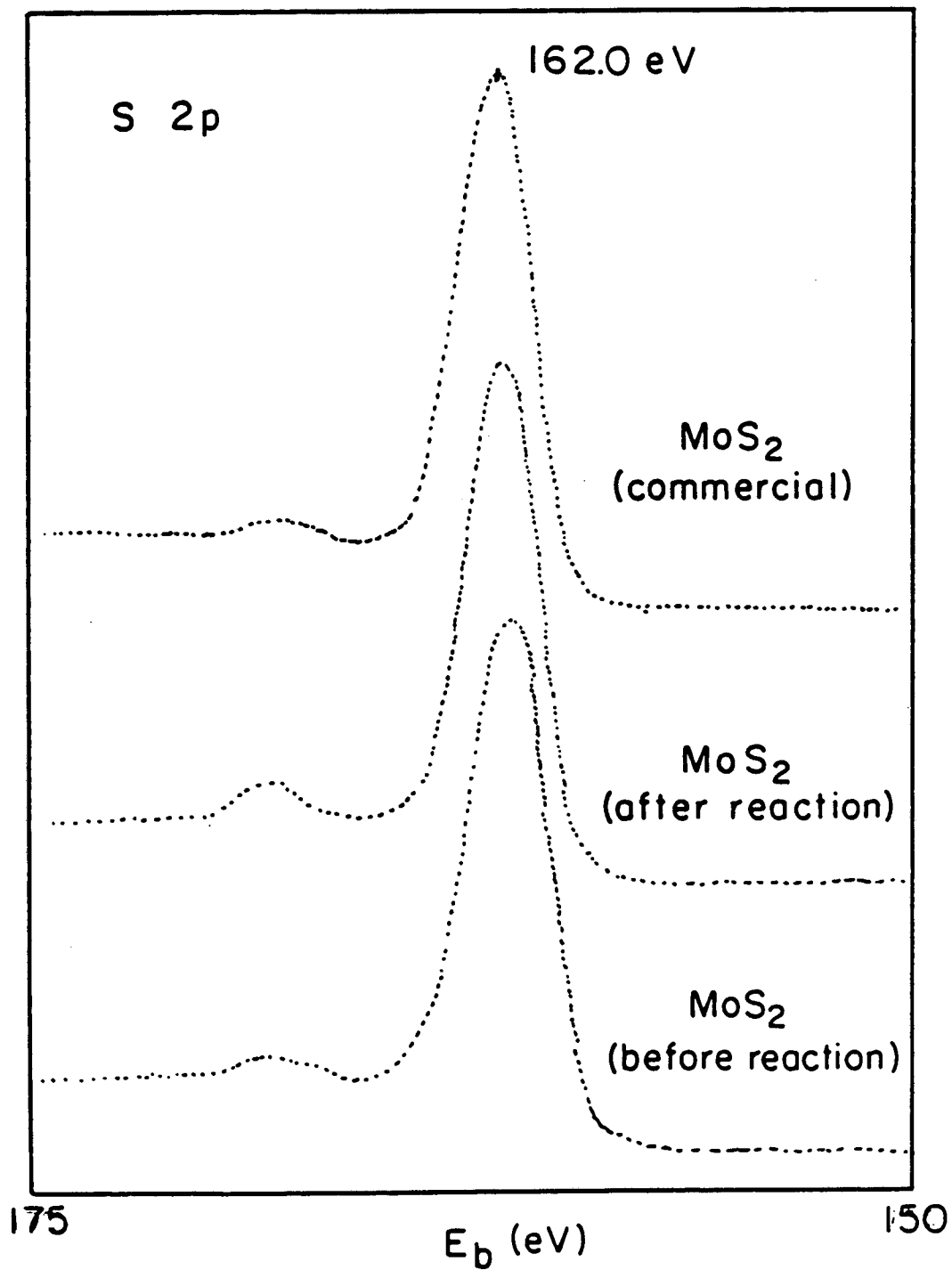
XPS Spectra of MoS$_2$

Fig. 6.3

XBL858-6525
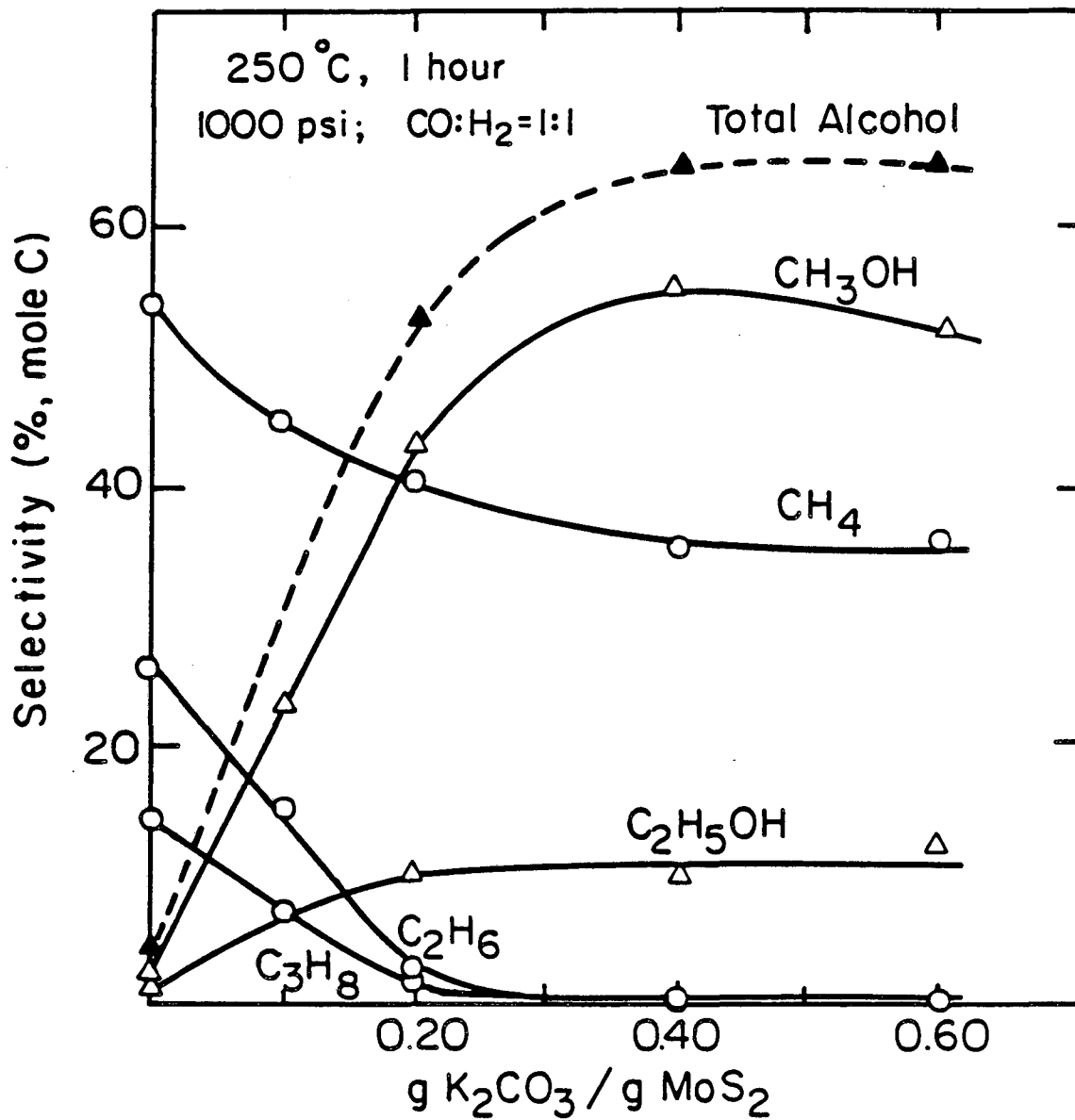
Effect of K_2CO_3 Content on Product Distribution of Promoted MoS_2 Catalyst

XBL 856-6370

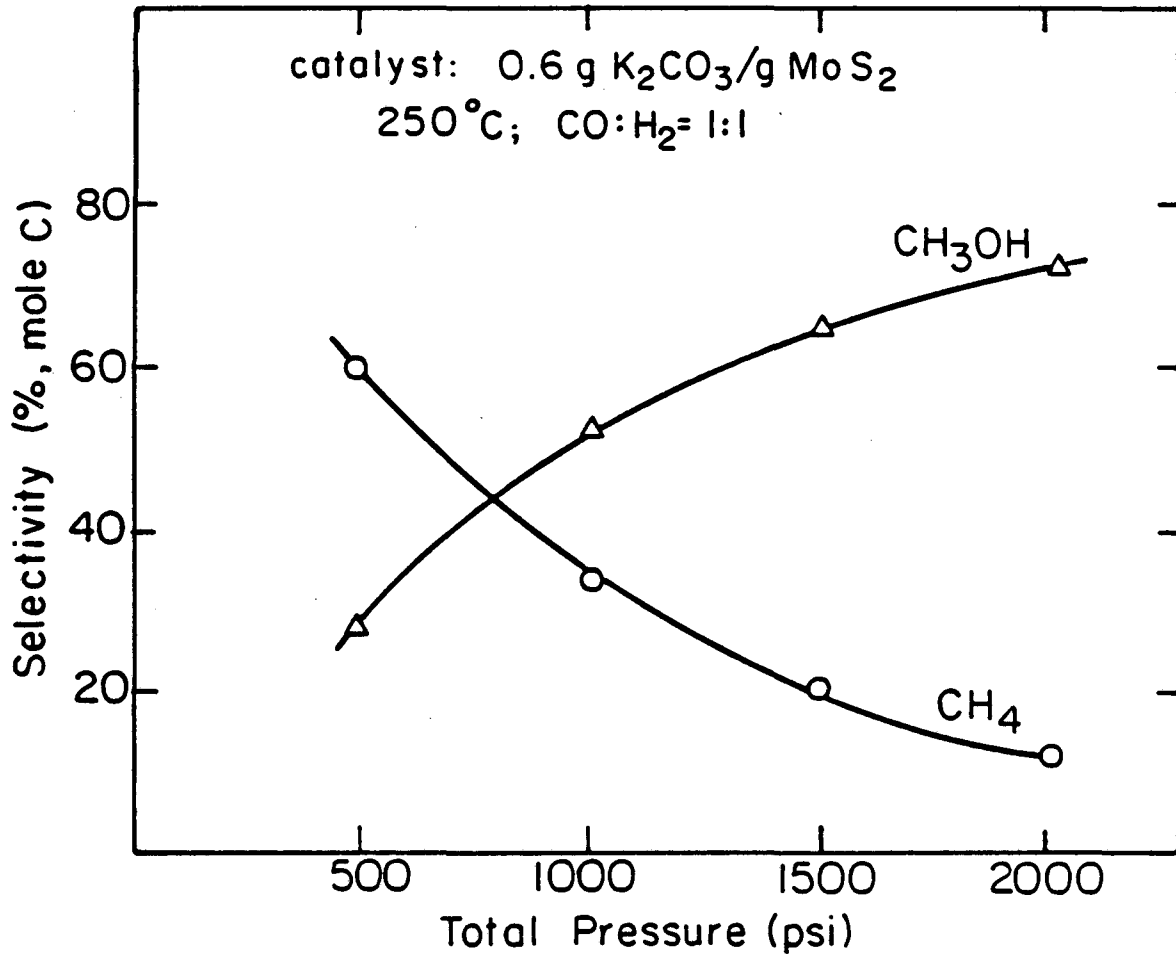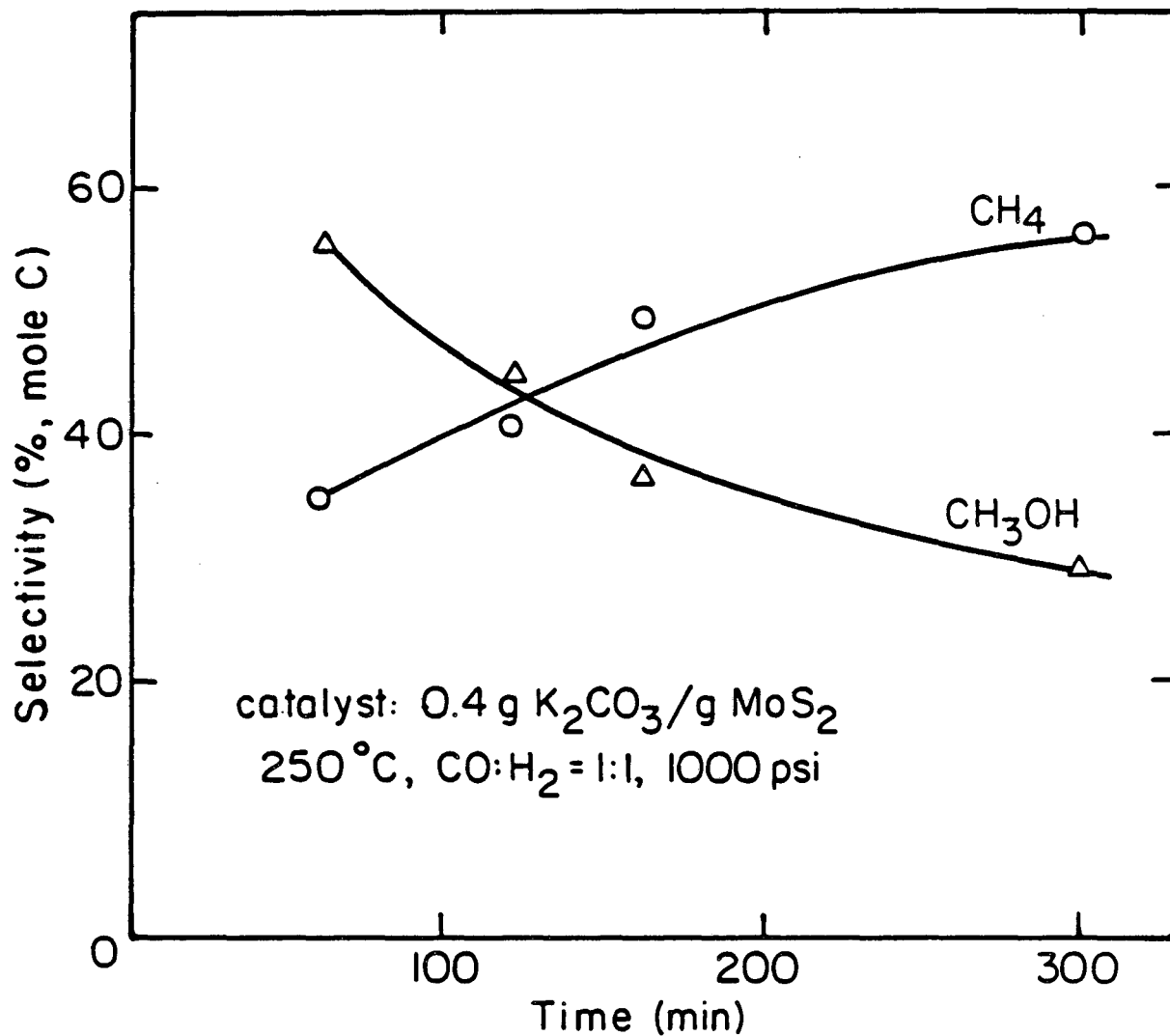Fig. 6.4

Effect of Pressure on Product Distribution of K$_2$CO$_3$/MoS$_2$ Catalyst

Fig. 6.5

XBL856-6369

Effect of Pressure on Selectivity

Fig. 6.6

XBL 858-6523

catalyst: 0.6 g K_2CO_3/g MoS_2
250°C; CO:H_2= I:I

Effect of Total Pressure on Selectivity of
K_2CO_3/MoS_2 Catalyst

Fig. 6.7   XBL 856-6368

Time Dependence of Selectivity

Fig. 6.8

XBL858-6524
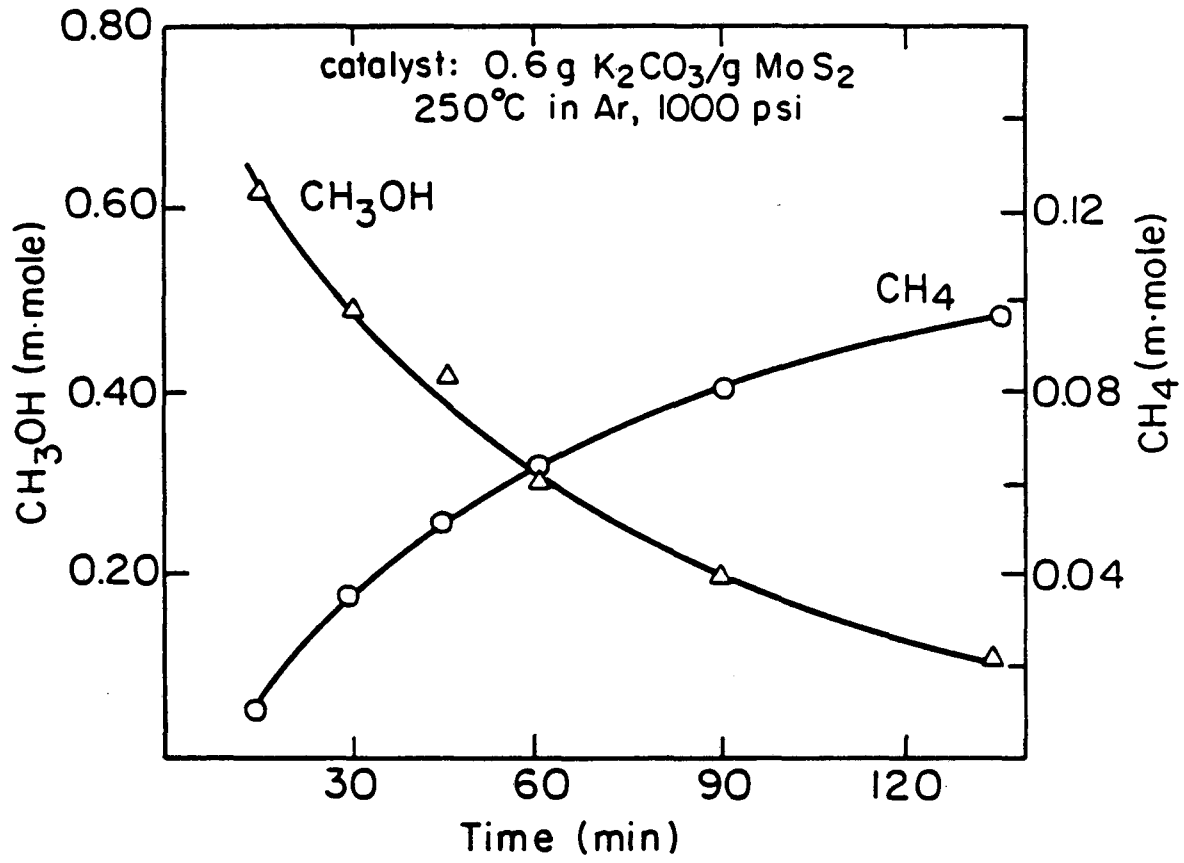
CH₃OH Decomposition on K₂CO₃/MoS₂ Catalyst

Fig. 6.9

XBL 856-6367